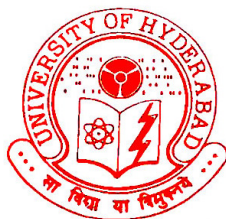# MICROWAVE-ASSISTED SOLUTION COMBUSTION SYNTHESIS AND CHARACTERIZATION OF CERIA-BASED OXIDES FOR CO OXIDATION

THESIS

SUBMITTED TO

UNIVERSITY OF HYDERABAD

FOR THE DEGREE OF

DOCTOR OF PHILOSOPHY

IN

CHEMISTRY

BY

L. HANUMA REDDY, M. Sc.
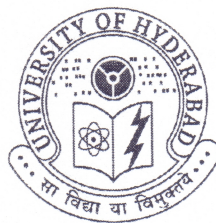
Reg. No: 09CHPH33

UNDER THE SUPERVISION OF

Dr. B. M. REDDY

INORGANIC & PHYSICAL CHEMISTRY DIVISION

CSIR–INDIAN INSTITUTE OF CHEMICAL TECHNOLOGY

HYDERABAD — 500 007, TELANGANA, INDIA

MARCH — 2017

This thesis is dedicated to my son Gokul Chandra, wife Kaanthi Srujana, beloved parents & parents in-law.

CERTIFICATE

This is to certify that the thesis entitled "**MICROWAVE-ASSISTED SOLUTION COMBUSTION SYNTHESIS AND CHARACTERIZATION OF CERIA-BASED OXIDES FOR CO OXIDATION**" submitted by **L. Hanuma Reddy** bearing registration number **09CHPH33** in partial-fulfilment of the requirements for award of Doctor of Philosophy in the school of **Inorganic and Physical Chemistry division, Indian Institute of Chemical Technology (CSIT-IICT)** is bonafide work carried out by him under my supervision and guidance.

This thesis is free from plagiarism and has not been submitted previously in part or full to this or any other university or institution for award of any degree or diploma.

Further, the student has the following publications before submission of the thesis for adjudication and has produced the evidence along with the thesis as annexure.

1. **Applied Catalysis A: General, 445– 446 (2012) 297– 305** (ISSN Number **0926-860X**), Chapter-3 i.e. Studies on CuO Promoted CeO_2-MxOy (M = Zr, La, Pr and Sm) Solid Solutions for CO Oxidation.

Further, the student has passed the following course towards fulfilment of coursework requirement for Ph.D/was exempted from doing course work (recommended by Doctorial Committee) on the basis of the following courses Passed during his M.Phil programme and the M.Phil degree was awarded.

	Course code	Name	Credits	Pass/Fail
1				
2		course work not done		
3				
4				

Supervisor   Head of Department   Dean of School

डॉ. बी. एम. रेड्डी, एफएनएई, एफएनएएससी, एफआरएससी, एफटीएएस
Dr. B. M. REDDY, FNAE, FNASc, FRSC, FTAS
मुख्य वैज्ञानिक एवं अध्यक्ष / Chief Scientist & Head (Rtd.)
अकर्बनिक एवं भौतिक रसायन प्रभाग
Inorganic & Physical Chemistry Division
सीएसआईआर-भारतीय रासायनिक प्रौद्योगिकी संस्थान
CSIR-Indian Institute of Chemical Technology
तारनाका, हैदराबाद, भारत/Tarnaka, Hyderabad - 500 007. India.

डॉ. क. एस. रामा राव
Dr. K. S. RAMA RAO
Senior Principal Scientist & Head
Inorganic & Physical Chemistry Division
एसआईआर-भारतीय रासायनिक प्रौद्योगिकी संस्थान
SIR-Indian Institute of Chemical Technology
Tarnaka, Hyderabad - 500 007.Telangana, India.

STATEMENT

I hereby declare that the matter embodied in this thesis entitled **"MICROWAVE-ASSISTED SOLUTION COMBUSTION SYNTHESIS AND CHARACTERIZATION OF CERIA-BASED OXIDES FOR CO OXIDATION"** is the result of investigation carried out by me in Inorganic and Physical Chemistry Division, Indian Institute of Chemical Technology (CSIR-IICT), Hyderabad, India, under the supervision of **Dr. B. Mahipal Reddy,** Chief Scientist, IICT.

In keeping with the general practice of reporting scientific observations, due acknowledgements have been made on the basis of the findings of other investigators. Any omission, which might have occurred by oversight or error, is regretted. This research work is free from Plagiarism. I hereby agree that my thesis can be deposited in shodganga/INFLIBNET. A report on plagiarism statistics from the University Librarian is enclosed.

March, 2017

L. Hanuma Reddy

09CHPH33

Dr. B. Mahipal Reddy
Supervisor

डॉ. बी. एम. रेड्डी, एफएनएई, एफएनएएससी, एफआरएससी, एफटीएएस
Dr. B. M. REDDY, FNAE, FNASc, FRSC, FTAS
मुख्य वैज्ञानिक एवं अध्यक्ष / Chief Scientist & Head (Rt d.)
अकर्बनिक एवं भौतिक रसायन प्रभाग
Inorganic & Physical Chemistry Division
सीएसआईआर-भारतीय रासायनिक प्रौद्योगिकी संस्थान
CSIR-Indian Institute of Chemical Technology
तारनाका, हैदराबाद, भारत / Tarnaka, Hyderabad - 500 007. India

I would like to acknowledge P.G. classmates at Department of Chemistry, Osmania University, Hyderabad, and all other friends from my school days to Ph.D for their constant support and encouragement in pursuing the venture. I would like to acknowledge my close friend **Dr. K. Nagarjuna** who has been with me from my school days to till today for his constant help and encouragement.

Words are few to express my appreciations to my family members, whose love, encouragement, and persistence confidence in me has taken the load off my shoulder. I would also like to thank everyone who is important to the successful realization of my journey, as well as express my apology that I could not mention personally one by one.

Date: March 2017   L. Hanuma Reddy

CONTENTS

CHAPTER 3: STUDIES ON CuO PROMOTED CeO_2-M_xO_y (M = Zr, La, Pr and Sm) SOLID SOLUTIONS FOR CO OXIDATION

CHAPTER 4: STUDIES ON CeO$_2$-MxOy (M=Mn, Fe, Co) FOR CO OXIDATION

CHAPTER 5: STUDIES ON CeO$_2$ and Ce$_{0.8}$Sm$_{0.2}$O$_2$ FOR CO OXIDATION-INFLUENCE OF BALL-MILL METHOD

CHAPTER 1

AN INTRODUCTION TO CeO$_2$, ITS OXIDES - SIGNIFICANCE OF MICROWAVE-ASSISTED COMBUSTION SYNTHESIS

Metal oxides, a group of catalysts being widely used as active supports to organize the industrial based heterogeneous catalysis because of their redox properties [1-6]. Most important features of metal oxides those responsible for their applicative catalysis are redox properties of the metal oxide, coordination chemistry of surface metal atoms, oxidation states of metal on metal oxide surface. Most of the metal oxide catalysts belong to transition metals because they exhibit variable oxidation states. The redox properties of metal cations of transition metals make them popularized in catalysis. The charge and size determine the acidity of lattice oxanions, whereas ionic nature of M-O bond decides the basicity of the metal cation [1, 7, 8]. Metal oxides and metals are widely used in heterogeneous catalysis. Metal oxides are prepared from calcinating metal hydroxides. Petroleum and petro chemical industries, complex inorganic and fine chemicals industries, various food industries are widely dependent on the metal oxides for their great catalytic applications [9]. Cerium metal, an f-block element with two variable oxidation states 3+ and 4+, exists in two oxides forms as Ce$_3$O$_4$ and CeO$_2$. Among these we consider CeO$_2$ for further studies because of its intrinsic properties.

1.1 Cerium Dioxide (CeO$_2$)

Ceria and its materials are the most important compounds belonging to ceramic materials with a wide range of applications. Ceria is recognized by its notable catalytic uses among those few of them are three way automotive catalysts (TWC's) [10], Ionic conductors [11], gas sensor [12], and electrolyte in solid fuel cells [13].

Nano particulate ceria has gained its importance from redox nature, in academic as well as industrial research. Non-stoichiometric studies related to the formation of anion vacancies (super structures) are well understood [14], and these vacancies are arranged in an order around the cubic fluorite crystal lattice of ceria [15]. These super structures are

linked to small localized polaron states of electrons those stay behind after desorption of O_2. A simple explanation for defect chemistry and its complexity, electrons released during loss of O_2 (g) from lattice, combines with Ce^{4+} ion and reduced to Ce^{3+} ions, results in expansion of lattice, as the ionic radii of Ce^{3+} ion is comparatively large compared to CeO_2 stoichiometric structure [14]. Morris et al. [16], Esch et al. [17] and Namia and co-workers [18] came up with vacancies those are labile and may also result in cluster formations. Nano particulate ceria has got specific interest from its higher catalytic activity resulted from surface area of nano particulates with rapid sinterability observed when compared to crude bulk materials [19].

Sensitivity of bands observed while characterization suggest that a slight change in the structure of ceria on nano-scale might show an impact in modification of physiochemical properties of ceria. On decreasing the size of nano particulate ceria, there observed a change in lattice constant 'a' of ionic crystallites which was completely studied yet [20], whereas Tsunekawa et al. reported that with a decrease in particle size there is an expansion in lattice structure from numerous preparations of ceria [21]. Many methods are used for preparing the nano particulate ceria. A few them includes micellar controlled, sol-gel, micro emulsion, co-precipitation, microwave-assisted, solution combustion, ball mill, and microwave-assisted combustion synthesis etc.

Ceria has wide applications in catalytic activity, even though its innovative properties are lost at higher temperatures for a long run in catalytic reactions due to rapid sintering. However, nanocrystallite ceria exhibits better catalytic activity and sinterability in comparison with coarse bulk material. Nanocrystallite ceria has gained special interest of scientific research due to its peculiar physiochemical properties with potential applications in present day situations. Ceria exhibits high mechanical hardness, thermal stability, temperature coupled redox activity, surface to volume ratio. It exhibits unique UV absorptivity, optical characteristics.

Nanocrystallite ceria is having research significance due to its high redox activity and surface area. Ceria has been continuously used in material science research for

developing scalable methods to synthesize nanocrystallite structures with variety of sizes, morphologies to study various applications involved with ceria and doped ceria solid solutions. Most of the chemical methods involved in preparation of ceria results in spherical nano particulates with a higher BET surface area, either weak agglomeration or no agglomeration seen. However, individual chemical methods produce solid solutions with different morphologies, defect densities resulting in the solid solutions with different rates of catalytic activity.

1.2   Fluorite Structure / Face Centered Cubic lattice of Ceria

Ceria is a white crystalline solid in pure state; exhibit cubic fluorite structure. Each unit cell of ceria has oxygen atoms as an array in cube form, acts as a framework for ceria atoms which are occupied in alternative cubes [22]. This is the fluorite structure of ceria, which is given its name after the CaF_2 as shown in figure 1.1. This fluorite crystal of ceria has FCC lattice which has a lattice constant 'a' value as 0.541134 nm and Fm3m space group. In this unit cell, ceria atoms occupy the face centered positions of the alternative cubes and the eight oxanions occupy the nearest edges of the cube, which are coordinated together. Tetrahedral positions are occupied by oxanions and are coordinated by the four metal ions in a lattice [23].
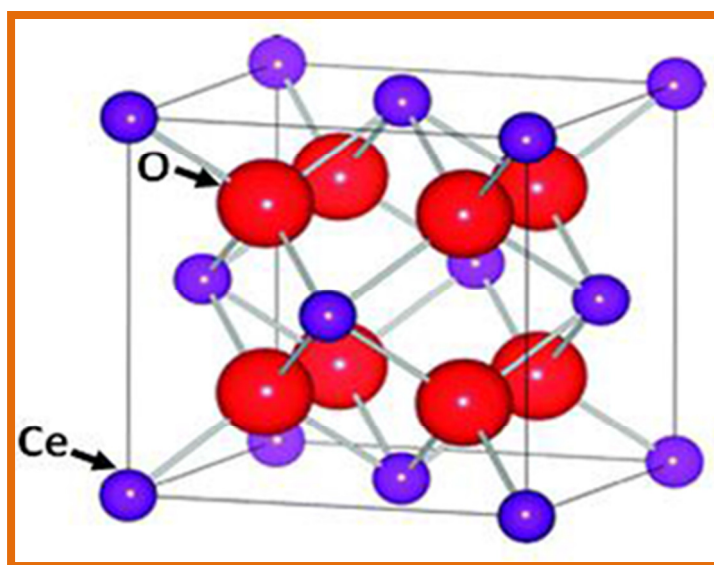
Figure 1.1:   Face centered cubic lattice structure of ceria

Oxygen deficient non-stoichiometric structures are formed in a series when ceria is subjected to reduction conditions and high temperatures [24, 25, 26]. Ceria has an affinity to create the isolated compositions when subjected to lower temperatures. Oxygen deficit non-stoichiometric structures are created from reducibility of ceria, as it release bulk O_2 to form huge oxanion vacancies. These reduced ceria particles still retain its crystal lattice, as its structure is thermodynamically stable and is readily convertible on exposure of oxidizing environment [27, 28, 29]. Apart from the arguments, it is clear that ceria is highly labile towards lattice oxygen and plays the most important role to be considered for its practical catalytic activity. This is explained as redox nature of ceria which has an utmost place in industry of catalysis.

As the OSC of ceria is high, and this decreases at higher temperatures because of thermal instability of ceria, which makes it important for further studies in developing the ceria as ceria based oxide catalysts. However, it is stated that ceria physiochemical properties can be increased by doping the metals of transition and inner transition groups into the FCC lattice [24-28]. A further explanation related to this statement is discussed in the later sections of this chapter and is practically observed in next upcoming chapters.

1.3   Stoichiometric properties of Ceria

1.3.1   Reduction reactions

Broad spectrum studies carried over the reduction of ceria is because it has wide range of applications in catalytic industry. Conversion of H_2 [30, 31] and CO [32,33] to their respective forms on reacting with ceria made it more specific and interesting to study the reductive mechanism involved with ceria.

From the characterization studies related to ceria collected over H_2-Temperature programmed reduction and X-ray diffraction spectrometry, a reductive scheme of ceria

involving the kinetics with 4 main steps involved and is proposed and summarized as follows which is as discussed by Trovarelli et. al [34].

Step1: Chemisorbed hydrogen on surface is dissociated as hydroxyl groups

Step2: Oxanion vacancies is formed along with the reduction of adjacent metal ions

Step3: Hydroxyl groups combined with H_2 leading to desorb the water.

Step4: Oxanions on surface layer are diffused to bulk lattice.

When a supporting oxide such as alumina or silica is used to modify the reduction ability of ceria, metal to oxide interactions play a vital role in deciding the modifications occurred. Similarly incorporating the dopant ion into bulk lattice ceria, the reduction capability can be modified.

Doping of small sized cations such as Zr, Hf, Pr, Mn, Fe, Co, Tb, La etc into the crystal lattice of ceria creates defects in lattice there by increasing the mobility of O_2. Reduction capability of mixed oxides depends on the crystal structure of base material.

1.3.2 Oxidation reactions

Most of the catalytic activities of ceria account for oxidation reactions of ceria and its mixed oxides. However, the redox nature and higher mobility towards lattice oxygen play a vital role in contribution towards the oxidative reactions of ceria. Even though ceria has proven for oxidative catalytic activities [32-38], partial and selective oxidations cannot be performed by ceria or even if it is performed the selectivity is poor.

Doping ceria with other metals, it's easy to modify the structure of ceria crystal leading to modification of oxidative properties of ceria. As ceria and doped ceria are reported with wide range of applications there is a huge demand for synthesizing in different sizes and morphologies. Formation of solid solution is very important with a special emphasis for CO oxidation as there is involvement of surface and bulk oxygen in the catalytic reaction.

1.4   Industrial applications of Ceria Nanoparticles

1.4.1   Automotive Catalysis

Using of ceria in automotive catalysis is seen during the start of 1980's for pollution control that has been more prevalent till today, supports the importance of ceria in this applicative catalysis [39]. Ceria is the main composition in formulations of TWCs, developing TWCs has got special interest because at a time conversion of HC's, CO, NO_X to H_2O, CO_2, N_2 decreases the percentage of harmful gaseous mixture being released from exhaust of automobiles. In the figures 1.2 and 1.3, the interactions of CO and hydrocarbons over ceria based oxides are displayed.
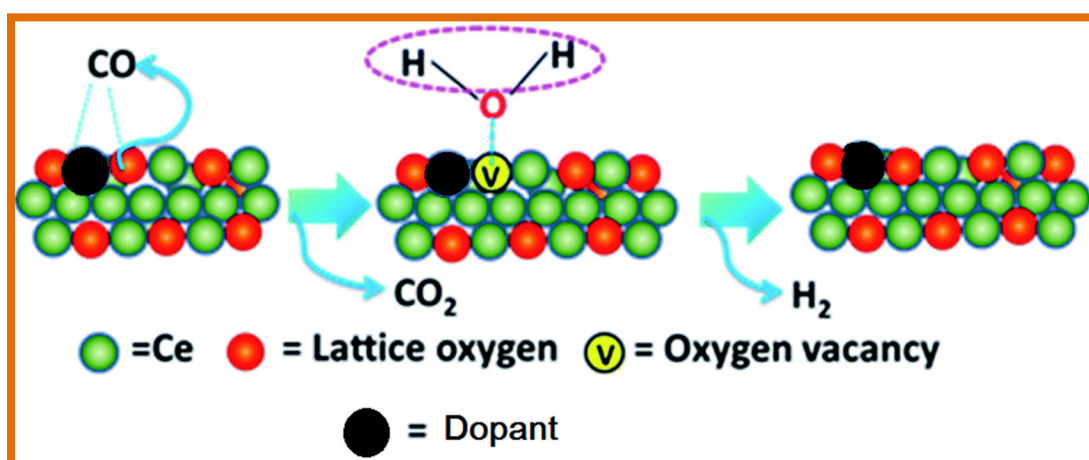
Figure 1.2:   CO oxidation and H_2O reduction over doped ceria [40]
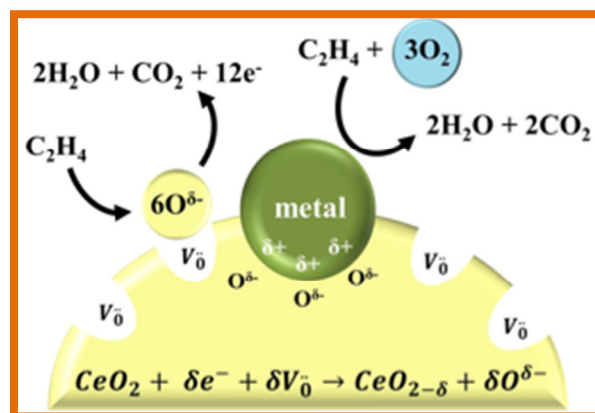
Figure 1.3:   Mechanism of conversion of HC's to H_2O and CO_2 over ceria. [41]

Formulation of TWCS is chiefly consisting of noble metals and their metal oxides which are dispersed over the pellets or the wash coat of alumina which is attached to the monolithic ceramic substrate. Monolith is designed in such a way to be resistant to thermal shocks because after ignition converter experiences a temperature increase up to 500 K within short interval duration. In order to maintain its catalytic property within this range of temperature, monolith should have a low thermal expansion coefficient.
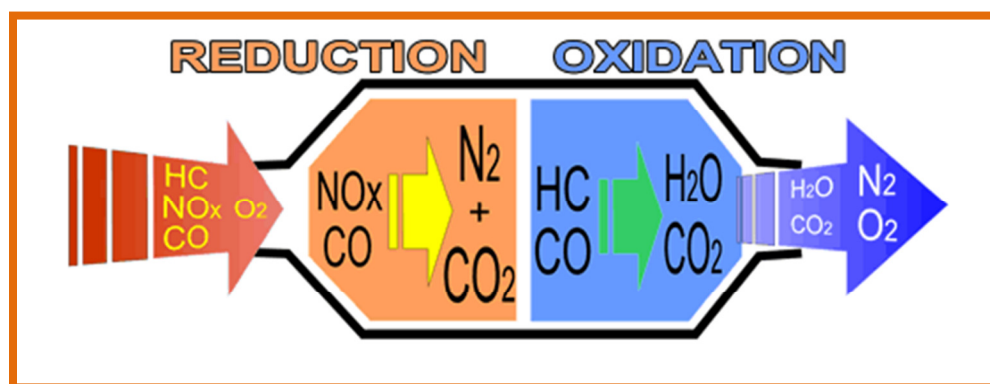
Figure 1.4:   Conversions taking place in TWC's.

For this reason the entire monolith is coated with solution of active metal salts, and its surface is deposited with alumina which has a great surface area with wash coat technique or slurry deposition.
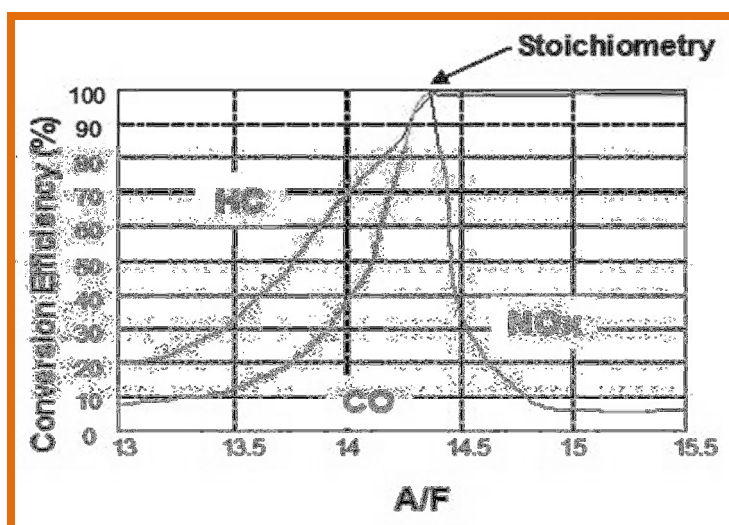
Figure 1.5:   Air-Fuel Ratio in TWC's

Higher rate of conversion of harmful pollutants is observed only when A/F ratio is approximately 14.6 which fall in the range named "window", during this conversion no pollutant falls below to the required value. But in reality, the exposed feed stream composition constantly varies from oxygen excess stoichiometry to oxygen deficient stoichiometry, results in decrease of catalytic efficiency of TWC's. Incorporating ceria in TWCS has many advantages, because of its ability to reduce to several $CeO_2\text{-}M_xO_y$ stoichiometry's, on exposure to O_2 vacancies, due to $Ce^{3+} \leftrightarrow Ce^{4+}$ redox couple.
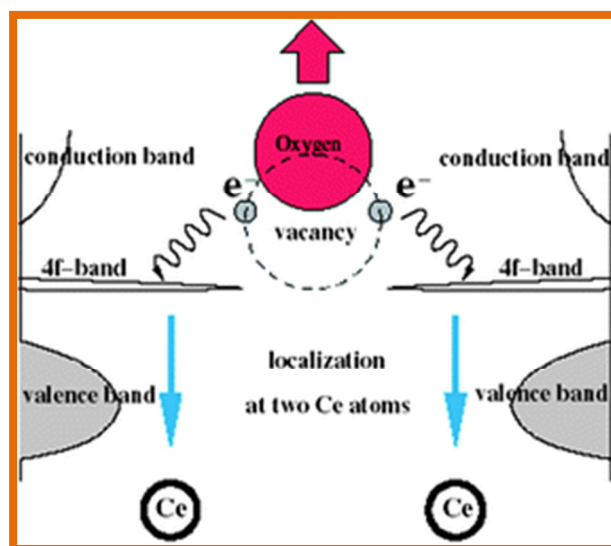
Figure 1.6:   Process of oxygen vacancy formation [42]

Below equations provide the information related to chemistry of ceria involved, `when passed over the exhaust feed stream:

i. CeO_2 + x CO → CeO_2-x   + xCO_2

ii. CeO_2 + CxHy → CeO_2-(2x+0.5y) + xCO_2 + $0.5yH_2O$
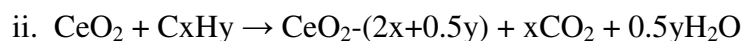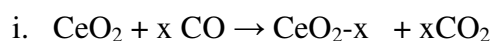
   (Lattice oxygen is involved in the above oxidation process)

iii. CeO_2 + x H_2 → CeO_{2-x} + x H_2O (Pt and Pd is involved in this reduction process)

iv. CeO_{2-x} + x NO → CeO_2 + $0.5xN_2$ (NO reduced to N_2 liberates the O_2 back to Ce lattice)

v. CeO_{2-x} + xH_2O → CeO_2 + xH_2 (Reduction reaction)

vi. CeO_{2-x} + $0.5xO_2$ → CeO_2 (Oxidation reaction)
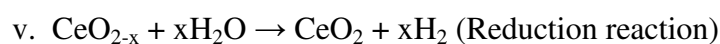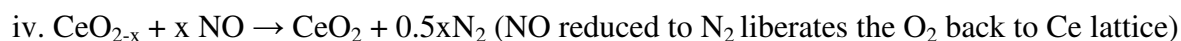
Reactions i-iii denotes ability of ceria to release the O_2 required for the conversions of carbon monoxide and hydrocarbons in the O_2 deficit part of cycle, while adsorption and storage of O_2 takes place in reactions iv – vi, This is the extra ordinary Oxygen Storage Capacity of CeO_2 which was reported by Gandhi et. al. [43] with specific and subtle balance between many factors namely, [44, 45] phase formation, rate of redox activity of $Ce^{+4/+3}$, presence of Ce^{3+} and Ce^{4+} ions on surface.

Various catalysts being profited from the use of ceria is also increasing, with further development in catalytic systems as combustion and oxidation catalysts [37, 38]. Oxidation capabilities completely depend on the redox couple of cerium and their high labile nature, which made these materials more interesting to use them in different catalysts having bio applications. To optimize or improve these material properties, study of complete nano particulate structural information of ceria and its mixed oxides and their relations helps in designing the multi component catalytic systems.

1.5   Defect Chemistry of Cerium Dioxide

Defect chemistry has got its own significance in the recent years as there is increased catalytic activity observed for modified ceria catalysts specially when doped with transition metal oxides and lanthanide oxides [46, 47]. When a M^{3+} cation is doped into the crystal lattice of ceria, it is neutralized by the negative ion (A^-) vacancies created in the lattice in general. Dopant cations are associated with the random distribution over the vacancies present within the crystal fluorite structure. This is considered to be thermodynamically significant defect mechanism where additional defects possible occur as minor species [48]. The intrinsic oxygen vacancies found for nano ceria has the experimental evidence [49]. These possible interstitial defects might be from thermal disorders or the interactions of solid to surrounded atmosphere on surface of ceria. Extrinsic defects are resulted when doped with impurities or aliovalent species. So, two types of defects observed with ceria, are intrinsic as well as extrinsic. The possible intrinsic defects from thermal disorders which do not involve gas phase during exchange. These

defects are Schottky, Frenkel defects and the equations are shown in 1.3, 1.4, 1.5 respectively [23].
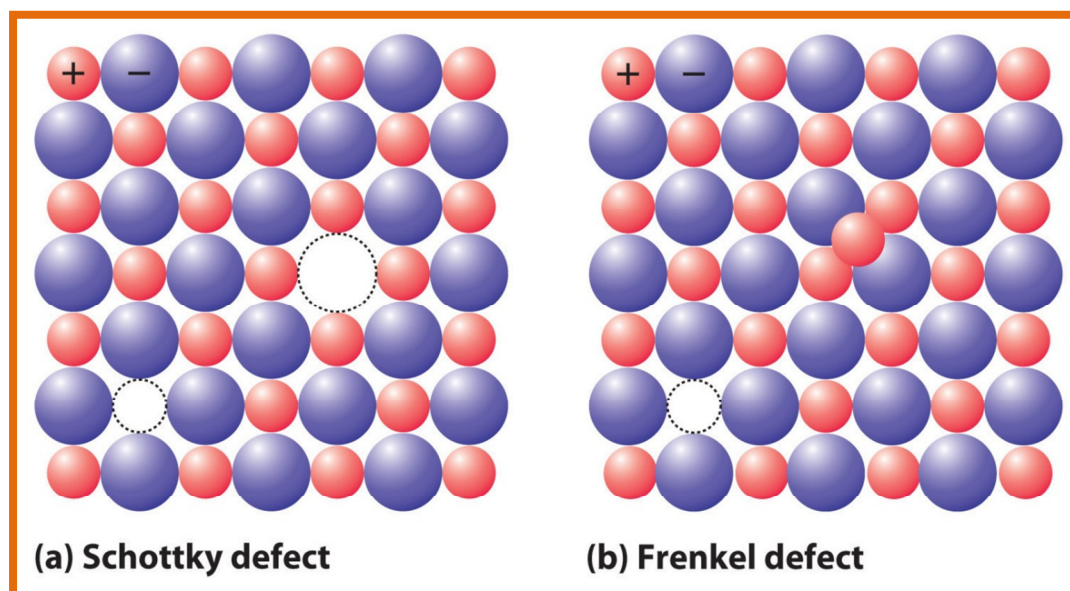
Figure 1.7:   Displays Schottky and Frenkel defects in crystal lattice

- When an atom migrates from its original site to the crystal surface creates a Schottky defect.
- When an atom migrates from its original site and resides in the interstitial site creates a Frenkel defect.
- Kroger and Vink defect notation is used to represent the above described defects as below:

$$CeCe + 2OO \leftrightarrow V''''Ce + 2VO + CeO_2 ....eq(1.3)$$
$$CeCe \leftrightarrow Cei.... + V''''Ce...................................eq(1.4)$$
$$OO \leftrightarrow Oi'' + V\ddot{O}...eq(1.5)$$
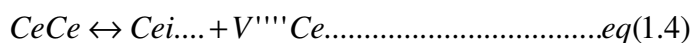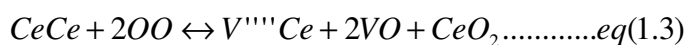
CeCe, OO, VO, Cei...., V'''' denotes cerium at a cerium site, oxygen at an oxygen site, vacancy at an oxygen site, the e- number, positive charge respectively.

The above equations indicate the formation of oxygen vacancies as well as the oxygen interstitial sites. When a reducing gas is passed over it, leads to an increase in concentration of those defects. After completion of reduction, excessive ceria left over compared to the anions resulting in a C+/A- ratio >0.5. Using two standard ways we can accommodate this difference. Oxygen vacancies compensate the holes resulted from reduction of Ce^{4+} to Ce^{3+}, followed by removal of O_2 ends up with +ve charge on crystal, to maintain the neutrality of crystal, 2 e's for each O_2 escaped is added. Anion vacancies present in the crystal will accompany the increase in lattice parameter of ceria. This is resulted from the large size of Ce^{3+} ion, and there occurs and expansion in lattice size, which was discussed in upcoming chapters, how Ce^{3+} ion influence the increase in lattice parameter of ceria and mixed oxides.

1.6   Doping in Ceria Lattice

Catalytic activity of ceria can be increased by doping with other metals [50, 51, 52]. Even after doping with higher concentration of metals, ceria based mixed oxides restore the fluorite crystal structure, mainly the sub-lattice of cation. By doping the metals in ceria, we can increase the physiochemical properties of ceria, such as increase in the thermal stability of the catalytic system and favor the transportation of O_2 leading to Ce^{3+} to Ce^{4+} conversions and vice versa. These doped ceria nano particles play an active role in catalysts for water gas shifts and SO_2 destruction [23, 49]. This is obtained by dispersion of noble metals, but the mechanism is not completely known [53, 54, 55]. However these doped catalysts preparation requires high cost estimation. To replace these noble metals the present studies over doping of ceria is continued with various transition metals and inner transition metals.

Two physiochemical properties of ceria based mixed oxides plays a vital role in deciding the effectiveness of catalyst. Those include the local M-O bonds, and distance between them, and the paths involved to attain the charge neutrality of the crystal lattice. In the ceria case it is principally through the number of oxygen vacancies present. For using these doped ceria based oxides at higher temperatures, we need to obtain a dopant metal

which can successfully create a large number of oxygen vacancies required in the ceria lattice [56]. The data collected from literature, clearly states that on doping ceria, in most cases thermal stability is increased for ceria based oxide when compared to pure ceria. These two properties discussed above depend on the various factors and are studied using different spectroscopic and non-spectroscopic characterization techniques.

1.7   Preparation methods of Nano Ceria and Mixed oxides of Ceria:

The production of nano ceria and ceria based mixed oxides can be achieved by various physical and chemical methods available such as precipitation method, Sol-gel method, hydrothermal method, combustion synthesis, ball milling, flame spray pyrolysis, chemical vapor deposition, electro-chemical deposition, microwave-assisted combustion synthesis etc., Both the surface and bulk phenomenon can be prone to change with the synthetic methodology adopted. Among the different preparation methods microwave assisted combustion synthesis [MWCS] has gained a superior role in the synthesis of metal oxides with intriguing properties. This method can be considered as one of the green methods as it obeys the principles of green chemistry.

Solution Combustion synthesis (CS) is a one of the chemical methods that has been employed for producing the inter-metallics, alloys, metal oxides and mixed metal oxides [57-60]. The main reason is established from its characteristic saving of intrinsic energy; since much of the energy required during the CS synthesis is released from the reaction being carried out. Certainly, CS method uses the benefit from exothermic reactions resulted. When precursors and fuel are kept together as reactants, they start reacting in a profitable manner after exposure to suitable ignition, therefore no further requirement of energy from the outside source, because by controlling and making use of the produced heat by the resulted reaction, facilitates the completion of reaction acting as a driving force for the reaction throughout the process. So, in the combustion synthesis we need to heat the solution to attain the combustion between the metal precursors and fuel.

For the most combustion synthesis conventional heating sources such as hot plates, muffle furnaces etc. are employed. Recently microwave heating has gained lots of interest in the synthesis of materials. The microwave heating can be coupled with combustion synthesis instead of conventional heating source as it heats the reactants uniformly without any thermal gradients. This in turn results in the modified properties of the oxide material than conventional combustion synthesis.

There are many benefits associated with the microwave-assisted synthesis [61] while compared to conventional heating synthesis and are listed below point by point.

o   There is an enormous benefit in time saving which plays a key role for the industrial people where they will perform number reactions in different strategies for the development of drugs.

o   Second thing most important concern devoted to the green technology is the most energy efficient way and intern relates to the economic issue.

o   Another green avenue is the use of environmentally benign solvents such as water and ionic liquids.

o   The synthetic methods were reproducible and reliable and often associated with the dedicated microwave reactors.

o   Uniform heating of the material without super facial heating unlike in conventional heating and it is very crucial for Nanomaterial synthesis

o   Microwave induced synthesis can be coupled with many more chemical synthetic routes for the materials synthesis such as Microwave assisted sol-gel, Microwave assisted hydrothermal/Solvo-thermal, Microwave assisted combustion.

o   Heating was achieved without contact between the source and the sample.

o   Microwave heating is very quick in heating and cooling the materials when the microwave power is on and off respectively.

Therefore, accompanying microwave heating with solution combustion synthesis, we can attain the complete advantages from microwave assisted synthesis as well as solution combustion synthesis, there by naming it as microwave-assisted solution combustion synthesis (MWCS). A very few literature reports were present on the microwave assisted combustion synthesis compared with conventional combustion synthesis.

1.7.1   Microwave-Assisted Combustion Synthesis (MWCS)

If microwave dielectric heating is used to initiate the solution combustion synthesis, while preparation of ceria and its oxides, the process is termed as microwave-assisted combustion synthesis.

MWCS typically involves combustion of metal precursors and fuel in a microwave oven. The choice of fuel depends on the material, which we have to prepare. In the present investigation urea was used as a fuel due to its availability and high exothermicity.

MWCS has its own advantages over other synthetic preparation methods of ceria and its oxides. Few of them are listed below:

- Preparation method uses relatively a simple instrument
- Purity of the products obtained is comparatively high
- Heating rates are relatively high
- Control over heat supply
- saves the energy
- Very easy to control reaction
- improved chemical reactivity
- Cost effective and involves green chemistry

Figure 1.8:   **Combustion reaction performed in microwave oven during the preparation of catalysts.**

MWCS usually takes place by combustion of fuel and metal precursors in a microwave oven. Precursors used while preparations are metal nitrates, since nitrates support combustion reaction. Choice of fuel depends on the product to be prepared. During the present investigations being carried out, urea is used as fuel because of its high availability and exothermicity. Hence, the energy outcome is very high during the MWCS.

Ratio of fuel to precursor plays a vital role in the MWCS, and this is calculated from total number of oxidizing and reducing valences present in fuel component and precursors. In general the oxidizing valencies and reducing valencies are the numerical coefficients obtained from the stoichiometric balance of the chemical reaction. Hence, the ratio will be equivalent to unity.

1.8 **Genesis of Present Investigation**

In recent times, air pollution is being one of the major problems reported globally. Exhaust gas from automobiles is being the major cause for air pollution. Therefore treating exhaust gas of automobiles is necessary and development of TWC to transform hazardous gases such as CO, NO_x and hydrocarbons to less hazardous gases or environmental friendly gases has become one of the interesting topics of research. The research and development activities were concerned with development of catalysts which have higher thermal stability along with the good activity and selectivity. There are various metals and metal oxides, which shown the activity in reducing the CO concentration levels [62]. Synthesis and design of new catalysts for the CO oxidation plays a significant role in the field of heterogeneous catalysis due to the stringent environmental conditions laid down during the past several years [63].

Among the various metal oxides screened cerium dioxide CeO_2, a known rare-earth oxide has found to be great importance in the field of catalysis and is most important catalyst in particular to CO oxidation [64, 65]. Ceria is the main ingredient present in formulation of TWC [66-68], because of its ability to play an important role in oxygen storage and release by filling and releasing oxygen from oxygen vacancies under oxygen rich (oxidizing) and oxygen poor (reducing) conditions respectively to stabilize air to fuel oxygen ratio at desired levels [68]. This is due to its rapid change in the valence state from +4 to +3 and vice versa depends on the surrounding atmosphere with the formation of oxygen vacancies [64, 65].

Even though extensive studies are conducted on ceria, many of the physio-chemical properties get affected under elevated temperatures [69, 70]. As the temperature increases the nanoparticles will form aggregates and leads to the formation of bulk particles [71]. Hence at elevated conditions ceria loses its intriguing properties such as surface area, oxygen storage capacity, etc. There could be an alternative way to avoid this drawback. One such could be modifying the ceria by doping with other metal ions.

Modifications of ceria solid solutions are to develop an efficient catalyst formulation for treating the exhaust gas from automobiles and few more applications. Besides, there are a wide range of bio applications and technological applications those are benefited from this unique redox properties and transportation properties of ceria and ceria-based oxide materials [72, 73, 74-76].

Doping ceria with other metals, increases surface area and sustain towards sintering on exposure to higher temperatures for a longer duration, because of mixed oxide cations co-operation [77, 78]. Ceria has been doped using a wide range of variable and invariable cations (transition and rare earth metal cations), since the host lattice is compatible to different types of substitutions. Here the metal cation doped plays a vital role in modification of physiochemical properties of mixed oxide produced. Oxidation state of doped metal ion is the deciding factor of oxygen vacancies concentration present in mixed oxide produced, and energy of association between doped ion and oxygen vacancy decides the mobility of oxide ions / oxygen vacancies.

Motivated by the unique and favourable characteristics of ceria–based materials for various catalytic applications, a systematic and comprehensive investigation was undertaken against the above background. In this present investigation, a various combination of ceria based oxides such as CuO promoted CeO_2-M_xO_y (M = Zr, La, Pr and Sm) catalysts and transition metal doped ceria (CeO_2-M_xO_y (M = Mn, Fe, Co)) and ceria–samarium (CeO_2-Sm_2O_3; 8:2 based on molar ratio) mixed oxide composites possessing high specific surface area, better thermal stability, superior sintering resistance, and desired redox properties have been synthesized

CO oxidation studies are carried over CeO_2, CeO_2–ZrO_2, CeO_2–La_2O_3, CeO_2–Pr_2O_3, CeO_2–Sm_2O_3, prepared from different methods. But lower temperature CO oxidation studies have their own significance. To analyze those studies, 5 Wt. % CuO is supported to the above catalysts [CuO/ CeO_2, CuO/ CeO_2–ZrO_2, CuO/ CeO_2–La_2O_3, CuO/ CeO_2–Pr_2O_3, CuO/ CeO_2–Sm_2O_3]. Synthesized the copper supported ceria and its oxides by MWCS and taken for the lower Temperature CO oxidation activity.

Mixed oxides of ceria are responsible for the incredible attention on TWC's. However, ceria and its oxides are the main composition of the formulation present in TWC's. Most of the research studies are mainly concentrated on CO oxidation studies of transition metal doped ceria oxides, as they are cost effective. But very few studied using microwave-assisted combustion synthesis. Hence, synthesized CeO_2-M_xO_y (M=Fe, Co, Mn)**,** ratio of ceria to metal is (7:3) by MWCS and characterized by various spectroscopic and non-spectroscopic techniques followed by oxygen storage activity and CO oxidation activity studies were carried out on the as-synthesized catalysts and correlated to pure ceria.

Oxygen vacancies developed in the lattice structure plays an important role in the OSC capacity as well as CO oxidation activity. In order to study the OSC capacity and CO oxidation activity of ball milled catalysts prepared from MWCS, we prepared CeO_2 and $CeO_2-Sm_2O_3$ (8:2) using MWCS method to prepare the samples and bill mill is applied over and a comparative study is conducted on the samples before to and after ball mill method over the as-synthesized catalysts from MWCS.

.1.9   Aims and Objectives of the Thesis

The main objective of the present project is to prepare ceria and its oxides by microwave-assisted solution combustion synthesis and study the CO oxidation activity.

Physiochemical characterization and evaluation of the prepared oxides is performed by various spectroscopic techniques and non-spectroscopic techniques. Investigations to be carried out to obtain the correlation between the pure ceria and its oxides are as follows:

Investigating the control of dopants over the redox properties of ceria and stability of defects present in the solid solutions

Evaluating the OSC properties of the solid solutions synthesized and the Catalytic activity studies by performing CO oxidation reaction

Present investigations also involve the study of changes in physiochemical properties of mixed oxides of ceria and doped ceria on correlation with pure ceria. Changes in physiochemical properties are as follows: improved redox properties there by enhanced BET surface area, thermal stability, OSC, sustained towards sintering, and better CO oxidation.

In the present project, the CeO_2 and its oxides are prepared by MWCS and the as-synthesized CeO_2 and modified ceria catalysts are subjected to evaluation by XRD, UV-Vis, BET Method, H_2-TPR, XPS to study the modified physiochemical properties, and CO oxidation activity.

1.10 References:

[1] C. Noguera, Physics and Chemistry at Oxide Surfaces; Cambridge University Press: Cambridge, UK, 1996.

[2] H.H. Kung, Transition Metal Oxides: Surface Chemistry and Catalysis; Elsevier: Amsterdam, 1989.

[3] V.E. Henrich, P.A. Cox, The Surface Chemistry of Metal Oxides; Cambridge University Press: Cambridge, UK, 1994.

[4] A.F. Wells, Structural Inorganic Chemistry, 6th ed; Oxford University Press: New York, 1987.

[5] W.A. Harrison, Electronic Structure and the Properties of Solids; Dover: New York, 1989.

[6] M. Fernández-García, A. Martínez-Arias, J.C. Hanson, J.A. Rodríguez, Chem. Rev. 104 (2004) 4063.

[7] A. Bruckner, Catal. Rev. Sci. Eng. 45 (2003) 97.

[8] B.M. Reddy, In Metal Oxides: Chemistry and Applications; J.L.G. Fierro, CRC Press, Taylor and Francis Group: Boca Raton, FL, chapter 8, 2006, 215.

[9] G. Ertl, H. Knozinger, J. Weitkamp (Editors), Handbook of Heterogeneous Catalysis; Wiley-VHC: Weinheim, 1997.

[10]   A. Trovarelli, C. de Leiterburg, M. Boaro, G. Dolcetti, 1 Catal. Today, 50 (1999) 173.

[11]   D. Waller, J.A. Lane, J.A. Kilner, B.C.H. Steele, Solid State Ion. 86 (1996) 767 and references therein.

[12]   T.S. Stefanik, H.L. Tuller, J. Eur. Ceram. Soc. 21 (2001) 1967.

[13]   A. Tsoga, A. Gupta, A. Naoumidis, P. Nikolopoulos, Acta. Mater. 48 (2000) 4709.

[14]   B.C. Morris, W.R. Flavell, W.C. Mackrodt, M.A. Morris, J. Mat. Chem. 3 (1993) 1007.

[15]   E.A. Kummerle, G. Heger, J. Sol. State Chem. 147 (1999) 485.

[16]   W.M. O'Neill, M.A. Morris, Chem. Phys. Lett. 305 (1999) 389

[17]   F. Esch, S. Fabris, L. Zhou, T. Montini, C. Africh, P. Fornasiero, G. Comelli, R. Posei, Science, 309 (2005) 752.

[18]   Y. Namia, K.I. Fukai, Y. Iwasawa, Catal. Today, 85 (2003) 79.

[19]   P. Fornasiero, R. di Monte, G.R. Rao, J. Kaspan, S. Meriani, A. Trovarelli, M. Grazizni, J. Catal. 151 (1995) 168.

[20]   C.W. Mays, J. S. Vermaak, D.K. Wilsdorf, Surf. Sci. 12 (1968) 134.

[21]   S. Tsunekawa, R. Sahara, Y. Kawazoe, K. Ishikawa, 1999, Appl. Surf. Sci. 152 (1999) 53.

[22]   P. Li, I.W. Chen, J.E. Penner-Hahn, T.Y. Tien, J. Am. Ceram. Soc. 74 (1991) 958.

[23]   A. Trovarelli, Catal. Rev. Sci. Eng. 38 (1996) 439.

[24]   M. Ricken, J. Nolting, I. Reiss, J. Solid State Chem. 54 (1984) 89.

[25]   R. Korner, M. Ricken, J. Nolting, I. Reiss, J. Solid Chem. 78 (1989) 136.

[26]   O.T. Sorenson, (ed.). Non-Stoichiometric Oxides, Academic Press, New York, 1981.

[27]   A. Laachir, V. Perichon, A. Badri, J. Lamotte, J. Chem. Soc. Faraday Trans. 87 (1991) 1601.

[28]   A. Badri, J. Lamotte, A. Laachir, V. Perichon, Eur. J. Solid State Inorg. Chem. 28 (1991) 445.

[29]   J. L. Duplan, H. Praliand, Appl. Catal. 67 (1991) 325.

[30]   H.C. Yao, Y.F.Y. Yao, J. Catal. 89 (1984) 254.

[31]   M.F.L. Johnson, J. Mooi, J. Catal. 103 (1987) 502.

[32]   C. Padeste, N.W. Cant, L. Trimm, Catal. Lett. 18 (1993) 305.

[33]   B. Harrison, A. F. Diwell, C. Hallett, Platinum Metals Rev. 32 (1988) 73.

[34]   ETC Group, Occasional Paper Series, 1 (2003) 7.

[35]   S. Bernal, F. Blanco, J. Botana, J. M. Gatica, J. A. Perez Omil, J. Alloys & Cmpds. 207 (1994) 196.

[36]   A.D Logan, M. Shelef, J. Mater. Res. 9 (1994) 468.

[37]   W.C. Mackrodt, M. Fowles, M.A. Morris, Euro. Pat 913716.5 (1991)

[38]   F. Zamar, A. Trovarelli, C. de Leitenburg, G. DolcettI, J. Chem. Soc. Chem Com. (1995) 965.

[39]   A. Trovarelli, M. Boaro, E. Rocchini, C.de Leitenburg, G. Dolcetti, J. Alloys & Cmpds. 323-324 (2001) 584.

[40]   A. Jha, D.-W. Jeong, Y.-L. Lee, I.W. Nah, H.-S. Roh, RSC Adv. 5 (2015) 103023.

[41]   H.A.E. Dole, E.A. Baranova, Chem Cat Chem. 8 (2016) 1977.

[42]   C. Sun, H. Li, L. Chen, Energy Environ. Sci. 5 (2012) 8475.

[43]   H.S. Gandhi, A.G. Piken, M. Shelef, R.G. Delossh, SAE 163 (1976) 760201.

[44]   J. Kaspar, P. Fornasiero, M. Graziani, Catal Today, 50 (1999) 285.

[45]   K.C. Taylor, J.R. Anderson, M. Boudart, Catalysis Science & Technology, Springer, Berlin, 5 (1984) 120.

[46]   T.J. Treux, at al in "Catalysis and Automotive Pollution Control", Elsevier, Amsterdam 77 (2) (1991) 175.

[47]   M. Breysse, M. Guenin, B. Claudel, J. Veron, J. Catal. 28 (1973) 54.

[48]   L. Minervini, M.O. Zacate, R.W. Grimes, Solid State Ion. 116 (1999) 339.

[49]   E. Mamontov, T. Egami, J. Phys. Chem. Solids, 61 (2000) 1345.

[50]   Q. Fu, H. Saltsburg, M. Flytzani-Stephanopoulous, Science, 301 (2003) 935.

[51]   M. Fernaandez-Garcia, A. Martinez-Arias, A. Guerrero-Ruiz, J.C. Conesa, J. Soria, J. Catal. 211 (2002) 326.

[52]   G. Vlaic, R. Di Monte, P. Fornasiero, E. Fonda, J. Kaspar, M. Graziani, J. Catal. 182 (1999) 378.

[53]   W. Liu, C. Wadia, M. Flytzani-Stephanopoulos, Catal. Today, 28 (1996) 391.

[54]   J.A. Rodriguez, T. Jirsak, A. Freitag, J.C. Hanson, J.Z. Larese, S. Chaturvedi, Catal. Lett. 62 (1999) 113.

[55]   Q. Fu, A. Weber, M. Flytzani-Stephanopoulos, Catal. Lett. 77 (2001) 87.

[56]   K. Schermanz, in Catalysis by Ceria and Related Materials; Trovarelli, A., Ed.; World Scientific: London; Chapter 1, 2002.

[57]   C. Aliotta, L.F. Liotta, V. La Parola, A. Martorana, E.N.S Muccillo, R. Muccillo, F. Deganello, Appl. Catal. B: Environ. 197 (2016) 14.

[58]   A. Varma, A.S. Mukasyan, A.S. Rogachev, K.V. Manukyan, Chem. Rev. 116 (2016) 14493.

[59]   F.T. Li, J. Ran, M. Jaroniec, S.Z. Qiao, Nanoscale, 7 (2015) 17590.

[60]   K. Rajeshwar, N.R. de Tacconi, Chem. Soc. Rev.38 (2009) 1984.

[61]   L.H. Reddy, D.Devaiah, B.M. Reddy, Microwave Assisted Synthesis: A Versatile Tool for Process Intensification: In Industrial Catalysis and Separations: Innovations for Process Intensification, Eds., K V Raghavan, B M Reddy, AAP/CRC Press, NJ, USA, Chapter 10, 2014, pp. 375 – 405.

[62]   D. Mukherjee, B. Govinda Rao, B.M. Reddy Appl. Catal. B: Environ. 197 (2016) 105.

[63]   P. Venkataswamy, K.N. Rao, D. Jampaiah, B.M. Reddy, Appl. Catal. B: Environ. 162 (2015) 122.

[64]   G. Dutta, U.V. Waghmare, T. Baidya, M.S. Hegde, K.R. Priolkar, P.R. Sarode, Chem. Mater. 18 (2006) 3249.

[65]   K. Mudiyanselage, H.Y. Kim, S.D. Senanayake, A.E. Baber, P. Liub, D. Stacchiola, Phys. Chem. Chem. Phys. 15 (2013) 15856.

[66]   Q. Fu, H. Saltsburg, M.F. Stephanopoulos, Science, 301 (2003) 935.

[67]   B.C.H. Steele, A. Heinzel, Nature, 414 (2001) 345.

[68]   A. Trovarelli, in: Catalysis by Ceria and Related Materials, Catalytic Science Series, Hutchings, G. J. Ed., Imperial College Press, London, vol. 2, 2002.

[69]   T. Masui, Y. Peng, K.I. Machida, G.Y. Adachi, Chem. Mater. 10 (1998) 4005.

[70]   H. Li, L. Zhang, H. Dai, H. He, Inorg. Chem. 48 (2009) 4421.

[71]   B.M. Reddy, G. Thrimurthulu, L. Katta, J. Phys. Chem. C 113 (2009) 15882.

[72]   M. Machida, Y. Murata, K. Kishikawa, D. Zhang, K. Ikeue, Chem. Mater. 20 (2008) 4489.

[73]   B.M. Reddy, P. Bharali, P. Saikia, S.E. Park, M.W.E. van den Berg, M. Muhler, W. Grunert, J. Phys. Chem. C 112 (2008) 11729.

[74]   K.J.D. Vries, G.Y. Meng, Mater. Res. Bull. 33 (1998) 357.

[75]   A.M. Arias, A.B. Hungria, M.F. Garcia, A.I. Juez, J.C. Conesa, G.C. Mather, G. Munuera, J. Power Sources, 151 (2005) 43.

[76]   J. Chen, S. Patil, S. Seal, J.F. Mc Ginnis, Nat. Nanotech. 1 (2006) 142.

[77]   R. Wang, P.A. Crozier, R. Sharma, J.B. Adams, J. Phys. Chem. B 110 (2006) 18278.

[78]   X. Wang, J.C. Hanson, G. Liu, J.A. Rodriguez, J. Chem. Phys. 121 (2004) 5434.

CHAPTER 2

PREPARATIONS AND CHARACTERIZATION TECHNIQUES

2.1 Preparation of catalysts

2.1.1 Preparation of 5 wt % CuO/ CeO$_2$–M$_x$O$_y$ (8:2 based on oxide ratio; M$_x$O$_y$ = La$_2$O$_3$, Pr$_2$O$_3$ and Sm$_2$O$_3$) Solid Solutions.

The following copper oxide promoted metal doped ceria catalytic formulations were synthesized in this investigation.

$$5 \text{ wt \% CuO/ CeO}_2 \qquad \text{(CC)}$$
$$5 \text{ wt \% CuO/ CeO}_2\text{–ZrO}_2 \quad \text{(CCZ)}$$
$$5 \text{ wt \% CuO/ CeO}_2\text{–La}_2\text{O}_3 \quad \text{(CCL)}$$
$$5 \text{ wt \% CuO/ CeO}_2\text{–Pr}_2\text{O}_3 \quad \text{(CCP)}$$
$$5 \text{ wt \% CuO/ CeO}_2\text{–Sm}_2\text{O}_3 \quad \text{(CCS)}$$

Preparation of 5 wt % CuO/ CeO$_2$–M$_x$O$_y$ (8:2 based on oxide ratio; M$_x$O$_y$ = La$_2$O$_3$, Pr$_2$O$_3$ and Sm$_2$O$_3$) and 5 wt % CuO/ CeO$_2$–ZrO$_2$ (1:1 based on oxide ratio) by microwave-assisted solution combustion synthesis (MWCS) for CO oxidation. The precursors used for synthesizing the above catalytic formulations are Cerium(III) nitrate hexa hydrate [(Ce(NO$_3$)$_3$· 6H$_2$O) (Aldrich, 99%)], zirconium(IV) oxy nitrate hydrate [(ZrO(NO$_3$)$_2$.XH$_2$O) (Aldrich, 99%)], lanthanum(III) nitrate hexa hydrate [(La(NO$_3$)$_3$·6H$_2$O) (Aldrich, 99%)], Samarium(III) nitrate hexa hydrate [(Sm(NO$_3$)$_3$·6H$_2$O), (Aldrich, 99%)], Praseodymium(III) nitrate hexa hydrate [(Pr(NO$_3$)$_3$·6H$_2$O), (Aldrich 99%)] and solid urea (300 Fluka, AR grade) are used directly without any further purification. All the metal precursors used are metal nitrates because they favor the combustion synthesis. In this procedure to synthesize 5 wt % Cu /CeO$_2$–ZrO$_2$, the required amount of the corresponding precursors (metal nitrates) taken in a pyrex dish and dissolved in deionized water separately and mixed all the above solutions. The required stoichiometric quantity of urea (considered from propellant chemistry) (1,2) is used for the

preparation of above solution, mixed thoroughly to obtain a homogenous solution at ambient conditions. We have adopted the microwave oven used for domestic purpose, modified with an outlet for exhaust gases (BPL, India Limited, 2.54 GHz, BMO-700T, 700 W). This modified oven is used as a heating source to initiate combustion between metal nitrates and urea. The dish containing the metal precursors and urea was introduced into the center of microwave oven and was operated. Initially, the solution boils with slow removal of water from the system followed by decomposition and spontaneous combustion synthesis leading to the flame generation for a short time. Along with the flame there occurs liberation of gases such as N_2, CO_2, H_2O, NH_3 and NO_2 resulting the light yellow solid material. The resultant powders were grinded for 10 min with mortar and pestle in order to get the homogenous powder form. The obtained catalyst was named as CCZ. Similarly all other catalytic materials were prepared in the same manner.

2.1.2 Preparation of CeO_2-MO_x (7:3 based on oxide ratio; M=Fe, Co, Mn) Solid Solutions

The following transition metal doped ceria samples were synthesized by using MWCS and for the purpose of comparison of physiochemical properties pure ceria is also synthesized.

$$CeO_2 \qquad (MC)$$
$$CeO_2-MnO_2 \quad (MCM)$$
$$CeO_2-Fe_2O_3 \quad (MCF)$$
$$CeO_2-Co_2O_3 \quad (MCC)$$
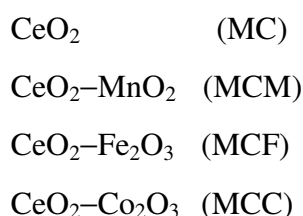
The precursors used for the preparation of above catalysts are Cerium (III) nitrate hexa hydrate [$(Ce(NO_3)_3 \cdot 6H_2O)$, (Aldrich, 99%)], Manganese (II) nitrate tetra hydrate [$(Mn(NO_3)_2 \cdot 4H_2O)$, (Merck, AR grade)], Iron (III) nitrate nonahydrate [$(Fe(NO_3)_3 \cdot 9H_2O)$, (Aldrich, AR grade)] and cobalt (II) nitrate hexahydrate [$(Co(NO_3)_2 \cdot 6H_2O)$, (Aldrich, AR grade) materials. The required quantity of metal precursors and the urea is dissolved in water and remaining process is the same as above discussed in 2.1.1.

2.1.3   Preparation of CeO_2 and CeO_2–Sm_2O_3 (8:2 based on oxide ratio)

The following pure ceria and samarium doped ceria samples were synthesized for the purpose of comparison of physiochemical properties.

CeO_2	(MC)
CeO_2– Sm_2O_3	(MCS)
Ball milled CeO_2	(MCB)
Ball milled CeO_2– Sm_2O_3	(MCSB)

The precursors used for synthesizing the CeO_2 and CeO_2–Sm_2O_3 catalytic formulations are Cerium (III) nitrate hexa hydrate [($Ce(NO_3)_3 \cdot 6H_2O$), (Aldrich, 99%)], Samarium(III) nitrate hexa hydrate [($Sm(NO_3)_3 \cdot 6H_2O$), (Aldrich, 99%)].

Here, the MWCS procedure was employed for the preparation of pure ceria (MC) and CeO_2–Sm_2O_3 (8:2 based on oxide ratio) (MCS). The synthesis procedure is same as outlined in section 2.1.1. Further, ball mill procedure is applied over as synthesized catalysts obtained from MWCS in order to study the changes in physiochemical properties. For this a bench top FRITSCH Pulverisette 7 planetary Micro Mill was used to perform the ball mill procedure over obtained catalysts from MWCS.

The obtained materials in the MWCS were dried at 383 K for 5 hrs in order to remove the moisture content adsorbed on the catalysts. The dried powders are taken up for the processing by ball mill method. The mass ratio between the ball and powder was maintained at 10:1 with a running speed of 500 rpm for 2 hr. The grinding tools are made up of stainless steel.

The milling was carried out in 45 ml capacity bowl with the 5 mm balls. The as synthesized ball milled catalysts are considered for analysis, for handiness naming of catalysts is as MCB for ball milled-CeO_2, MCSB for ball milled-(CeO_2– Sm_2O_3).

2.2   Catalyst Characterization

Listed in table below are the following spectroscopic and non-spectroscopic characterization techniques employed on catalytic samples for investigation studies during the project:

S. No	Characterization Technique	Abbreviated
Non-Spectroscopic		
1.	Brunauer Emmett Teller Method	BET
2.	Thermal Analysis	TG/DTA
3.	H_2-Temperature Programmed Reduction	H_2-TPR
Spectroscopic		
4.	X-ray Diffraction	XRD
5.	UV-Vis Diffuse Reflectance	UV-vis DRS
6.	Laser Raman	LRS
7.	X-ray Photoelectron	XPS
8.	Fourier Transform Infrared	FTIR
9.	Scanning Electron Microscope	SEM

Table 2.1:   Displays the characterization techniques used for analysis of samples

2.2.1   Specific Surface Area: BET Method

During 1938, Stephen Brunauer, Paul Hugh Emmett, and Edward Teller have published BET theory as an article in a journal [3] for the first time; and given the name from initials of their last names. BET is a well-accepted method for the measurement of specific surface area through physical adsorption and desorption phenomenon of gases [4]. From this technique we can also investigate size distribution volume, and specific surface area of pores. For characterizing solid catalysts, two fundamental parameters namely pore size distribution and specific surface area are required. Specific surface area of solid sample in powdered form is measured from the mass of nitrogen adsorbed in correlation

with its pressure, at boiling temperature of liq. N_2 under standard atmospheric pressure. This N_2 gas is adsorbed at 77 K, and the variation in amount of N_2 gas absorbed varies with the applied pressure, as related in adsorption isotherm. Adsorption of gas over powdered solid surface is physisorption, used to compute total surface area and pore size of nano-porous, micro-porus particles. Langmuir theory is the theory for monolayer molecular adsorptions and multilayer molecular adsorptions [5, 6]. BET theory is said to be an extended addition over Langmuir theory. Amount of nitrogen adsorbed to a molecular monolayer on surface of catalyst is given as [7-9]:

$$\frac{P}{V_a(P_0 - P)}(y-component) = \frac{1}{V_m C}(c, \text{int} ercept) + \frac{C-1}{V_m C}(m, slope)\frac{P}{P_0}(x-component) \quad 2.1$$

Where,

P = pressure,

P_0 = saturation vapor pressure,

V_a = amount of gas adsorbed at the relative pressure P/P_0,

V_m = monolayer capacity, and

C = BET constant.

A plot drawn against y-component ($\frac{p}{V_a(p_0 - p)}$) and x-component ($\frac{p}{p_0}$) is a straight line

with slope and intercept values as $\frac{(C-1)}{V_m C}$ and $\frac{1}{V_m C}$, respectively. If the value of intercept

and slope is obtained from graph plotted, we can calculate the Vm. From which the specific surface area can be calculated using the formula as shown in equation 2.2.

$$\text{Specific Surface Area } (m^2 g^{-1}) = \frac{V_m * L * Am}{W * V_0} \quad 2.2$$

Where,

L = Avogadro constant (6.023 X 10^{23} molecules mol^{-1})

A_m = cross sectional area of N_2 molecule, 0.162 nm^2 at 77 K

W = Sample weighed

V_0 = 22414 mL mol^{-1}

In the present analysis, BET surface areas were determined using the following analyzer, micrometrics Gemini 2360 Instrument. Before we perform analysis, the samples were dried in an oven for 12 h at 393 K, followed by flushing with Argon gas for 2 h. All the Specific surface area values obtained while performing the analysis was measured is accurate within ± 5 %.

2.2.2 Thermal Analysis

Gain or loss in weight of sample reported as functions of temperature to be measured by thermogravimetry. In this analysis, mass of sample is continuously recorded against increase in temperature (ambient to high). Without any changes in magnitude of mass of sample this characterization technique cannot be studied. Three main factors to be noted while studying the TG curve: shape of the curve obtained, changes in mass of sample at a particular temperature, and change in magnitude of mass of sample. Differential thermo analysis, absorption and emission of heat by sample are recorded by measuring the temperature difference between sample and reference compounds as a function of increased temperature of both.

$$\Delta T = Ts - Tr \qquad 2.3$$

This is an appropriate technique to analyze solid-gas systems. Temperature as a main parameter involved with analysis of sample, hence the name thermal analysis. When particular substance is subjected to cooling or heating phenomenon, those result in physical and chemical changes of sample which comprises variations in mass of sample when subjected to different temperatures. In the present investigations we have adopted this technique for measuring the OSC of the catalysts.

Instrument is comprised with an ultra-sensitive weighing device, which enables to record small variations in mass of sample. All the TG-DTA values in this analysis were obtained on Mettler Toledo TG-DTA analyzer. During the procedure solids are heated in this range (RT to 1273 K) under a N_2 flow. Rate of heating is limited at 10 K/min during the complete analysis.

2.2.3 X-ray Diffraction Studies

X-ray diffraction (XRD) is an appropriate characterizing technique used to examine different bulk phases existed within the solid sample. X-rays of electromagnetic radiation are involved in penetration while analyzing the sample. These rays penetrate through material with an ease and their order of wavelengths are similar to inter-atomic distance values. Thus, according to Bragg's law, crystalline phases present in sample diffract the collimated beam of X-rays [10-12]. Diffraction profiles of powdered solid are obtained by measuring the angle at which the sample diffracts the X-ray beam wavelength 'λ'.
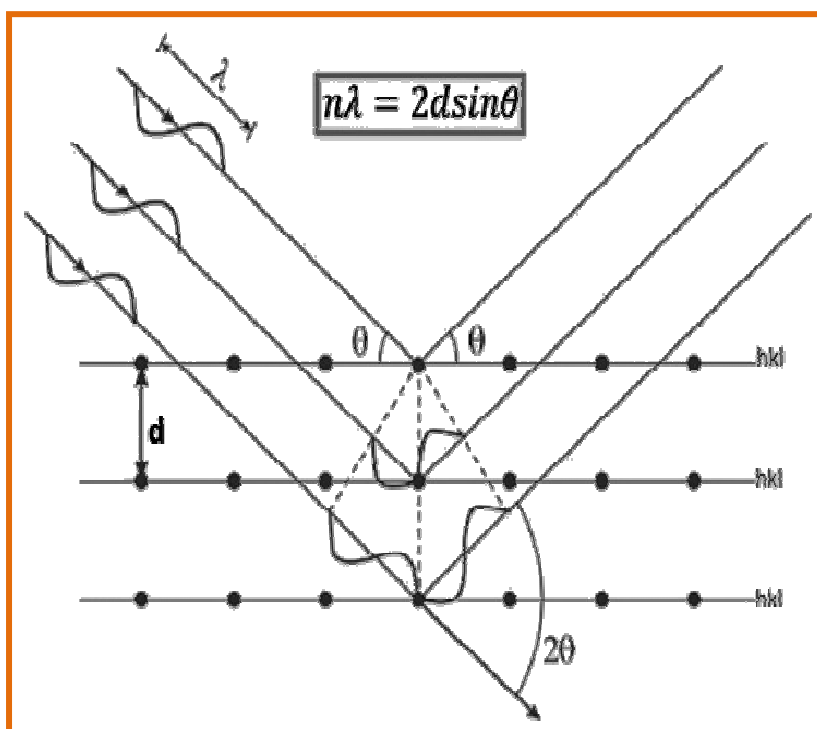
Figure 2.1: Phenomenon of diffraction of X-rays on crystal layers

As shown in the above figure 2.1 the spacing between planes (*hkl*) *d* is correlated to 2θ, and equation 2.4 is given by Bragg's law:

$$n\lambda = 2d \sin \theta \qquad\qquad 2.4$$

Where,

λ = wavelength,

d = distance between the consecutive atomic planes present in crystalline phase,

n = order of the diffraction, and

θ = diffraction angle.

The most commonly used reference data of single phase XRD patterns, distinctive interplanar spacing's, relative intensities and crystallographic properties are obtained from Powder diffraction file (PDF) [13]. PDF is distributed by ICDD (international center for Diffraction Data). *Bruker* D8 ADVANCE instrument is used to obtain XRD patterns of sample. Cu Kα is the radiation source with λ = 0.15418 nm used during analysis. The intensity data was collected in range of 2θ from 20 to 80 with a 0.02° step size by using a count time of 1 s per point. Diffraction patterns assigned in XRD are taken from PDF database.

2.2.3.1 Crystallite Size Determination

Average size of crystallite particle is predicted by Scherrer formula using data of important diffraction lines obtained in the XRD. According to principle, diffraction lines must be narrow. Broadened diffraction lines appear as the crystallite size of polycrystalline sample gets below 1000 A^o. Line broadening might be due to strain in lattice crystal or limitations in instrument.

The Scherrer formula gives relation between the broadening lines and crystallite size of a sample:

$$hkl = \frac{K\lambda}{\beta_{hkl} Cos\theta} \qquad 2.5$$

Where, K is a constant (ranges from (0.98 to 1.39) but set to 1 because of uncertainty in experiment being performed and K depends on the definition of 'β', i.e. integral breadth which is the volume of average size of crystallite particle [5].

2.2.3.2 Cell Parameter Estimation

The cell parameter is indicated by 'a'. This is calculated by SCI method. This method uses the intensity of significant XRD lines (111) of CeO_2 crystallite phases of individual samples. For calculating the cell parameter of a unit crystal, individual solid samples cell parameters are used in cubic relation with d_{hkl} and is given as below [14,15]:

$$1/d^2_{hkl} = (h^2 + k^2 + l^2) / a^2 \qquad 2.6$$

2.2.4   Temperature Programmed Reduction

Using hydrogen or carbon monoxide as reducing agent temperature programmed reduction (TPR) technique is performed for the characterization of reducible samples. In this technique, reducible sample or precursor is open to the flow of reduction gas mixture (i.e. H_2 / CO in Ar) with gradual increase of temperature in linear pattern. Reduction rate of the sample catalyst or sample solid is constantly noted by measuring H_2 / CO composition of gas mixture at reactor exit channel. The experiment limits the determination of total amount of H_2 / CO consumed, which assists in calculation of degree of reduction and there by assisting in calculation of average oxidation state of sample solid or catalyst after reduction. A detailed depiction of the basic physical principles of the H_2-TPR method is presented in relevant reviews and journals [16–20].

In the present investigation H_2 is used as reducing agent for the TPR measurements. Micromeritics model auto-chem2910 is used for performing H_2-TPR

analysis. About 50 mg of catalyst sample was weighed down in H_2-TPR in an isothermal zone for runs at heating rate of 10 K min^{-1} and heated to 473 K with flow rate of 30 mL min^{-1}. Desorption of water is facilitated by 'He' gas. After cooling the sample to RT, 'He' gas was switched at a rate of 20 mL min^{-1} along with the reducing gas (5% H_2/Ar) and at heating rate of 5 K min^{-1}, with raise in temperature to 1073 K. To remove the water formed in the reactor, effluent gas is passed through the molecular sieve trap and is taken for analysis by gas chromatography (GC) with a thermal conductivity detector (TCD) at the end of outlet.

2.2.5   UV-Vis Diffuse Reflectance Spectroscopy

To obtain the information related to electronic structure of solid catalysts, absorption bands appearing in near UV and visible regions are useful. Many of the powdered heterogeneous catalysts are opaque in nature, which facilitates the reflection of light radiated but not transmission. The reflected radiation from the surface of sample catalysts has two different components. The diffused component that is absorbed into solid surface later after multiple scatterings those reappear at surface and the reflected component from the surface without any transmission, otherwise known as mirror reflection. Commercial spectrophotometers are designed to minimize the mirror reflection and diffusely reflected radiation is termed as reflectance [21−24].

In the DRS, function of wavelength is measured as the ratio of the light scattered from surface of the sample (2-3nm) to light scattered from the surface of reference sample (i.e. ideal non-absorbing) (i.e. F_{SKM} / (R∞) vs λ in nm). The scattering coefficient (S), sample diffuse reflectance (R∞), and absorption (K), are related by the Schuster-Kubelka-Munk remission function (SKM) [22,23]:

$$F(R_\infty) = (1- R_\infty)^2/2\ R_\infty = K/S \qquad\qquad 2.7$$

The sample was diluted with KBr matrix acts as a baseline standard,. Dilution is done by pelletization procedure, 200-800nm range of wavelength used in obtaining the

spectra. GBS-Cintra 10e UV-Vis NIR spectrophotometer instrument is used for characterization sample with an integration sphere diffuse reflectance attachment.

2.2.6   Laser Raman Spectroscopy

The most efficient technique among those used for analyzing solid catalyst is Laser-Raman spectroscopy. Raman is used to obtain metal–oxygen bond arrangement and the oxygen vacancies present in lattice. Cubic fluorite type of oxides is characterized by oxygen lattice vibrations in Raman spectra. It can distinguish numerous oxidation states of the metal oxides, as individual oxidation states is characterized by an exceptional vibrational spectrums related to individual structures respectively. It is reported that intensity of bands in spectra may vary with the laser source used while performing the experiment. Recently, a study was reported on the Raman spectral investigations performed on surface properties, bulk properties of fluorite-type crystal oxide material using four unlike excited lasers by Raman spectroscopy [25]. When the beam of illuminated light is exposed over the surface of the material, both elastic and inelastic scattered light is reflected, among which 10^{-5} % of incident light is Raman or Inelastic scattered light (composition of Strokes and Anti-strokes scattered light) and the rest of the light is scattered as Rayleigh or Elastic scattered light. Scattering of reflected light in the Raman spectra is as shown in the figure 2.2.
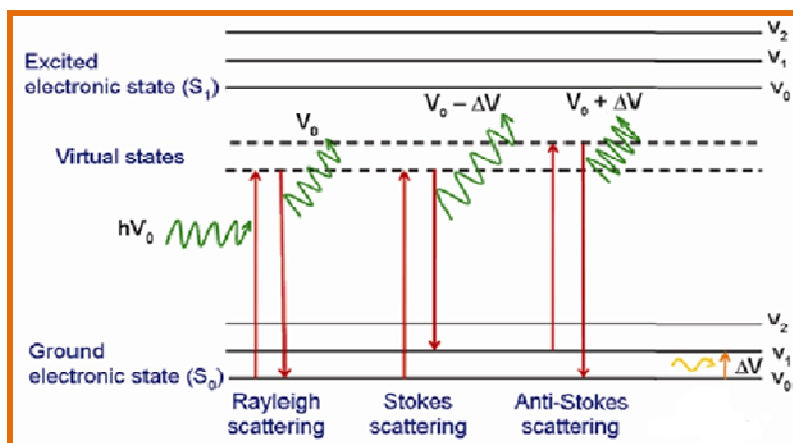
Figure 2.2: Represents the energy level diagram of scattered lines in Raman spectra [26].

From the literature sources it is clear that samples investigated shows laser beam with shorter λ is nearer to electronic adsorption of samples, while using excited laser beam shorter λ is more sensitive to surface region of samples.

Investigations of vis-RS were recorded with an instrument named Lab Ram HR800, attached with a CCD detector. Ar^+ ion laser is used to focus emission line of wavelength 638.2nm on sample solids. Acquisition time used was tuned with respect to intensity of scattering light. Spectra of various samples are recorded within a range followed by comparison of data to determine the homogeneity observed between the samples. All the samples investigated were found to have homogeneity [27−29]. Precise λ values are reported from Laser Raman spectra.

2.2.7 X-ray Photoelectron Spectroscopy (XPS)

XPS is a renowned technique applied to surface of samples, which is otherwise known as Electron Spectroscopy for Chemical Analysis (ESCA). This is an extensively used technique for analyzing the elemental detailing present in solid surfaces with its shrinking depth of 20 Å. Mono-energetic x-rays are used to irradiate the solid sample to obtain the XPS of sample by studying the electrons emitted. Mg Kα, Al Kα x-rays with (1253.6 eV), (1486.6 eV) are used for irradiation. However, the photons in radiation have an inadequate penetration in a solid, at a range of 1-10 micrometers. These photons interact with elements present on surface of sample by photoelectric effect, thereby causes the emission of electrons, is shown in the below figure 2.3. Kinetic energy (KE) is associated with the emitted electrons, which is given by:

$$KE = h\upsilon - BE - \varphi_s \qquad 2.8$$

Where,

$h\upsilon$ = energy of photon

BE = binding energy

φ_s = spectrometer work function
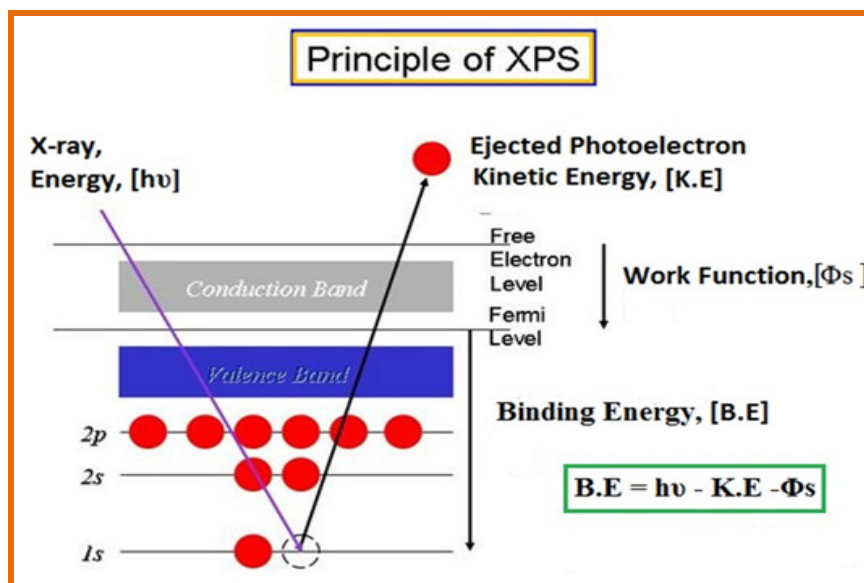
Figure 2.3: Schematic photoemission of electron from core level.

Binding energy (BE) is otherwise termed as Ionization potential of element for the particular atomic orbital from which electron is evolved. Various oxidation states are possible for individual atom; therefore various KE's are associated with electrons.

The XPS of all the samples investigated were recorded on a KRATOS AXIS 165. Mg Kα X-ray with 1253.6 eV is used as source for excitation of electron. Charges present on surface of samples was set by correcting the binding energy of the adventitious carbon (C 1s) at 284.6 eV. This analysis was performed at optimal temperatures and pressures less than 10^{-6} Pa. Prior to analyze; samples were out-gassed for about 12 h in a vacuum oven. All B.E's quoted in this analysis were measured are accurate with ±0.1 eV [30, 31].

2.2.8 Fourier Transform Infrared Spectroscopy (FTIR)

FTIR spectra of the samples were recorded on Bio-Rad Excalibur series equipment in the range of 400–4000 cm^{-1} employing the KBr disc method.

2.2.9   Scanning Electron Microscopy (SEM)

SEM is a versatile electron microscopic technique used widely to examine the surface morphology and topology to determine the particle shape and size respectively. SEM also provides the information related to internal composition, dispersion of active components over surface of material and structure of particles.

Working principle of SEM is explained as the interaction between the characteristic X-rays and electrons present in the matter and there by analyzing the electrons are diffracted [32].
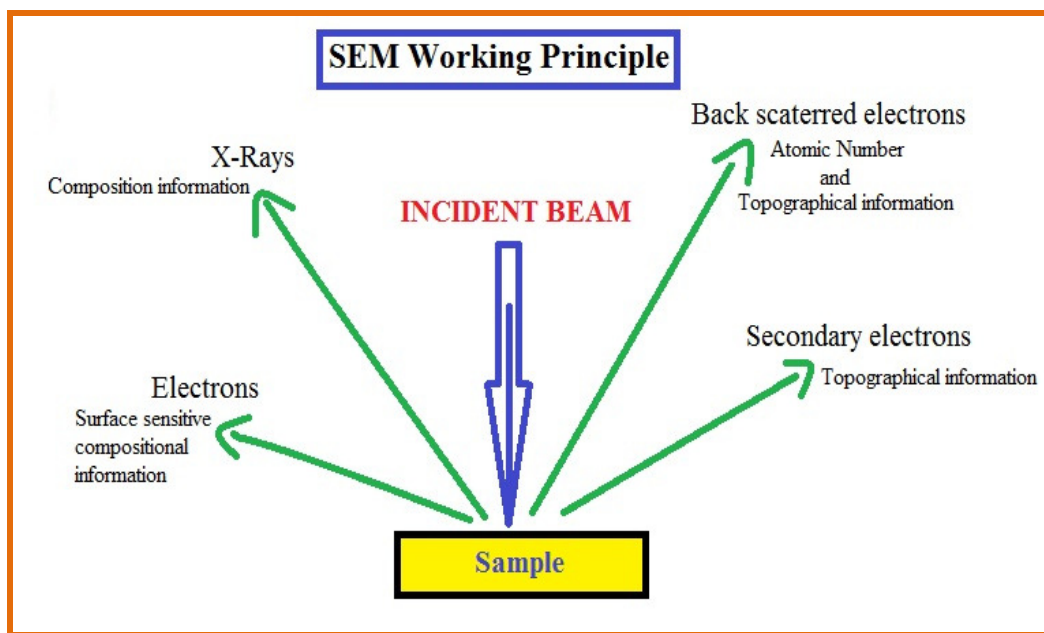
Figure 2.4: Schematic representation of principle of SEM.

To carry out SEM on a sample, rafter the narrow e- beam above the material surface there by detecting the back scattered e-'s, X-rays, secondary electrons and photons as a function of primary beam position to analyze the specific properties of the material. SEM analysis is carried out by Hitachi X650 microscope, operating with an accelerating voltage of 15 kV. SEM micrographs were taken after coating by gold sputtering.

2.3   Catalytic Activity Studies

The composite oxides synthesized and characterized by spectroscopic and non-spectroscopic techniques in the present analysis were evaluated by these catalytic activity reactions:

1.   Potential Oxygen Storage Capacity (OSC)
2.   CO Oxidation Reaction

2.3.1   Potential Oxygen Storage Capacity (OSC)

Potential catalytic performance of powders was analyzed by oxygen releasing capacity in dry air at temperatures from 573K to 1073 K. The TG instrument under cyclic heat treatment in flowing air monitors the difference in weight of the sample. TG/DTA instrument was employed to estimate the OSC of the investigated samples. The heat cycle involves heating, then cooling followed by heating again to 1073 K, 423 K and 1073K respectively. All the rates of heating and cooling were in 5 K min^{-1}.

Loss in weight of samples occurs with heating at last step of the procedure. TG data was used as assess for oxygen storage/release capacity (OSC) of the mixed powdered samples between 573K and 1073 K temperatures. The heat treatment temperature (1073 K) maxima relate to the optimal thermal condition of exhaust gases liberated from automobiles [33, 34].

2.3.2   CO Oxidation Activity

Exhaust gas from automobiles is being the major cause for air pollution. Treatment of exhaust gas is necessary and development of Three-way catalyst (TWC) to transform hazardous gases such as CO, NO_x and hydrocarbons to less hazardous gases or environmental friendly gases has become one of the interesting topic of research. CO oxidation is the main step involved in overall progression of the TWC's. Therefore CO

oxidation is used as an investigation reaction over ceria and ceria-based mixed oxides to quantify and analyze the catalytic formulations and their mechanistic issues [35–42].

The CO oxidation activity of catalyst is evaluated using fixed-bed micro reactor at optimized atmospheric pressure and temperature range at 300–773K with rate of heating i.e. 5 K/min. While evaluating the sample ($\approx$ 50mg) is placed in quartz reactor by diluting it with fraction of sieved quartz particles. Thermocouple is used for measuring the temperature directly in hollow shaft bed reactor.

Used gases and gaseous mixtures were supplied by Air Liquide, as pure CO is not passed over the catalyst. Simplified experiment set up used for CO oxidation is shown in figure 2.5. This gaseous mixture has Ar, 9.98% CO in Ar, and 10.2% O_2 in Ar (purity of Ar, CO, O_2 is >99.995%). Mass flow controllers were used to maintain the total flow rates in the range of 50-100NmL min^{-1} (mL at STP).
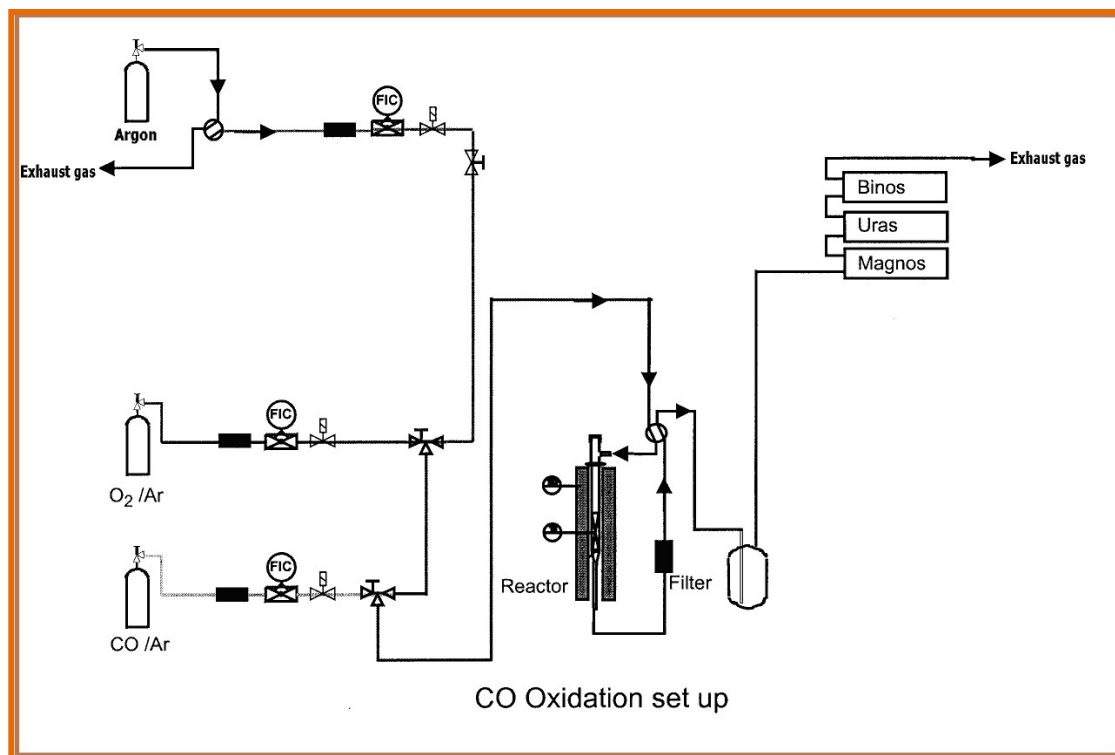
Figure 2.5:   **Experimental setT up for CO oxidation details the used gases, analyzer and reactor [38].**

Following equations were used to calculate the % of CO, O_2 which was converted during the process and % of CO_2 yielded:

$$Conversion\ of\ CO(\%) = \frac{[CO]^{in} - [CO]^{out}}{[CO]^{in}} x100 \qquad 2.9$$

$[CO]^{in}$, $[CO]^{out}$ the inlet and outlet concentrations of CO respectively.

2.4   References

[1]   R.D. Purohit, B.P. Sharma, K.T. Pillai, A.K. Tyagi, Mater. Res. Bull. 36 (2001) 2711.

[2]   K.C. Patil, S.T. Aruna, S. Ekambaram, Curr. Opin, Solid State Mater Sci. 2 (1997) 158.

[3]   S. Brunauer, P.H. Emmett, E. Teller, J. Am. Chem. Soc. 60 (1938) 309.

[4]   A.S. Deshpande, N. Pinna, P. Beato, M. Antonietti, M. Niederberger, Chem. Mater. 16 (2004) 2599.

[5]   J.R. Anderson, K.C. Pratt, Introduction to the Characterization and Testing of Catalysts, Academic press, Sydney, 1985.

[6]   A. Auroux, Catalyst Characterization: Physical Techniques for Solid Materials, Plenum Press, New York, Chapter 22, 1994.

[7]   H. Borchert, Y. Borchert, V.V. Kaichev, I.P. Prosvirin, G.M. Alikina, I. Lukashevich, V.I. Zaikovskii, V.I. Moroz, E M. Paukshtis, E.A. Bukhtiyarov, V.I. Sadykov, J. Phys. Chem. B. 109 (2005) 20077.

[8]   J. Villarroel-Rocha, D. Barrera and K. Sapag, Microporous Mesoporous Mater. 200 (2014) 68.

[9]   N.W. Hurst, S.J. Gentry, A. Jones, B.D. Mc. Nicol, Catal. Rev. Sci. Eng. 24 (1982) 233.

[10] H.P. Klug, L.E. Alexander, X-Ray Diffraction Procedures for Polycrystalline and Amorphous Material, 2nd ed., Wiley, New York, 1974.

[11] P. Gallezot in Catalysis, Science and Technology, Springer, Berlin, Vol. 5, pp. 221-273, 1984.

[12] G. Bergeret, P. Gallezot in Catalyst Characterization: Physical Techniques for Solid Materials, Plenum Press, New York, Chapter 15, 1994.

[13] International Centre for Diffraction Data, 12 Campus Boulevard, Newton Square, PA 19073-3273, USA.

[14] A. Bozo, F. Gaillard, N. Guilhaume, Appl. Catal. A: Gen. 220 (2001) 69.

[15] G. Colon, M. Pijolat, F. Valdivieso, H. Vidal, J. Kaspar, E. Finocchio, M. Daturi, C. Binet, J.C. Lavalley, R.T. Baker, S. Bernal, J. Chem. Soc. Faraday Trans. 94 (1998) 3717.

[16] M. Wlodzimierz, A. Malgorzata, A. Malecka, P. K. Leszek, Appl. Catal. A: Gen. 368 (2009) 71.

[17] D.A.M. Monti, A. Baiker, J. Catal. 83 (1983) 323.

[18] A. Jones, B. Mc. Nicol, Temperature-Programmed Reduction for Solid Materials Characterization in Chemical Industries, Marcel Dekker, New York, Vol. 25, 1986.

[19] P. Malet, A. Caballero, J. Chem. Soc. Faraday Trans. 84 (1988) 2369.

[20] G. Ertl, H. Knozinger, J. Weitkamp (Ed.) Handbook of Heterogeneous Catalysis, VCH, Weinheim, Vol. 2, 1997.

[21] B.M. Weckhuysen, R.A. Schoonheydt, Catal. Today, 49 (1999) 441.

[22] G. Kortum, Reflectance Spectroscopy: Principles, Methods and Applications, Springler Verlag, Berlin, 1969.

[22] W.N. Delgass. G.L. Haller, R. Kellerman, J.H. Lunsford, Spectroscopy in Heterogeneous Catalysis, Academic Press, New York.

[24] X. Gao, I.E. Wachs, J. Phys. Chem. B 104 (2000) 1261.

[25] M.F. Luo, Z.L. Yan, L.Y. Jin, M. He, J. Phys. Chem. B. 110 (2006) 13068.

[26] M.S.M. Ibrahim, M.M. Bajaj, V.R. Singh, Ruchika, S.A.S. Farhana, Internat. J. Bisosciences Vol. 3 No.1 (2014), pp. 52-73.

[27] H. Knozinger, Fundamental Aspects of Heterogeneous Catalysis Studies by Particle Beams (Ed: H.H. Brongersma, R.A. van Santen), Plenum Press, New York, 1991.

[28]   J.M. Stencel, Raman Spectroscopy for Catalysis, van Nostrand Reinhold, New York, 1990.

[29]   E. Garbowski, G. Coudurier in Catalyst Characterization: Physical Techniques for Solid Materials (Ed: B. Imelik, J.C. Vedrine), Plenum Press, New York, Chapter 3, 1994.

[30]   A. Briggs, M.P. Seah, Eds. Practical Surface Analysis, 2nd ed.; Auger and X - Ray Photoelectron Spectroscopy, Wiley, New York, Vol. 1,1990.

[31]   C.D. Wagner, W.M. Riggs, L.E. Davis, J.F. Moulder, in: G.E. Muilenberg, Ed. Handbook of X-Ray Photoelectron Spectroscopy, Perkin-Elmer Corporation, Minnesota, 1978.

[32]   G. Ertl and J. Kuppers, Low Energy Electrons and Surface Chemistry, VCH, Weinheim. (1985).

[33]   M. Ozawa, C.K. Loong, Catal. Today. 50 (1999) 329.

[34]   A.D. Logan, M. Shelef, J. Mater. Res. 9 (1994) 468.

[35]   A. Trovarelli, Catal. Rev. Sci. Eng. 38 (1996) 439.

[36]   E. Aneggi, J. Llorca, M. Boaro, A. Trovarelli, J. Catal. 234 (2005) 88.

[37]   M.F. Milkes, P. Hayden, A.K. Bhattacharya, J. Catal. 219 (2003) 295.

[38]   W. Liu, M. Flytzani-Stephanopoulos, J. Catal. 153 (1995) 304.

[39]   Y. Madier, C. Descorme, A.M. LeGovic, D. Duprez, J. Phys. Chem. B. 103 (1999) 10999.

[40]   R.H. Nibbelke, A.J.H. Nievergeld, J.H.B.H. Hoebnik, G.B. Marin, Appl. Catal. B: Environ. 19 (1998) 245.

[41]   L. Zhua, J. Yu, X. Wang, J. Hazardous Mater. 140 (2007) 205.

[42]   J. Liu, Z. Zhao, C. Xu, A. Duan, L. Wang, S. Zhang, Catal. Commun. 8 (2007) 220.

CHAPTER 3

STUDIES ON CuO PROMOTED CeO$_2$-MxOy (M = Zr, La, Pr and Sm) CATALYSTS FOR CO OXIDATION

3.1.   Introduction

Carbon monoxide treatment by catalytic oxidation, such as water-gas-shift reaction (WGSR), preferential CO oxidation in the H_2 rich streams (PROX) and its simple oxidation either in the presence of O_2 or NO have received much attention by the scientific community. The presence of CO in the atmosphere (100 ppm or above) causes severe environmental and human health problems [1−4]. CO oxidation reaction is also considered in few other fields which include air fresher indoor devices, vehicle exhaust pollution-control device, carbon dioxide lasers, solid oxide fuel cells and so on [5,6]. In many cases, the noble metal-based catalysts have proven to be the highly effective candidates towards the CO oxidation [7−9]. However, some disadvantages of noble metals; lower abundance, Costlier metals, highly sensitive towards catalyst poisoning. These listed factors initiated for a wide research for substitute catalysts [10, 11].

In recent years, copper−cerium based catalysts have received much attention because they are easy to prepare, inexpensive and environmentally benign materials [12,13]. The synergism between copper and ceria shows a remarkable influence on various oxidation reactions and exhibit comparable activity with that of noble metal catalysts [14−17]. Particularly, ceria is a significant inner-transition metal oxide used widely in heterogeneous catalysis because of its high OSC value and easily inter-convertible Ce^{4+}/Ce^{3+} redox couple [3, 18−20]. However, pure ceria is not an ideal candidate for increasing practical applications because of its limited OSC and poor thermal stability.

Modification of ceria with other metals is a key issue to overcome the aforesaid drawbacks. Hence, several research efforts are going on towards doping of CeO_2 with other aliovalent cations [La^{3+}, Tb^{3+}, Sm^{3+}, $Mn^{2+/3+}$, Eu^{3+}, $Fe^{2+/3+}$, etc.] or isovalent cations [Ti^{4+}, Hf^{4+}, Zr^{4+}, etc.]. In both the cases of doping physio chemical properties i.e. redox nature and chemical reactivity of the doped CeO_2 is improved when compared with activity of pure CeO_2 [21−23]. Therefore, the synergism between copper and ceria as well as enhanced physicochemical properties of doped ceria have inspired the researchers to design copper promoted ceria-based mixed oxides [24−27]. Papavasiliou et al. [28, 29] investigated the

effect of different dopants on the copper–ceria for methanol steam reforming and WGSR. It was found that dopants such as Zn and Sm show a positive effect, whereas Zr, La, Gd and Y exhibit negative effect on the activity of copper−ceria catalysts.

Numerous research efforts have been undertaken to prepare Cu promoted CeO_2-based mixed oxides, of which solution-based methods are of particular interest in the laboratory and industry. Various techniques including, co-precipitation, sol-gel, micro-emulsion, hydrothermal synthesis, wet-impregnation and so on have been reported in the literature. However, most of the solution-based processes utilize conventional heating that result in high inclined thermal gradient effect, ineffective, futile, non-productive reaction conditions all the way through the bulk solution.

Additionally, they even they entail calcination at higher temperatures for longer period of time that prolonged times that ultimately result in adverse crystallite size, with lower BET surface area and hence, insignificant catalytic activity. Particularly, it is very difficult to obtain mono-dispersed and regularly-shaped particles with homogeneous composition by co-precipitation methods because different species precipitate at different pH ranges with different rates [30, 31]. Microwave-assisted route for the synthesis of nano materials is one of the promising techniques to overcome the above said drawbacks. The main advantages of MW irradiation are i) Constant heating and uniform distribution of heat to the reaction mixture; ii) production of gradually higher temperatures confine to the reaction sites; iii) very short time is required to complete the reaction; iv) Selectivity is observed for definite morphology; v) very less energy is consumed; vi) very high percentage of product yield. Because of all these advantages, a uniformly dispersed nano-crystalline particulate matter with enhanced properties can be prepared in a single pot synthesis within a short span of time [32, 33].

The current investigation was commenced in contradiction of the above-mentioned context and designed at developing a new class of copper promoted metal doped CeO_2 catalysts using microwave-assisted combustion method. The prepared samples were probed for CO oxidation. Structural characterization studies demonstrated that all the doped

foreign metal cations form uniform solid solutions and result in the better OSC materials than Cu−CeO$_2$. Among the various metal doped catalysts, the Cu/CeO$_2$−ZrO$_2$ combination exhibited superior CO oxidation activity due to its better OSC and other favourable characteristics.

3.2.   Experimental

The investigated copper promoted CeO$_2$−M$_x$O$_y$ (8:2 based on oxide ratio; M$_x$O$_y$ = La$_2$O$_3$, Pr$_2$O$_3$ and Sm$_2$O$_3$) and copper promoted CeO$_2$−ZrO$_2$ (1:1) were prepared by MWCS, using urea as the fuel. Complete preparation details are described under experimental section of chapter 2. Whereas numerous characterization techniques; XRD, Raman, TPR/TPO, XPS, OSC, BET surface are studied to investigate the structural properties and surface properties of sample prepared.

3.3.   Results and discussion

XRD technique was used to analyze the structural parameters (crystallite size, lattice parameter) and purity of crystalline phases. The XRD patterns of the metal doped Cu/CeO$_2$ and pure Cu/CeO$_2$ catalysts are shown in Figure 3.1. All diffraction patterns resemble the characteristic standard FCC peak of ceria as reported in the literature. There are no peaks related to ZrO$_2$, La$_2$O$_3$, Pr$_2$O$_3$ and Sm$_2$O$_3$, thus confirming the formation of single phase ceria solid solutions. Additionally, the patterns relating to either CuO or other combinations between Cu and Ce were not found in the investigated region. This desperate feature can be explained as due to the low percentage of copper or existence of strong interaction between finely dispersed copper and the supports. Remarkable peak shift is observed in diffractogram, which is due to variation in ionic radius of the dopant ions. In the case of zirconium doped catalyst (CCZ), diffraction peaks are shifted to higher angle side due to the smaller ionic radius of Zr^{4+} (0.84 Å) in comparison to Ce^{4+} (0.97 Å). On the other hand, due to the larger ionic radii of La^{3+} (1.10 Å), Pr^{3+} (1.13 Å) and Sm^{3+} (1.09 Å) ions in relation to Ce^{4+} (0.97Å), the respective XRD peaks are shifted to lower angle side [34].
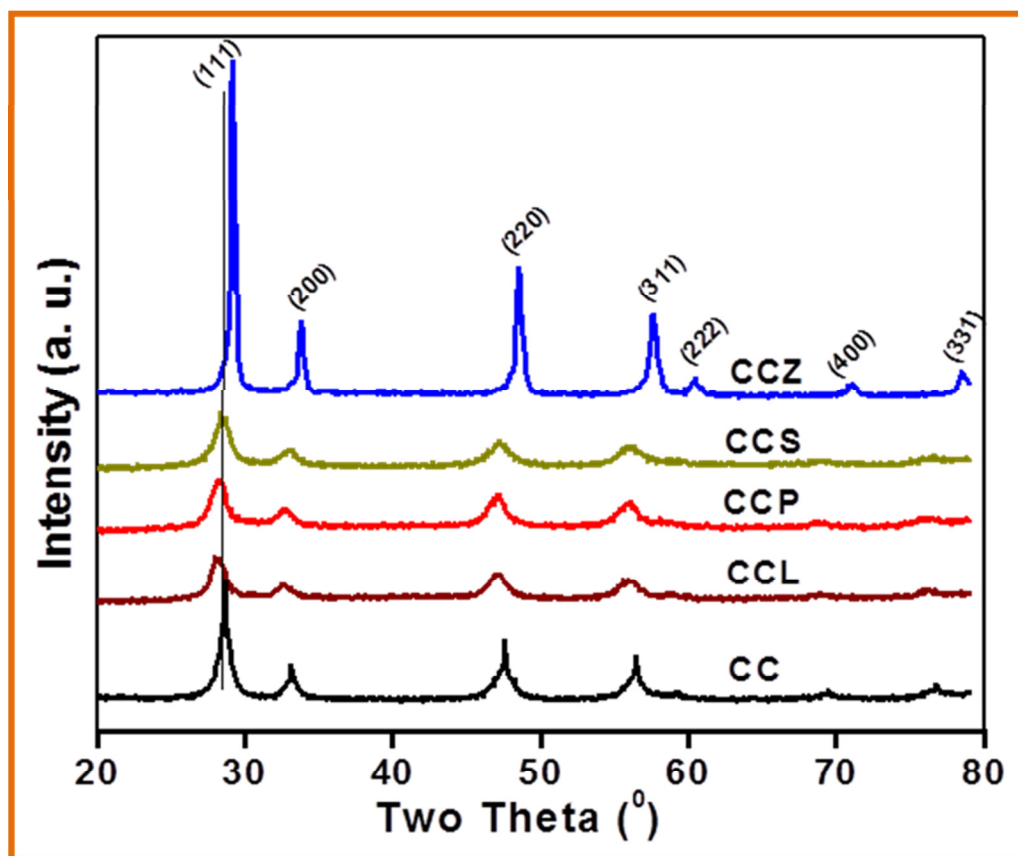
Figure 3.1:   **Powder X-ray diffraction patterns of Cu/CeO₂ (CC), Cu/CeO₂–ZrO₂ (CCZ), Cu/CeO₂-La₂O₃ (CCL), Cu/CeO₂–Sm₂O₃ (CCS) and Cu/CeO₂–Pr₂O₃ (CCP) catalysts.**

The values of lattice parameter 'a' and average crystallite size of various catalysts are presented in Table 3.1. The measured crystallite sizes obtained by employing the Scherrer's equation reveal that the samples prepared by microwave-assisted method are in the nano size range. Except Cu/CeO₂−ZrO₂ sample (29 nm), remaining copper promoted ceria-based mixed oxides exhibited smaller crystallite sizes (~8 nm) compared to the Cu/CeO₂ (19 nm).

Table 3.1. BET surface area, average crystallite size, lattice Parameter, oxygen storage capacity (OSC) and light off ($T_{1/2}$) temperature values of pure and metal doped Cu-CeO$_2$ mixed oxides

Catalyst	Surface area (m^2/g)	Crystallite size (nm)	Lattice parameter (Å)	OSC μmol of O$_2$/g ceria	$T_{1/2}$ (K)	H$_2$ Consumption (umol/gm)
CC	36	19.31	5.394	258	486	412
CCZ	56	29.05	5.302	358	378	590
CCL	48	7.82	5.494	278	442	485
CCP	47	8.02	5.477	332	411	523
CCS	52	8.37	5.443	335	406	556

The utmost penetrating line (111) of the diffractogram is used to measure the lattice parameter by cubic indexation method (Table 1). It was found that Zr^{4+} doped Cu/CeO$_2$ sample exhibits smaller lattice parameter (5.302 Å) compared to Cu/CeO$_2$ (5.394 Å) this results in contraction of lattice because of substitution of fewer Ce^{4+} ions with Zr^{4+} ions. Conversely, all other samples showed higher lattice parameters (lattice expansion) than that of Cu/CeO$_2$ due to the replacement of fewer Ce^{4+} ions with large size La^{3+}, Sm^{3+}, Pr^{3+} ions. The obtained lattice parameters for the catalyst supports were well matched with the corresponding literature reported mixed oxides [22, 23, 35]. Further, there is a linear increase in the lattice parameters values with respects to the ionic radius of the dopants indicating that the doped oxide is in single oxidation state rather than mixed valence states [36]. The specific surface areas of copper promoted ceria-based mixed oxides are shown in Table 3.1. It can be illustrated from the Table 3.1 that the addition of foreign cations to the Cu/CeO$_2$ increases the surface area significantly. This observation can be explained as the resultant solid solutions formed are porous in nature with decreased crystallite size. Among all the materials, the CCZ shown high BET surface area of 56 m^2/g. However, there is a contradiction with average crystallite size values obtained from the diffractogram analysis

for the CCZ, which shows a crystallite size of 29.6 nm, whereas CC material exhibited ~19 nm sizes with a BET surface area of 36 m^2/g. In general, the materials with larger crystallite sizes show low specific surface area. The observed abnormal feature was confirmed from the scanning electron micrographs of the representative materials as shown in Figure.3.2.
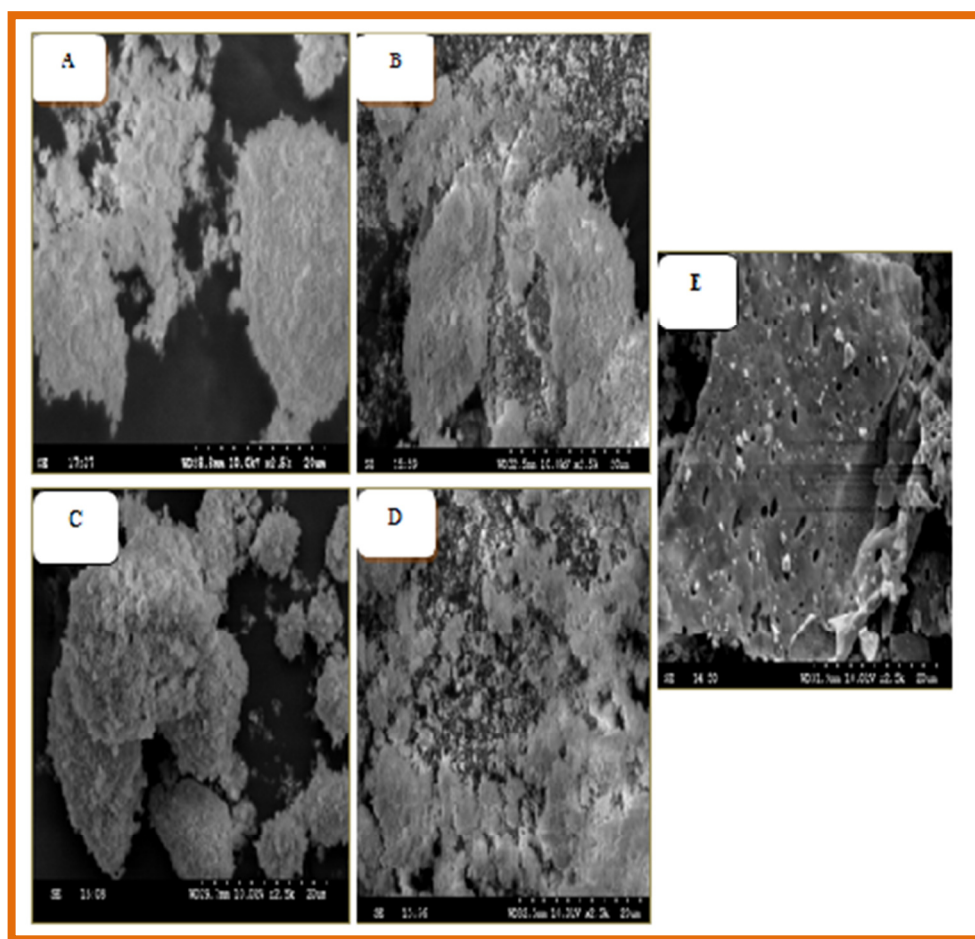
Figure 3.2:   **SEM images of (A) Cu/CeO$_2$ (CC), (B) Cu/CeO$_2$–La$_2$O$_3$ (CCL), (C) Cu/CeO$_2$–Sm$_2$O$_3$ (CCS) (D) Cu/CeO$_2$–Pr$_2$O$_3$ (CCP) and (E) Cu/CeO$_2$– ZrO$_2$ (CCZ) samples.**

All the materials showed same type of morphology except the CCZ sample. The CCZ sample exhibited a large number of voids as shown in the Figure 3.2. Najjir and Batis [37] have also reported the same morphology prepared by combustion synthesis method.

These voids are observed to contribute to an increase in the surface area although CCZ sample shows larger crystallites.

The Raman spectra of various samples were recorded to know the oxygen defect sites and crystalline phases present. Figure 3.3 displays the Raman spectra of CC, CCZ, CCL, CCP, and CCS. Pure ceria exhibits a characteristic peak at 461 cm^{-1}, which relates to the Raman active F_{2g} mode of ceria [38, 39]. For CC, CCZ, CCL, CCP and CCS samples, there is a substantial shift in the F_{2g} band towards lower wavenumber side compared to the ceria spectrum. The peak shift in the Raman spectra depends on numerous aspects, such as in-homogeneity in distribution of size, strain, phonon confinement, deviations in particle size and lattice defects. Raman spectra of Zr^{4+} doped Cu/CeO_2 sample (CCZ) exhibited two more additional peaks at ~300 and 630 cm^{-1}. The band at 300 cm^{-1} relates to the dislocation of oxygen atoms from their actual positions of fluorite lattice. As well, the peak at 630 cm^{-1} is due to non-degenerate longitudinal optical mode of the CeO_2 ascending from the moderation of symmetry that specifies the existence of lattice oxygen vacancies [40,41]. Shift in the peak position of F_{2g} band is not observed in the case of CCZ sample, which is generally observed towards right side for the ceria-zirconia materials. This anomaly is due to the fact that copper oxide was doped into the lattice of the ceria-zirconia lattice during the preparation. Similar observations were also made by other groups in the literature [42,43]. The shifting in the peak position of F_{2g} mode of ceria in all the catalysts is resulted from the solid solutions formed between the dopant and ceria thereby increasing the strain in the lattice. The solid solution formation is also confirmed from the XRD analysis also. The $Sm^{3+}-$ and $Pr^{3+}-$ doped Cu/CeO_2 samples (CCS and CCP) also exhibited an additional peak at around 579 cm^{-1}, can be related to the existence of oxygen vacancies in the CeO_2 lattice due to the charge compensation mechanism [37-41]. On the other hand, any band corresponding to the existence of the oxygen vacancies was not found in the case of La^{3+} doped Cu/CeO_2 sample. Further, no characteristic Raman bands pertaining to the individual dopants obviously reveal the formation of ceria solid solutions as observed from XRD measurements.
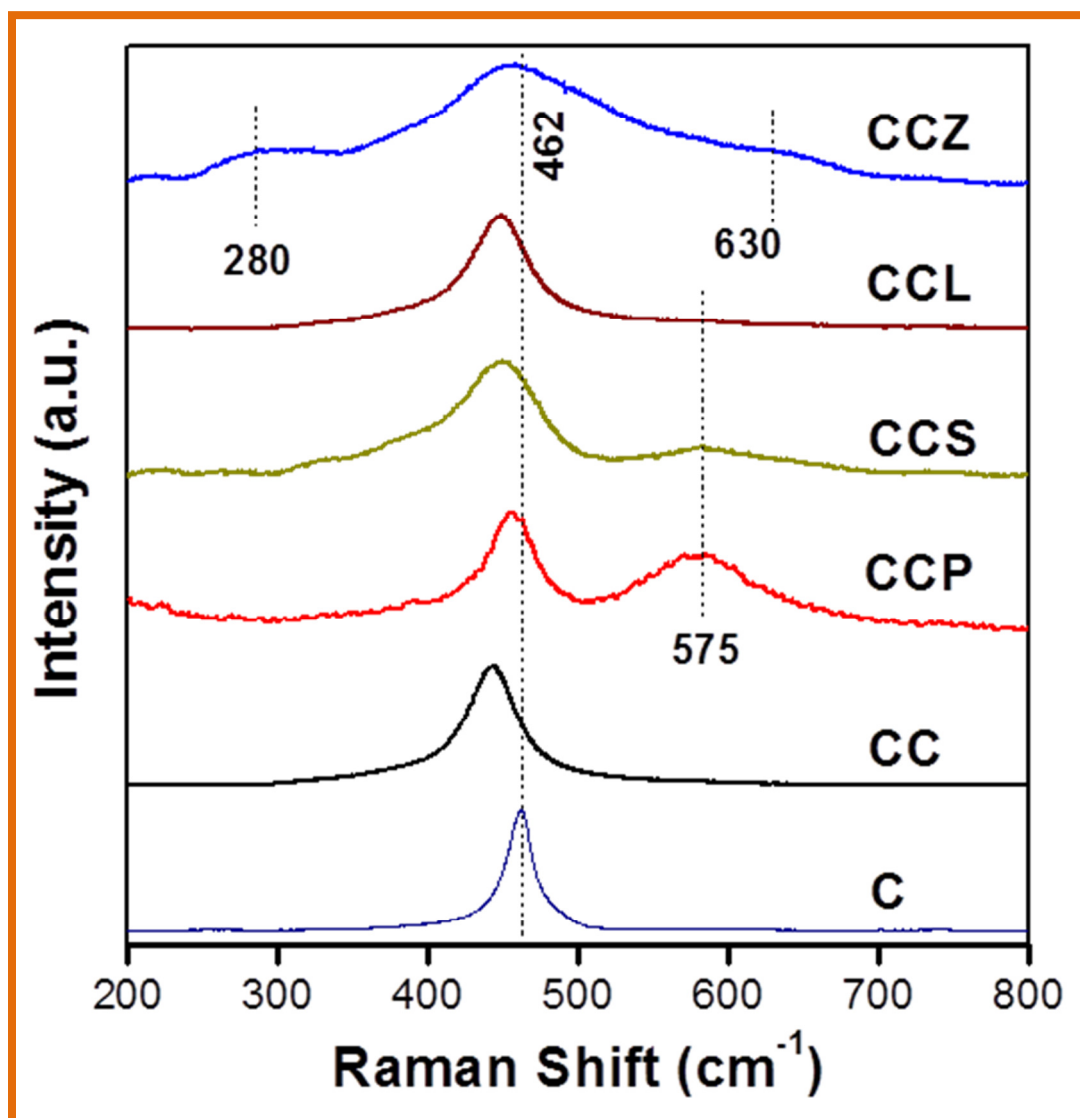
Figure 3.3: **Vis-Raman spectra of pure CeO_2 (C), Cu/CeO_2 (CC), $Cu/CeO_2–ZrO_2$ (CCZ), $Cu/CeO_2–La_2O_3$ (CCL), $Cu/CeO_2–Sm_2O_3$ (CCS) and $Cu/CeO_2–Pr_2O_3$ (CCP) catalysts.**

The vibrational characteristics of the powdered samples were analyzed by FTIR spectroscopy as shown in Figure 3.4. In addition to the major bands observed in the region of $1345–1630$ cm^{-1}, some additional bands were also noticed at 3447, 1050 and 840 cm^{-1} for all the samples. All these bands could be attributed to the presence of traces of

carbonate species in different modes, except the bands present at 3447 and 1630 cm^{-1}. The presence of IR bands at 1379 and 1490 cm^{-1} is due to the physically adsorbed surface mono-dentate carbonate species. The intensity of latter band is low for the Zr^{4+} doped Cu/CeO_2 and pure Cu/CeO_2 samples, whereas other dopant containing samples (CCL, CCP and CCS) exhibited both bands (1379 and 1490 cm^{-1}) in high intensity.

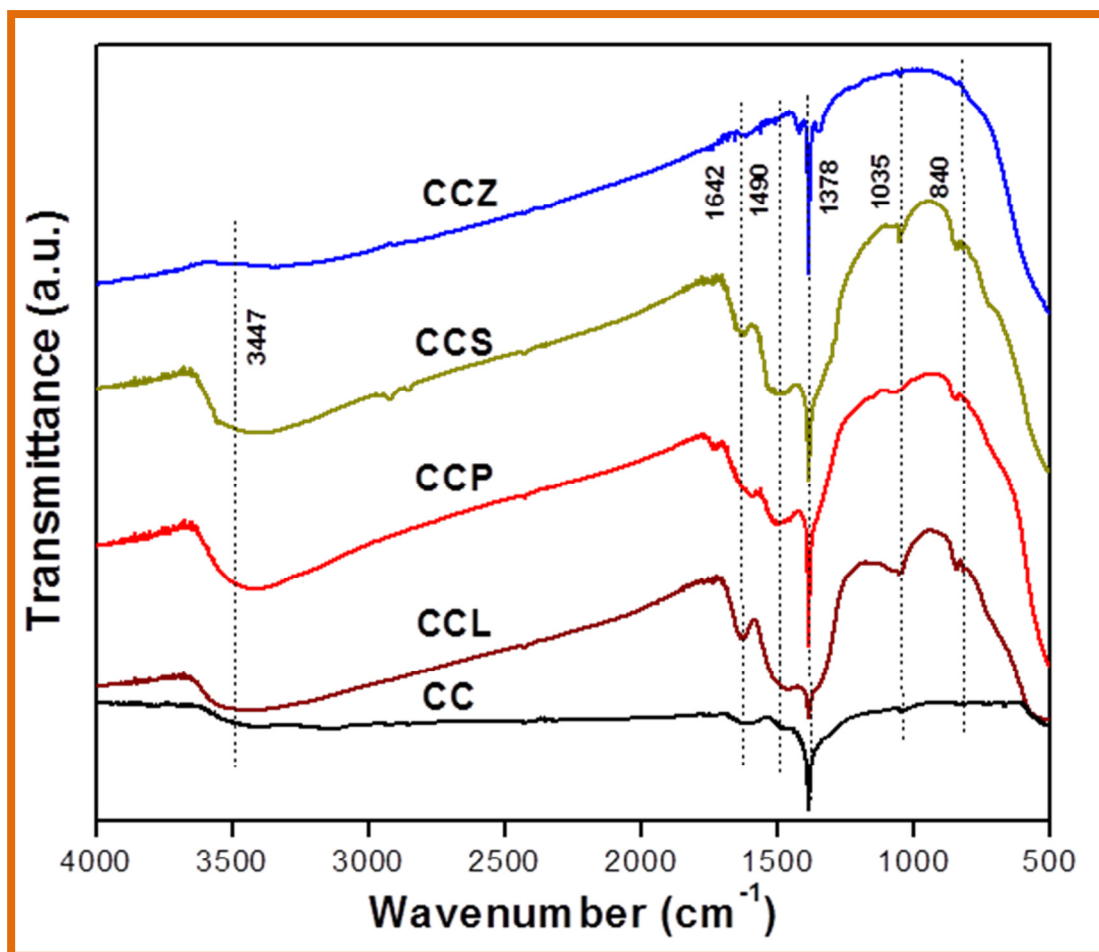**Figure. 3.4:** **Infrared spectra of Cu/CeO₂ (CC), Cu/CeO₂–ZrO₂ (CCZ), Cu/CeO₂–La₂O₃ (CCL), Cu/CeO₂–Sm₂O₃ (CCS) and Cu/CeO₂–Pr₂O₃ (CCP) catalysts.**

These results suggest that more carbonate species are formed in the basic (Pr, La and Sm) oxide doped catalysts. The difference in the intensity of these bands suggest that at least two types of carbonate species are formed i.e., cerium carbonate and other dopant

metal carbonates (Pr, La, Sm and Zr) as explained by Najjir and Battis [37]. The bands at 1050 and 846 cm^{-1} are owing to stretching vibrations of the CO_3^{2-} and the out of plane vibrations of 'C' atom respectively. The band at 3447 cm^{-1} characterizes the stretching of O-H bond of hydroxyl group of physisorbed water or the surface Ce−OH group. The band at 1630 cm^{-1} relates to the H-O-H "scissor" bending peaks, which may have a role in the CO oxidation reaction [42]. The presence of CO_3^{2-} species and -OH species for the combustion synthesized materials are well documented in the literature [34, 43].

TPR and TPO techniques are used to study the redox properties of the catalytic samples prepared. TPR profiles as a function of temperature for CC, CCZ, CCL, CCP, and CCS are shown in Figure 3.5. Generally, pure ceria exhibits two step reduction processes: one is at low temperature (~800 K), due to surface reduction, second is at high temperature (~1000 K) from the bulk reduction [44]. Interestingly, the reduction behavior of ceria was found to depend on the type of metal doped.

On analyzing, reduction peak of ceria is shifted to lower temperature side and is explained as hydrogen dissociated over surface of CuO, is further spilled over and reduced on the surface of CeO_2. For pure Cu/CeO_2 sample, the reduction of $Cu^{2+} \leftrightarrow Cu^0$ occurred at around 494 K and surface ceria reduction at around 524 K.

Further, there is a great difference in the theoretical and experimental calculated H_2 consumption for the copper oxide which is indicated that the copper oxide has strong interaction with the ceria and the reduction of ceria occurs along with the copper oxide which is observed in the peak fit of TPR profiles as shown in the Fig. 5. The doped catalysts have consumed more amounts of H_2 than undoped catalyst and the calculated H_2 consumed value is more for the CCZ catalyst among all other other catalysts as shown in Table 1 indication of the more reducible species on the surface of the CCZ catalyst.
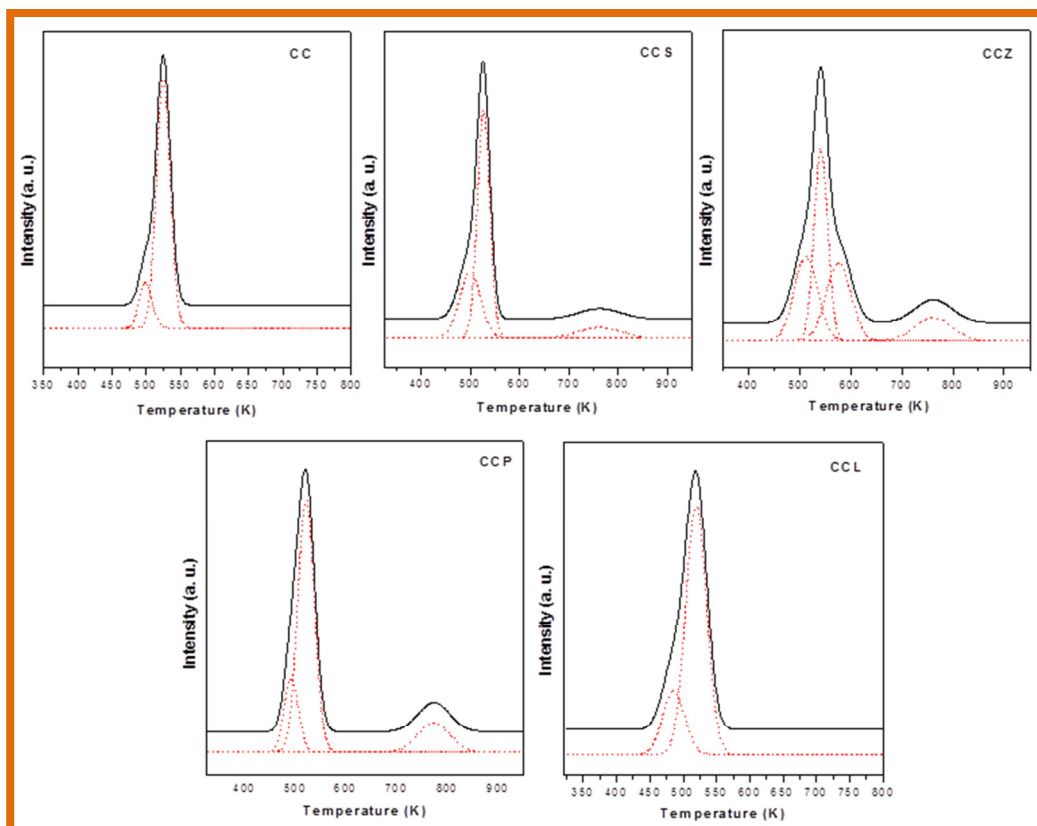
Figure 3.5:   **H$_2$-TPR profiles of Cu/CeO$_2$ (CC), Cu/CeO$_2$–ZrO$_2$ (CCZ), Cu/CeO$_2$–La$_2$O$_3$ (CCL), Cu/CeO$_2$–Sm$_2$O$_3$ (CCS) and Cu/ CeO$_2$–Pr$_2$O$_3$ (CCP) catalysts.**

Interestingly, bulk ceria reduction peak was not observed in the case of Cu/CeO$_2$ sample. The TPR profile of La^{3+} doped sample is similar to the Cu/CeO$_2$ which exhibits Cu reduction at around 493 K and surface ceria reduction at around 523 K. Here also, the peak due to bulk reduction was not observed.

On the other hand, both Sm^{3+}– and Pr^{3+}– doped Cu/CeO$_2$ catalysts exhibited three peaks in their TPR profiles. The reduction of Cu^{2+} occurred at around 493 K and surface ceria reduction occurred at 523 K similar to the Cu/CeO$_2$ sample. Interestingly, the bulk ceria reduction was observed in the case of Sm^{3+}– and Pr^{3+}– doped samples at around 773 K. The TPR profile of Zr^{4+} doped Cu/CeO$_2$ sample is completely different from the other metal doped oxides. It exhibited a total of four peaks in the TPR profile. These results

suggest that there is more than one type of cerium species in the zirconium doped sample. Same behavior was observed in the previous studies [45].

An immediate performance of the TPO analysis was undertaken after the TPR run and the experimental results are shown in Figure 3. 6.
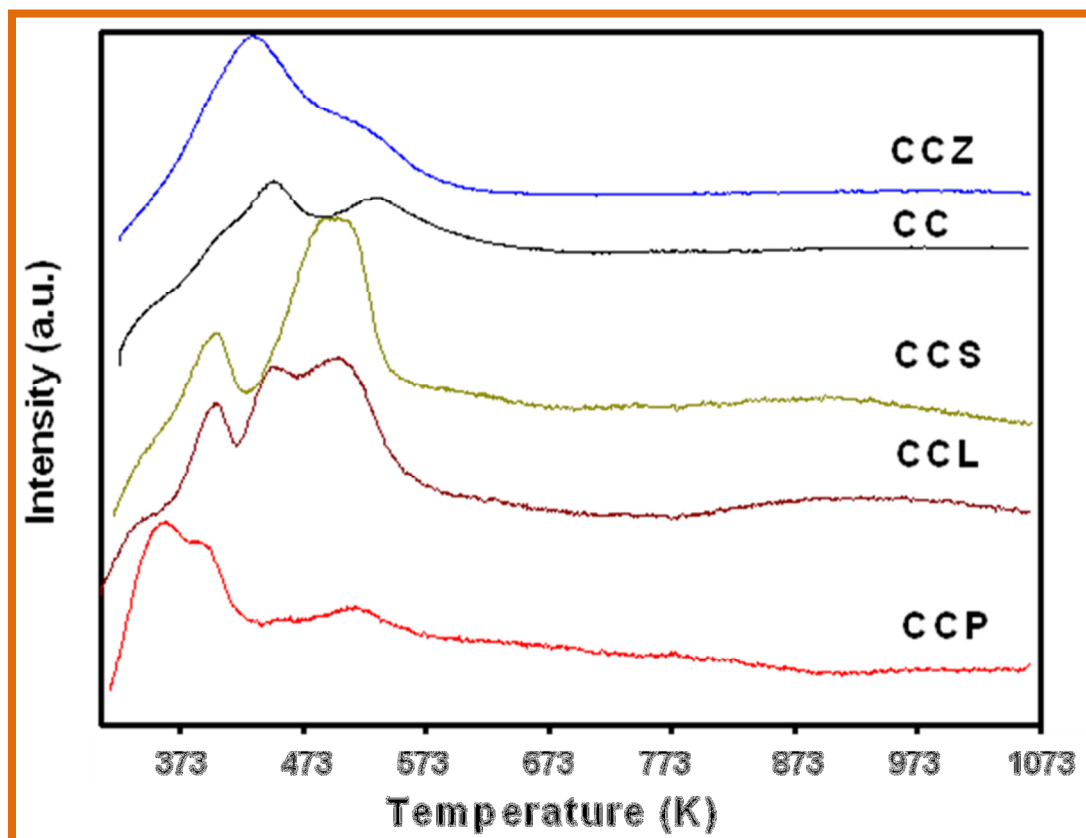
Figure 3.6: **TPO profiles of Cu/CeO$_2$ (CC), Cu/CeO$_2$–ZrO$_2$ (CCZ), Cu/CeO$_2$–La$_2$O$_3$ (CCL), Cu/CeO$_2$–Sm$_2$O$_3$ (CCS) and Cu/CeO$_2$–Pr$_2$O$_3$ (CCP) catalysts.**

The peaks corresponding to the oxidation were found to coincide well with the TPR results. Interestingly, complete oxidation of all the catalysts occurred below 573 K. All the catalysts exhibited oxygen adsorption in two or three stages which explain that the oxidation of copper, surface ceria and bulk ceria occurs separately. An important observation noted here was that the temperature for the oxidation of reducible copper was fairly lowered compared to the reduction temperature. Moreover, no peaks corresponding

to the oxygen release by the decomposition of copper oxide were identified with in the experimental range as envisaged by Luo et al. [46]. These observations can be explained by either due to the strong interaction of finely dispersed copper oxide with the ceria doped mixed oxides or incorporation of copper into the ceria lattice.

To investigate elemental oxidation states as well as the consequence of foreign metal cations on the redox behavior of the $Ce^{3+}\leftrightarrow Ce^{4+}$ couple, XPS measurements were undertaken. The O 1s, Ce 3d and Cu 2p binding energy values of CC, CCZ, CCL, CCP, CCS are accessible in Table 3.2. The O 1s spectra of metal doped Cu/CeO_2 catalysts (not shown) are broad and complex due to overlying commencement of Cu, Ce and the dopants. The binding energy of the most intense peak in the case of metal doped Cu/CeO_2 catalysts is observed at around 530.3 eV, corresponding to lattice oxygen of ceria [47,48]. In addition to the peak at 530.3 eV, all catalysts exhibited a peak at around 534 eV due to the formation of either carbonate or –OH species. The FTIR spectroscopy studies also confirmed the formation of carbonate and –OH species.

Table 3.2: XPS binding energies (eV) of metal doped copper promoted ceria based oxides

Sample	O 1s	Ce 3d	% of Ce^{+3}	Cu 2p
CCZ	529.8	883.3	17	934.3
CCP	530.3	883.4	13	934.5
CCS	530.3	883.1	12	934.5
CCL	530.3	883.4	7	934.2

Figure 3.7 demonstrates the Ce 3d XP core level spectra of metal doped Cu/CeO_2 samples. As shown in Figure 3.7, complex XPS spectra is resulted because of overlapping peaks obtained because of various oxidation states of CeO_2 and hybrid orbitals of Ce 4f

level- O 2p valence band. Hence, Burroughs et al. [49] notation can be aimed to obtain a well stated XPS spectra as shown in Figure 3.7 [22, 23].

The Ce 3d core level spectra is consisting two sets of peaks labeled as 'u' and 'v' featured as $3d_{3/2}$ spin state, $3d_{5/2}$ spin state, respectively. As presented in Fig. 7, the labels u, u$'$, u$''$ and u$'''$ represent Ce $3d_{3/2}$ ionization, whereas the labels v, v$'$, v$''$ and v$'''$ are corresponding to the Ce $3d_{5/2}$ ionization. Here, the labels v/u and v$''$/u$''$ are due to a mixer of Ce $3d^9$ $4f^2$ O $2p^4$ and Ce $3d^9$ $4f^1$ O $2p^5$ of Ce(IV), whereas the peaks labeled v$'''$/u$'''$ correspond to the Ce $3d^9$ $4f^0$ O $2p^6$ of Ce(IV) final state. On the other hand, the labels v$'$/u$'$ are assigned to Ce $3d^9$ $4f^2$ O $2p^5$ and Ce $3d^9$ $4f^1$ O $2p^6$ of Ce(III). It can be concluded from the figure that all samples have surface cerium species in both 4+ and 3+ oxidation states. Interestingly, the Zr^{4+} doped Cu/CeO$_2$ sample showed a progressive reduction in the intensity of the peaks u$'''$/v$'''$ (Ce^{4+}) and an increase in u$'$/v$'$ peaks (Ce^{3+}) compared to other metal doped Cu/CeO$_2$ samples.

The amount of Ce^{3+} present on the catalyst surface was determined by calculating the ratio of area under the peaks u$'$ and v$'$ to the total area and the values are presented in Table 2. As presented in Table 2, Cu/CeO$_2$–ZrO$_2$ sample contains higher amount of Ce^{3+} ions (17%) followed by Sm^{3+}– (13%), Pr^{3+}– (12%) and La^{3+}– (7%) doped Cu/CeO$_2$ samples respectively. Creation of more defective sites due to copper–ceria interactions, doping of zirconium into the ceria lattice and instantaneous high temperature preparation conditions may be responsible for more reducibility of Cu/CeO$_2$–ZrO$_2$ sample.

The Cu $2p_{3/2}$ spectrum of all metal doped Cu/CeO$_2$ catalysts exhibited an intense peak in the range of 934.2-934.6 eV as shown in the Figure 3.8 which is related to the presence of surface Cu^{2+} species [50]. The observed binding energy values are higher than in the literature reported which is generally in the region of 933 to 933.6, indicating that the copper oxide has strong interaction with the ceria/support. The strong interaction between the copper and the ceria/support is also observed by the analysis of XRD, TPR/TPO as discussed above. The observed high full-width at half-maximum (FWHM) value seems to be a strong evidence for the presence of Cu ions in different binding states.
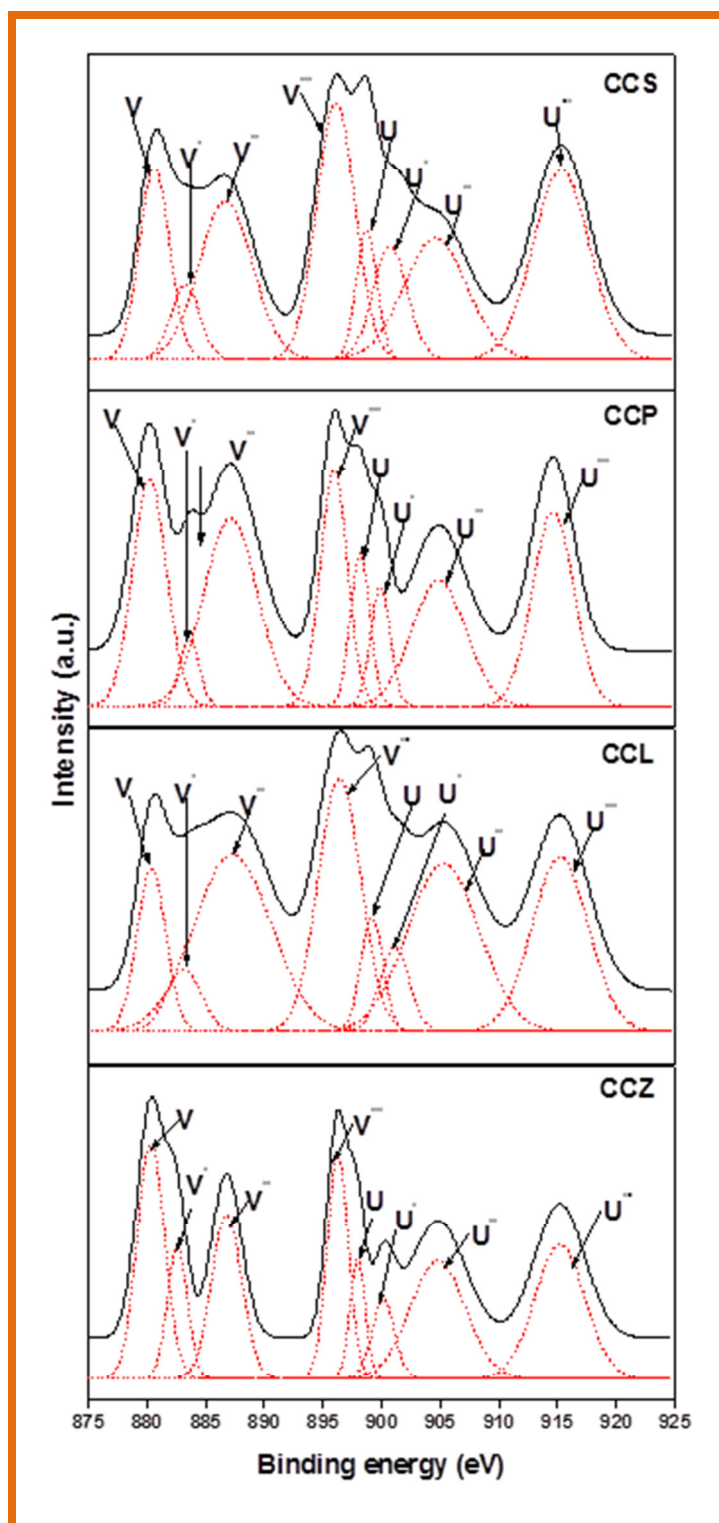
Figure 3.7:   **Ce 3d XPS spectra of Cu/CeO$_2$ (CC), Cu/CeO$_2$–ZrO$_2$ (CCZ), Cu/CeO$_2$–La$_2$O$_3$ (CCL),   Cu/CeO$_2$–Sm$_2$O$_3$ (CCS) and Cu/CeO$_2$–Pr$_2$O$_3$ (CCP) catalysts.**
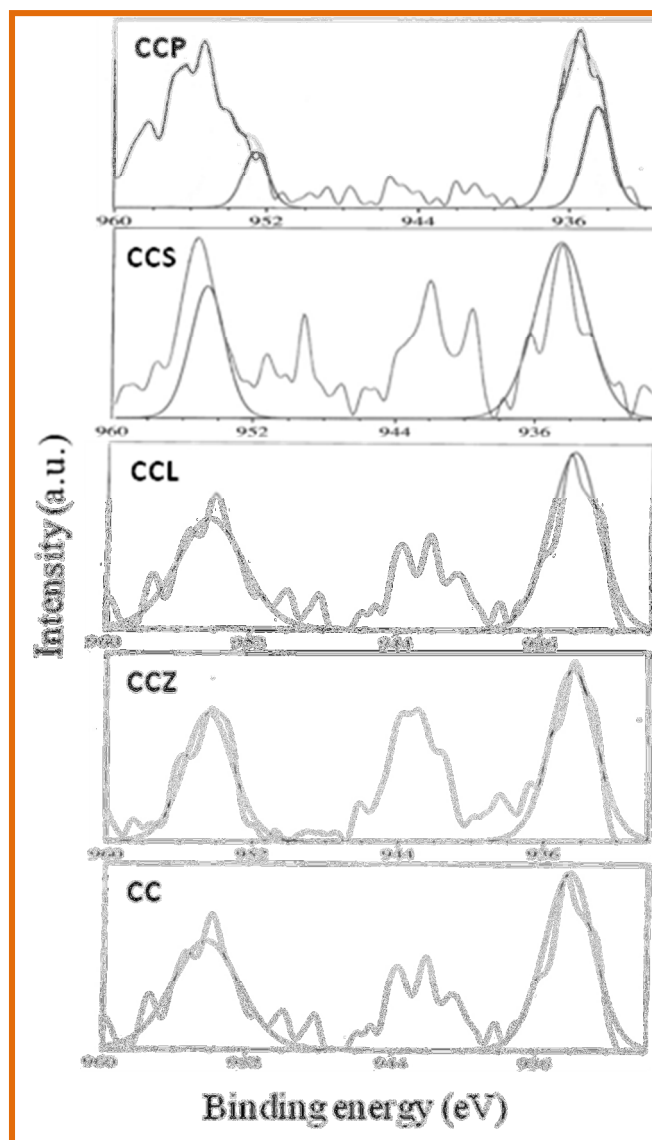
Figure 3.8: **Cu 2P XPS spectra of Cu/CeO$_2$ (CC), Cu/CeO$_2$–ZrO$_2$ (CCZ), Cu/CeO$_2$–La$_2$O$_3$ (CCL), Cu/CeO$_2$–Sm$_2$O$_3$ (CCS) and Cu/CeO$_2$–Pr$_2$O$_3$ (CCP) catalysts.**

The oxygen storage capacity of all catalytic materials was measured using thermo-gravimetric analyzer and the obtained values are presented in Table 3.1. The metal doped Cu/CeO$_2$ samples (CCZ, CCS, CCP and CCL) exhibited higher OSC values compared to undoped Cu/CeO$_2$ (CC), which is corroborated well with the TPR/TPO, Raman and XPS

measurements. As well, the OSC of all the materials is found to be 6–9 times more than the pure ceria reported elsewhere [23]. Amongst, Zr^{4+} doped Cu/CeO_2 sample showed a superior OSC of 358 μmol of O_2/g of ceria and the OSC of 258, 335, 330 and 278 μmol of O_2/g were obtained in the case of CC, CCS, CCP and CCL samples, respectively. The observed significant difference in the OSC values of metal doped Cu/CeO_2 samples and undoped Cu/CeO_2 revealed that the addition of dopants enhances the oxygen mobility in the ceria lattice, which is also supported by TPR/TPO and Raman studies.

The CO oxidation results of various metal doped Cu/CeO_2 catalysts as a function of reaction temperature are shown in Figure 3.9. To compare the activity of catalysts, the obtained light-off temperature ($T_{1/2}$) values are listed in Table 1, where $T_{1/2}$ represents the temperature at 50% conversion of CO. As could be seen from the figure, the conversion of CO is linearly increased with increase in the reaction temperature for all catalysts. All the metal doped Cu/CeO_2 samples exhibited excellent catalytic performance compared to pure Cu/CeO_2 ($T_{1/2}$ ~486 K) catalyst. Among the various metal doped oxides, the Cu/CeO_2–ZrO_2 sample showed better CO oxidation at low temperature. The Zr^{4+} doped Cu/CeO_2 catalyst exhibited light off temperature ($T_{1/2}$) of 378 K followed by Sm^{3+}– ($T_{1/2}$ ~ 406 K), Pr^{3+}– ($T_{1/2}$ ~ 411 K) and La^{3+}– doped Cu/CeO_2 ($T_{1/2}$ ~ 442 K) catalysts respectively.

Remarkably, the Cu/CeO_2–ZrO_2 catalyst showed 100% CO conversion below 423 K. As well, Sm^{3+}– and Pr^{3+}– doped Cu/CeO_2 catalysts exhibited 100% CO conversion at around 473 K, whereas La^{3+} doped Cu/CeO_2 and pure Cu/CeO_2 showed 100% CO conversion at 515 and 595 K, respectively. Cu/CeO_2–ZrO_2 is the more active catalyst for the titled reaction. Though, it has more average crystalline size, but at the same time it has more surface area, OSC and better redox properties and creation of more defective sites due to copper-ceria interactions, doping of zirconium into the ceria lattice and instantaneous high temperature preparation conditions may be responsible for more reducibility of Cu/CeO_2-ZrO_2.

XPS analysis also confirms the more reducibility of Cu/CeO_2-ZrO_2 as it has more amounts of Ce^{3+} ions (17%) and H_2 TPR analysis also supports the more reducible nature

of the catalyst i.e. consumed the more amount of hydrogen. The obtained activity results of all the catalysts were in linear relation with the combined studies of XPS, TPR, OSC and surface area of the catalysts. These observations suggest that the strong interaction between copper and ceria as well as the superior physicochemical properties of the doped ceria could be responsible for enhancement of CO oxidation activity.

It is generally accepted that the oxidation of CO on ceria occurs through Mars-van Krevelen redox type mechanism [51]. The mechanism generally involves an alternate reduction and oxidation of the ceria with the formation of surface oxygen vacancies (as the key step) and their successive replacement by gas-phase oxygen. Hence, the catalyst with more OSC exhibits superior CO oxidation activity. More than the total OSC, the local concentration of sites for O_2 adsorption would be a determining factor in CO oxidation.
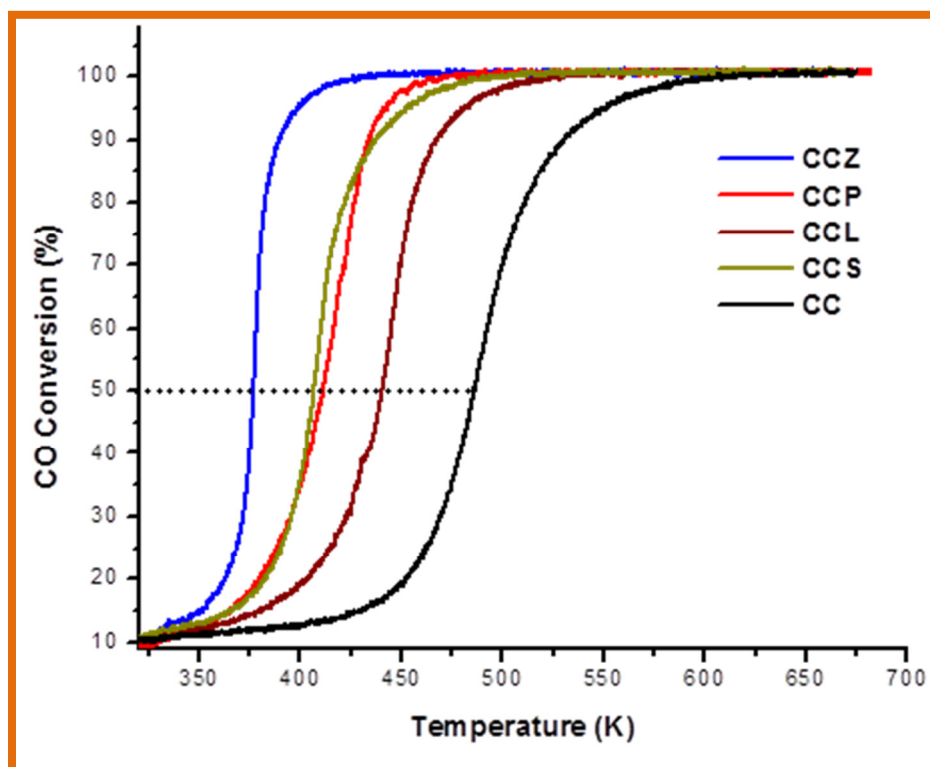
Figure 3.9:　Conversion of CO (%) versus temperature for Cu/CeO₂ (CC), Cu/CeO₂–ZrO₂ (CCZ), Cu/CeO₂–La₂O₃ (CCL), Cu/CeO₂–Sm₂O₃ (CCS) and Cu/CeO₂–Pr₂O₃ (CCP) catalysts.

To study the significance of preparation method, we have compared the CO oxidation activity of 5 wt.% Cu/CeO_2-ZrO_2 (microwave-induced combustion method, MWC) with 10 wt.% Cu/CeO_2-ZrO_2 catalyst (co-precipitation–impregnation method, CPI) [45]. The CO oxidation profiles of both catalysts are presented in Figure 3.10. Remarkably, the catalyst prepared by MWC method exhibited superior activity compared to the CPI−synthesized catalyst even though the Cu wt.% is half in the microwave method. The obtained $T_{1/2}$ values for the MWC− and CPI−synthesized catalysts are 378 and 400 K, respectively.
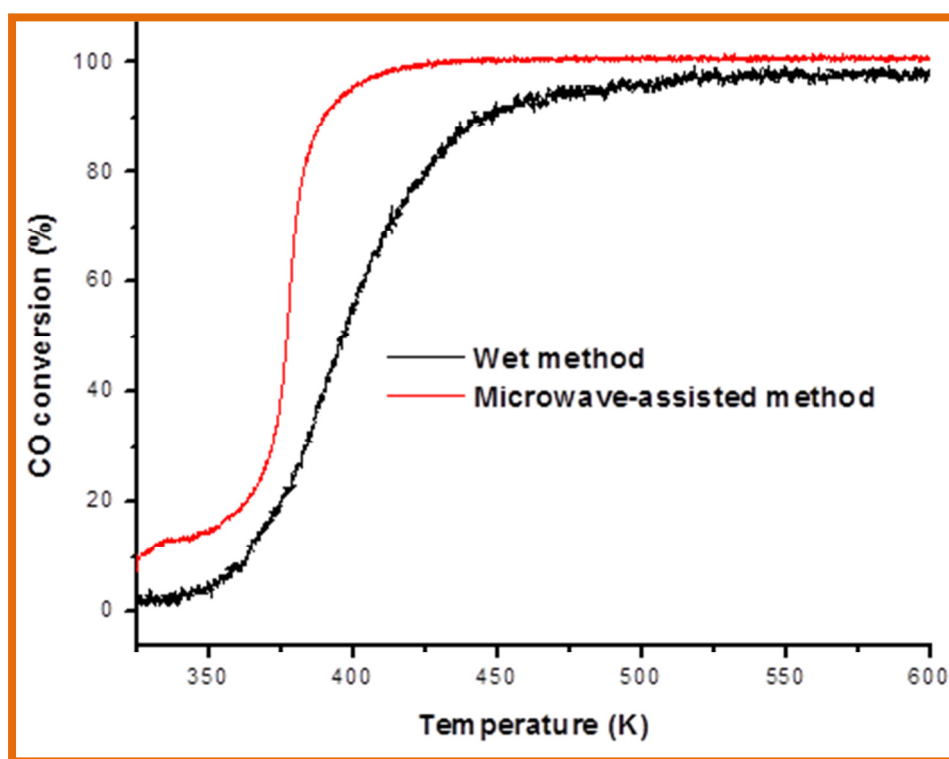
Figure 3.10: Conversion of CO (%) versus temperature for the micro-wave synthesized 5 wt % Cu/CeO_2-ZrO_2 and wet method synthesized 10 wt.% Cu/CeO_2-ZrO_2 catalysts.

Moreover, microwave synthesized 5 wt.% Cu/CeO_2-ZrO_2 exhibited 100 % CO conversion at 423 K, whereas wet method synthesized 10 wt.% Cu/CeO_2-ZrO_2 catalyst

showed a maximum of 97% CO conversion at 573 K. In the previous studies also, microwave synthesized CeO_2–ZrO_2 catalyst exhibited better CO oxidation activity compared to the co-precipitated synthesized CeO_2–ZrO_2 catalysts [52]. These interesting results indicate that microwave-assisted technique is a simple and cost-effective method for the synthesis of metal doped Cu/CeO_2 catalysts towards low temperature CO oxidation in comparison to the co-precipitation route.

3.4. Conclusions

The advantages associated with the microwave-assisted combustion method were considered for the synthesis of catalytic active materials. Accordingly, a series of copper promoted doped ceria catalysts were prepared successfully in a single step. The synthesized catalytic materials were characterized by various physicochemical techniques namely, XRD, BET surface area, Raman, TPR, and XPS. Among all the synthesized materials, CCZ mixed oxide exhibited better structural properties such as enhancement in the BET surface area, low temperature reducibility, more defects formation and a high OSC. Catalytic CO oxidation reaction was tested to evaluate the synthesized catalysts. All the doped catalytic materials showed an improvement in the CO oxidation activity compared to the Cu/CeO_2 catalyst. Among all the catalysts, Zr^{4+} doped Cu/CeO_2 exhibited excellent catalytic performance followed by Sm^{3+}–, Pr^{3+}– and La^{3+}– doped Cu/CeO_2 catalysts. The activity studies were well corroborated with Raman studies, reducibility, surface area and OSC measurements.

3.5   References

[1]   G. Avgouropoulos, T. Ioannides, Appl. Catal. A: Gen. 244 (2003) 155.

[2]   S. Royer, D. Duprez, ChemCatChem 3 (2011) 24.

[3]   R.J. Gorte, AIChE J. 56 (2010) 1126.

[4]   A. Martínez-Arias, M. Fernandez-Garcia, A.B. Hungría, A. Iglesias-Juez, O. Galvez, J.A. Anderson, J.C. Conesa, J. Soria, G. Munuera, J. Catal. 214 (2003) 261.

[5]   J. Kaspar, P. Fornasiero, N. Hickey, Catal. Today, 77 (2003) 419.

[6]   A. Weber, B. Sauer, A.C. Müller, D. Herbstritt, E. Ivers-Tiffee, Solid State Ionics, 152–153 (2002) 543.

[7]   H. Wang, H. Zhu, Z. Qin, F. Liang, G. Wang, J. Wang, J. Catal. 264 (2009) 154.

[8]   G.K. Bethke, H.H. Kung, Appl. Catal. A: Gen. 194 –195 (2000) 43.

[9]   Y.F. Han, M.J. Kahlich, M. Kinne, R.J. Behm, Appl. Catal. B: Environ. 50 (2004) 209.

[10]   K. Everaert, J. Baeyens, J. Hazard. Mater. 109 (2004) 113.

[11]   F. Marino, C. Descorme, D. Duprez, Appl. Catal. B: Envoron. 54 (2004) 5966.

[12]   M.E. Gunay, R. Yildirim, Ind. Eng. Chem. Res. 50 (2011) 12488.

[13]   W. Dow, T. Huang, J. Catal. 160 (1996) 171.

[14]   X. Tang, B. Zhang, Y. Li, Y. Xu, Q. Xin, W. Shen, Appl. Catal. A: Gen. 288 (2005) 116.

[15]   M. Manzoli, R.D. Monte, F. Boccuzzi, S. Coluccia, J. Kaspar, Appl. Catal. B: Environ. 61 (2005) 192.

[16]   R. Zhang, W.Y. Teoh, R. Amal, B. Chen, S. Kaliaguine, J. Catal. 272 (2010) 210.

[17]   K.N. Rao, P. Bharali, G. Thrimurthulu, B.M. Reddy, Catal. Commun. 11 (2010) 863.

[18]   L. Vivier, D. Duprez, ChemSusChem 3 (2010) 654.

[19]   A. Trovarelli, Catal. Rev. Sci. Eng. 38 (1996) 439.

[20]   A. Gupta, U.V. Waghmare, M.S. Hegde, Chem Mat. 22 (2010) 5184.

[21]   B.M. Reddy, P. Bharali, P. Saikia, S.-E. Park, Maurits W. E. van den Berg, M. Muhler, W. Grunert, J. Phys. Chem. C 112 (2008) 11729.

[22]   B.M. Reddy, L. Katta, P. Sudarsanam, G. Thrimurthulu, Appl. Catal. B: Environ. 101 (2010) 101.

[23]   B.M. Reddy, G. Thrimurthulu, L. Katta, Catal. Lett. 141 (2011) 572.

[24]   P. Ratnasamy, D. Srinivas, C.V.V. Satyanarayana, P. Manikandan, R.S. Senthil Kumaran, M. Sachin, V.N. Shetti, J. Catal. 221 (2004) 455.

[25]   Q. Liang, X. Wu, D. Weng, Z. Lu, Catal. Commun. 9 (2008) 202.

[26]   Y.Z. Chen, B.J. Liaw, H.C. Chen, Int. J. Hydrogen Energy 31 (2006) 427.

[27]   Y.Z. Chen, B.J. Liaw, C.W. Huang, Appl. Catal. A: Gen. 302 (2006) 168.

[28]   J. Papavasiliou, G. Avgouropoulos, T. Ioannides, Appl. Catal. B: Environ. 69 (2007) 226.

[29]   T. Tabakova, V. Idakiev, J. Papavasiliou, G. Avgouropoulos, T. Ioannides, Catal. Commun. 8 (2007) 101.

[30]   A.G. Jeffrey, M. Donny. W. Aaron, F.S. Geoffrey, J. Am. Chem. Soc. 127 (2005) 15791.

[31]   Y.C. Kang, S.B. Park, Mater. Lett. 40 (1999) 129.

[32]   M. Tsuji, M. Hashimoto, Y. Nishizawa, M. Kubokawa, T. Tsuj, Chem. Eur. J. 11 (2005) 440.

[33]   J.S. Xu, Y.J. Zhu, Cryst. Eng. Comm. 14 (2012) 2630.

[34]   B.M. Reddy, G.K. Reddy, I. Ganesh, J.M.F. Ferreira, J. Mater. Sci. 44 (2009) 2743.

[35]   M. Yashima, T. Takizawa, J. Phys. Chem. C 114 (2010) 2385.

[36]   D.H. Prasad, S.Y. Park, H.I. Ji, H.R. Kim, J.W. Son, B.K. Kim, H.W. Lee, J.H. Lee, J. Phys. Chem. C 116 (2012) 3467.

[37]   H. Najjar, H. Batis, Appl. Catal. A: Gen. 383 (2010) 192.

[38]   J.R. Mc. Bride, K.C. Hass, B.D. Poindexter, W.H. Weber, J. Appl. Phys. 76 (1994) 2435.

[39]   J.E. Spanier, R.D. Robinson, F. Zhang, S.W. Chan, I.P. Herman, Phys. Rev. B 64 (2001) 245.

[40]   B.M. Reddy, G.K. Reddy, I. Ganesh, J.M.F. Ferreira Catal. Lett. 130 (2009) 227.

[41]   B.M. Reddy, K.N. Rao, G.K. Reddy, A. Khan, J. Phys. Chem. C 111 (2007) 18751.

[42]   S.F. Parker, Chem. Commun. 47 (2011) 1988.

[43]   T. Mokkelbost, I. Kaus, T. Grande, M.A. Einarsrud, Chem. Mater. 16 (2004) 5489.

[44]   A. Trovarelli, Comments Inorg.Chem. 20 (1999) 263.

[45]   K.N. Rao, P. Bharali, G. Thrimurthulu, B.M. Reddy, Catal. Commun. 11 (2010) 863.

[46]   J.Y. Luo, M. Meng, Y.Q. Zha, L.H. Guo, J. Phys. Chem. C 112 (2008) 8694.

[47]   G.A. Sawatzky, D. Post, Phys. Rev. B 20 (1979) 1546.

[48]   J. Stubenrauch, J.M. Vohs, J. Catal. 159 (1996) 50.

[49]   A. Burroughs, A. Hamnett, A.F. Orchard, G. Thornton, J. Chem. Soc. Dalton Trans. 1 (1976) 1686.

[50]   C.D. Wagner, W.M. Riggs, L.E. Davis, J.F. Moulder: Handbook of X-ray Photoelectron Spectroscopy. (Edited by G.E. Muilenberg) Perkin-Elmer Corporation: Eden Prairie, MN, 1978.

[51]   M. Boaro, M. Vicario, C. de Leitenburg, G. Dolcetti, A. Trovarelli, Catal. Today, 77 (2003) 407.

[52]   G.K. Reddy, G. Thrimurthulu, B.M. Reddy, Catal. Surv. Asia, 13 (2009) 237.

CHAPTER 4

STUDIES ON CeO$_2$-M$_x$O$_y$ (M=Fe, Co, Mn) FOR CO OXIDATION

4.1.   Introduction

There has been a great interest in scientific research towards synthesizing new catalysts which are more advantageous to environmental issues [1-7]. In recent times, air pollution is being one of the major problems reported globally. Exhaust gas from automobiles is being the major cause for air pollution. Therefore treating exhaust gas of automobiles is necessary and development of Three-way catalyst (TWC) to transform hazardous gases such as CO, NO$_x$ and hydrocarbons to less hazardous gases or environmental friendly gases has become one of the interesting topics of research. Ceria is the main ingredient present in formulation of TWC [1-4], because of its ability to play an important role in oxygen storage and release by filling and releasing oxygen from oxygen vacancies under oxygen rich (oxidizing) and oxygen poor (reducing) conditions respectively to stabilize air to fuel oxygen ratio at desired levels [4]. However, oxygen storage/release capacity of ceria plays an important role in this concern.

Synthesis and design of new catalysts for the CO oxidation plays a significant role in the field of heterogeneous catalysis due to the stringent environmental conditions laid down during the past several years [8]. The research and development activities were concerned with development of catalysts which have higher thermal stability along with the good activity and selectivity. There are various metals and metal oxides, which shown the activity in reducing the CO concentration levels [9]. Among the various metal oxides screened cerium dioxide CeO$_2$, a known rare-earth oxide has found to be great importance in the field of catalysis and is most important catalyst in particular to CO oxidation [10, 11]. This is due to its rapid change in the valence state from +4 to +3 and vice versa depends on the surrounding atmosphere with the formation of oxygen vacancies [10-12]. Besides this when there is a change in the bulk ceria particles to nano regime, the particles have expected increase in the performance of redox properties to many fold. This is owing to its easy availability of both surface and bulk oxygen compared the bulk ceria relatively [13]. Therefore nano ceria grabbed an attention in the catalysis filed for various

applications. However, in general as the temperature increases the nanoparticles will form aggregates and leads to the formation of bulk particles [14]. Hence at elevated conditions ceria loses its intriguing properties such as surface area, oxygen storage capacity, etc. There could be an alternative way to avoid this drawback. One such could be modifying the ceria by doping with other metal ions. In the literature it is reported that the aforesaid issues were addressed. Apart from the stability, upon doping with other metal ions it is expected to be change, of novel structural and electronic properties of cerium dioxide [15-17].

Even though extensive studies are conducted on ceria, many of the physio-chemical properties get affected under elevated temperatures [18,19]. Modifications of ceria solid solutions are to develop an efficient catalyst formulation for treating the exhaust gas from automobiles and few more applications. Doping ceria with other metals, increases surface area and sustain towards sintering on exposure to higher temperatures for a longer duration, because of mixed oxide cations co-operation [20,21]. On further combination of different cations to oxide matrix produce solid solution samples with novel properties resulting in high catalytic activity.

Besides, there are a wide range of bio applications and technological applications those are benefited from this unique redox properties and transportation properties of ceria and ceria-based oxide materials [6,7,22-26]. As ceria and ceria-based oxides are reported with wide range of applications there is a huge demand for synthesizing in different sizes and morphologies. Doping ceria with other metals and metal oxides, it's easy to modify the structure of ceria crystal leading to changes in physiochemical properties. It is reported that at lower reduction temperatures compared to pure ceria, ceria based mixed oxide materials exhibited enhancement in OSC [27-30].

Ceria has been doped using a wide range of variable and invariable cations (transition and rare earth metal cations), since the host lattice is compatible to different types of substitutions [31, 32-34]. Here the metal cation doped plays a vital role in modification of physiochemical properties of mixed oxide produced. Oxidation state of doped metal ion is the deciding factor of oxygen vacancies concentration present in mixed

oxide produced, and energy of association between doped ion and oxygen vacancy decides the mobility of oxide ions / oxygen vacancies. To enhance the physiochemical properties of ceria by doping with metal cations, an appropriate ratio of dopant to host lattice has to be maintained to retain cubic crystalline structure of ceria. This facilitates oxygen migration through a channel that favors OSC.

Hence among the doped metals, transition metals have played a significant role because of their variable valency states and considerable redox properties. Among the different transition metals, Mn, Fe, Co has gained recent interest pertaining to the field of catalysis. Various literature reports were established with these metals for numerous catalytic applications [9, 35, 36]. It is observed that these metals have strong influence on the reduction properties and oxygen storage capacity of ceria upon doping by creating the lattice defects and oxygen vacancies. These vacancies and defects are the path makers for the mobility of oxygen atoms from the bulk to the surface and vice versa for the ceria particles. There by the easy liability of oxygen from the ceria particles leads to the requirement of low temperature for the aimed reaction.

This chapter was aimed at the doping of ceria with the Mn, Fe and Co for the carbon monoxide oxidation reaction which are synthesized by the MWCS method. The structural characterization has been examined using XRD, Raman, XPS, TPR and BET surface area techniques. The catalytic performance was considered for OSC and CO oxidation activity.

4.2.   Experimental Section

Transition metal (Fe, Mn, Co) doped ceria samples were synthesized using MWCS and for the purpose of comparison of physiochemical properties pure ceria is also synthesized. CeO_2, Ce−Mn, Ce−Fe, Ce−Co are synthesized and for handiness the obtained catalysts were coded as follows MC, MCM, MCF, MCC respectively. The ratio between the Ce and the respective dopants are kept 7:3 for all the catalysts. The structural

elucidation of synthesized catalysts has been carried out by physiochemical characterizations such as XRD, Raman, TPR and BET surface area techniques.

4.3   Results and Discussion

The recorded XRD patterns were shown in the figure 4.1. XRD patterns obtained for MC, MCM, MCF, MCC exhibit similar peaks as a cubic fluorite like structure of ceria. Diffractograms of MC, MCM, MCF, MCC have no peaks related to dopant metal oxides [8, 9, 35].
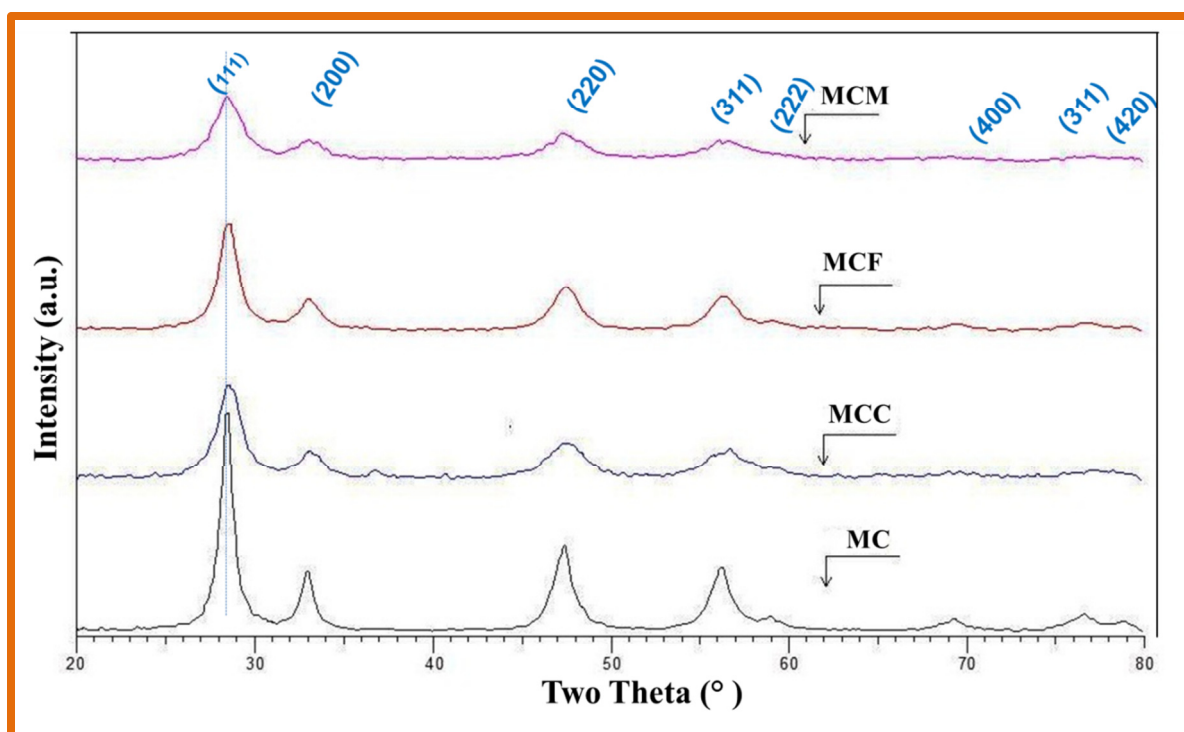
Figure 4.1:   Powder XRD patterns of CeO$_2$ (MC), Ce–Mn (MCM), Ce–Fe (MCF), and Ce–Co (MCC) catalysts.

Absence of Mn$_2$O$_3$ peaks is explained as follows: Mn^{3+} ions are replacing in Ce^{4+} ions of fluorite crystal lattice because of similarity in structure [11]. It is also reported as Mn$_2$O$_3$ crystallizes only when the content of Mn is >50% while preparing the doped ceria [36, 37]. Absence of iron oxide peaks in diffractogram might be because of decrease in cell

parameters after doping iron oxide over the ceria [38]. Besides this cobalt oxide peak is also not reported in the diffractogram of doped ceria oxide. According to Kraum et al. [39], when Co is doped over ceria, titania, zirconia, cobalt oxide peak is absent only when doped over ceria. This is because of no crystallite formation of cobalt oxide. The increase in dispersion of cobalt accredidates there is an effectual Co-CeO$_2$ interaction. From the above discussed it can be generalized as effectual dispersion of amorphous metal oxides takes place over ceria base. There is a slight shift in position of standard CeO$_2$ peak in MCM, MCF, MCC samples [37, 38]. This indicates the formation of solid solutions. The formation of solid solution is confirmed by measuring the crystallite size and lattice parameter values shown in table 4.1. The lattice parameter values calculated for MCM, MCF, MCC are slightly smaller when compared to pure ceria. This phenomenon is due to the smaller ionic radius of the dopants when compared to the Ce^{+4}. In case of MCM, Mn^{2+} and Mn^{4+} have ionic radius of 0.083 nm and 0.065 nm respectively, and on comparison to Ce^{4+} (0.097 nm) it is lower. In case of MCF, Fe^{3+} have ionic radius of 0.064 nm, which is lower to pure ceria. It is reported in literature, that lattice parameter of Fe^{3+} doped ceria was high because of high proportions of oxide ions in the solid solution [40-42]. This might be because of different method of preparation in synthesizing Iron doped ceria. Co^{2+} and Co^{3+} ions have an ionic radius of 0.078 nm and 0.063 nm respectively, and comparatively lower radius to Ce^{4+} which is 0.097 nm [40-42].

Average crystallite size is calculated by considering the broadened peak of (111) plane at $2\theta=28.5°$, by employing Debye–Scherer equation. Doped catalysts have low crystallite size compared to pure ceria. Among the doped catalysts investigated, cobalt doped ceria has lower crystallite size compared to the manganese and iron doped catalysts, and MCF has higher crystallite size when compared to MCM and MCC. The order of crystallite size is follows: MC > MCF > MCM > MCC. Lattice parameter values of MC, MCM, MCF, and MCC are shown in the table 4.1. From the values obtained it is clear that metal ions have shown a great influence in decreasing the lattice parameters when compared to pure ceria. Among those, Co metal ion has shown much decrease in lattice parameter of ceria. The difference in lattice parameter is because when the dopant was introduced into the ceria lattice, size decreases by lattice contraction.

The BET surface area value was estimated on the catalysts and obtained values are denoted in table 4.1. The surface area was much improved for MCM, MCF, and MCC when compared to MC. Among the doped catalysts, MCC has shown higher surface area on comparison with MCM and MCF. As the MCM, MCF and MCC are composed of 3 wt % of Mn, Fe, Co respectively. Increase in content of Co on ceria above 2 wt % shows an increase in surface area activity. But when considered with Mn and Fe, increased surface activity is observed for only 2 wt %, and on further increase of wt % of metal shows a decrease in surface activity. Neri et al [43] considerations show an increase of iron content over ceria shows an increase in surface area. This is explained as increase in structural defects created, resulting in increase of surface area. This might be because of method of preparation also influence characterization of metal doped ceria samples.

Table 4.1. BET surface area, average crystallite size, lattice Parameter, oxygen storage capacity (OSC) and light off ($T_{1/2}$) temperature values of pure and transition metal doped CeO_2 mixed oxides.

Catalyst	Surface area (m^2/g)	Crystallite size (nm)	Lattice parameter (Å)	OSC μ mol of O_2/g ceria
MC	35	16	5.405	46
MCM	48	11	5.370	192
MCF	45	14	5.402	168
MCC	52	09	5.390	209

The Raman spectra of all the catalysts were recorded to investigate the metal-oxygen bond and lattice defects. Figure 4.2 shows the recorded spectra of all the catalysts as-synthesized. All the catalysts were shown an intense peak at ~461 cm^{-1}, which represents the Raman active F_{2g} mode of ceria and it can be viewed as symmetrical breathing mode of oxygen atoms surrounding the cerium cations (O-Ce-O) in the crystal lattice [39]. The less intense peak observed at ~580 cm^{-1} is because of presence of intrinsic defects created by the presence of Ce^{3+} ions. However there is a shift in the peak position

of F_{2g} to the left side, i.e. towards lower frequency for the doped ceria compared to pure ceria. This shift is due to the decreased crystallite size and lattice strain, which is induced by the dopants [44].
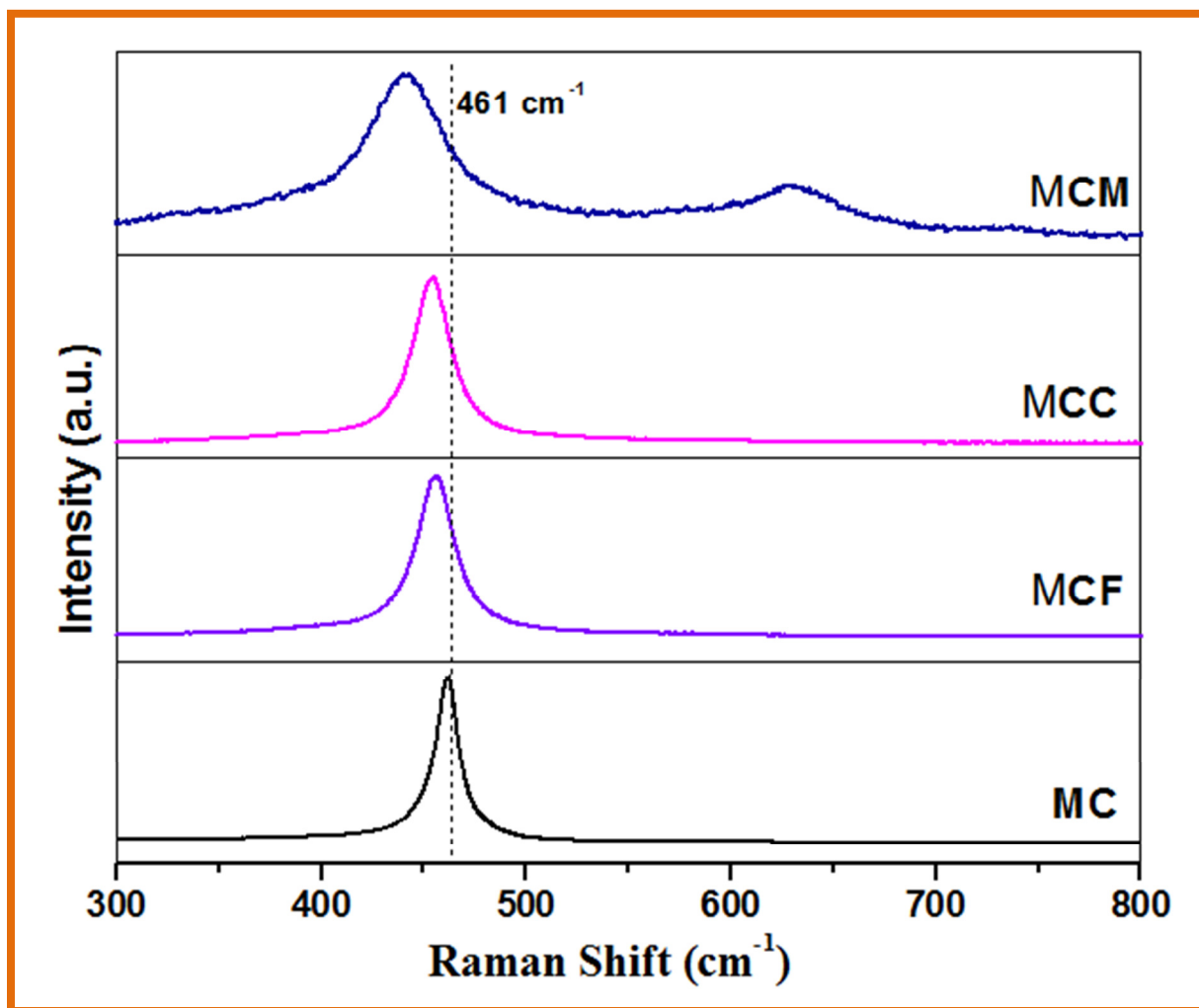
Figure 4.2:   **Vis-Raman spectra of CeO$_2$ (MC), Ce–Mn (MCM), Ce–Fe (MCF), and Ce–Co (MCC) catalysts.**

Apart from the shifting of the peaks towards lower frequency, there is a peak broadening for all the doped catalysts which is because of incorporated metals ions in the host lattice. It is noticed that there are bands pertaining to the individual oxides of cobalt, manganese and Iron [45, 46]. The presence of additional band in MCM at ~636 cm^{-1} is due to stretching of O-Mn-O of Mn$_3$O$_4$ crystallite solid phase, where as in MCF there are two

additional bands observed on the lower frequency side at 220 cm^{-1} and 285 cm^{-1} is due to presence of O-Fe-O vibrations. For MCC sample, a weak intense peak observed at 672 cm^{-1} represents the stretching peak of O-Co-O of Co_3O_4. However, these metal oxide peaks related to Mn, Fe, Co are not observed in XRD, because of effectual dispersion of amorphous metal oxides takes place over ceria base. Solid solution is formed between the dopants and ceria, also showed correlation with the XRD analysis [46].

CO oxidation reaction is strongly influenced by the redox nature of the catalysts which can be best studied by H_2 temperature programmed reduction experiment [47-49]. The consumption of the Hydrogen against the temperature of all the catalysts is shown in the figure 4.3.
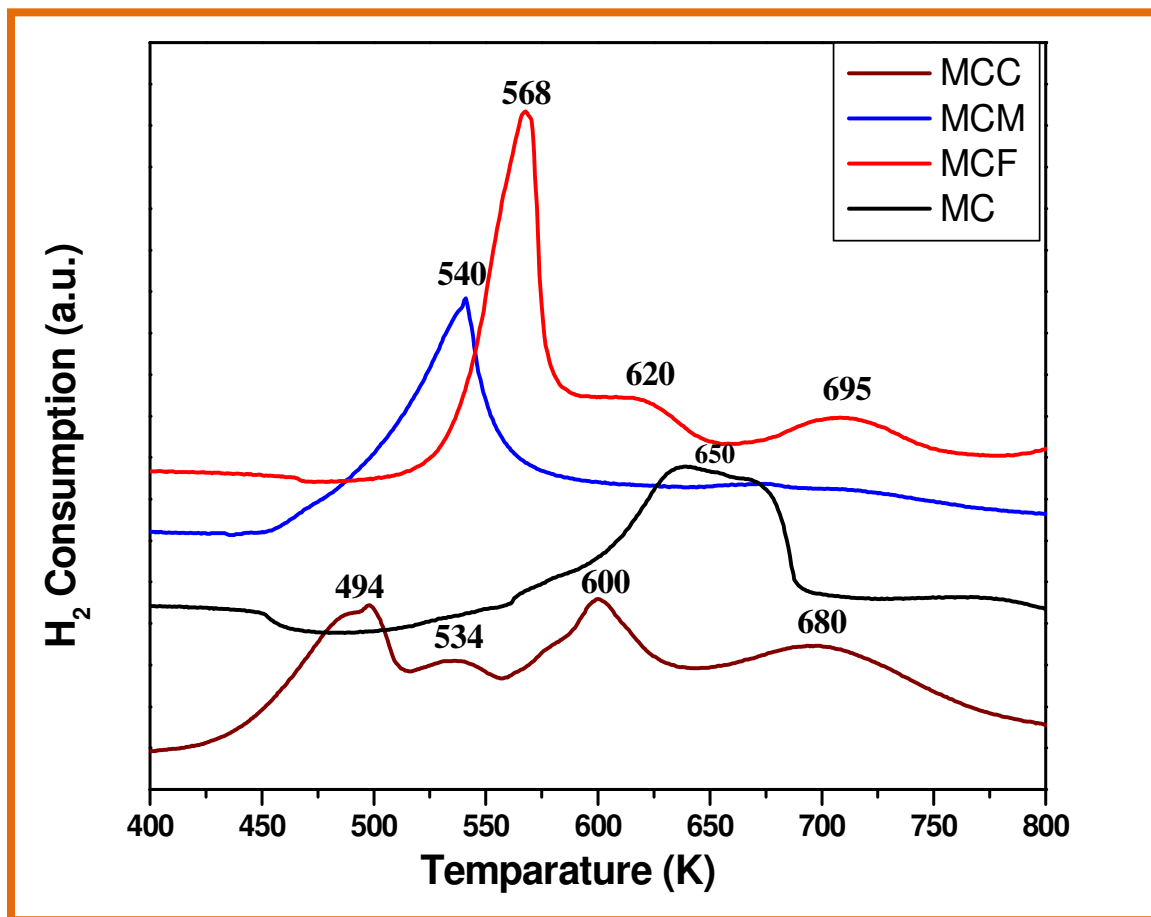

Figure 4.3:   **H_2 TPR profiles of CeO$_2$ (MC), Ce–Mn (MCM), Ce–Fe (MCF), and Ce–Co (MCC) catalysts.**

Interestingly the reduction profile patterns will vary strongly with the foreign ions doped into the ceria lattice. Among all the catalysts cobalt doped ceria catalyst exhibits lower reduction peaks located at 494 K, 534 K, 600 K and 680 K. First peak correspond to the reduction of Co_3O_4 to CoO, interacted with the ceria, second peak at (534 K) corresponds to reduction of CoO to Co, 600 K peak corresponds to reduction of surface reduction of ceria and 700 K peak corresponds to the reduction of bulk oxygen of ceria lattice [50]. The next low temperature reduced catalyst is manganese doped ceria catalyst peak corresponds to centers at 540 K with huge intensity which represents the reduction of manganese oxides (Mn-O-Mn) and surface oxygen reduction interaction with Ceria (Ce-O-Mn) [51]. Manganese oxides exhibit two step reduction, at first MnO_2/Mn_2O_3 is reduced to Mn_3O_4, which is further reduced to MnO. The iron doped ceria catalyst exhibits high temperature in reduction compared to cobalt and manganese doped ceria catalysts peaks centered at 568, 620, and 695 K represents the reduction of oxides of iron, as follows: $Fe_2O_3 \rightarrow Fe_3O_4$, consuming CeO_2 and overlapping with $Fe_3O_4 \rightarrow FeO$, followed by oxygen to bulk ceria followed by overlapping with FeO $\rightarrow Fe^0$ [52]. The reduction behavior of all the catalysts are in correlation with XRD patterns as the peaks were broadened with the doped catalysts compared to pure ceria and crystallite size and Raman shifting and BET surface area.

The oxygen storage capacity of the as-synthesized catalysts was measured. All the catalysts were shown higher OSC value compared pure ceria. In addition to the above there is three-four times increase in the OSC values compared to pure ceria. This is due to the solid solution formation between ceria and dopants. These values were shown in table 4.1. Interestingly among the doped catalysts MCC has high OSC compared to MCM and MCF. The OSC values order is as follows: MCC > MCM > MCF. This higher OSC value was due to presence higher proportions of labile oxygen from the surface and bulk level of ceria.

The catalytic activity of MC, MCM, MCF, and MCC in this present chapter was evaluated for CO oxidation. The conversion of CO against temperature is shown in figure

4.4. As the temperature increases, there is linear increase in the CO conversion for all the catalysts.
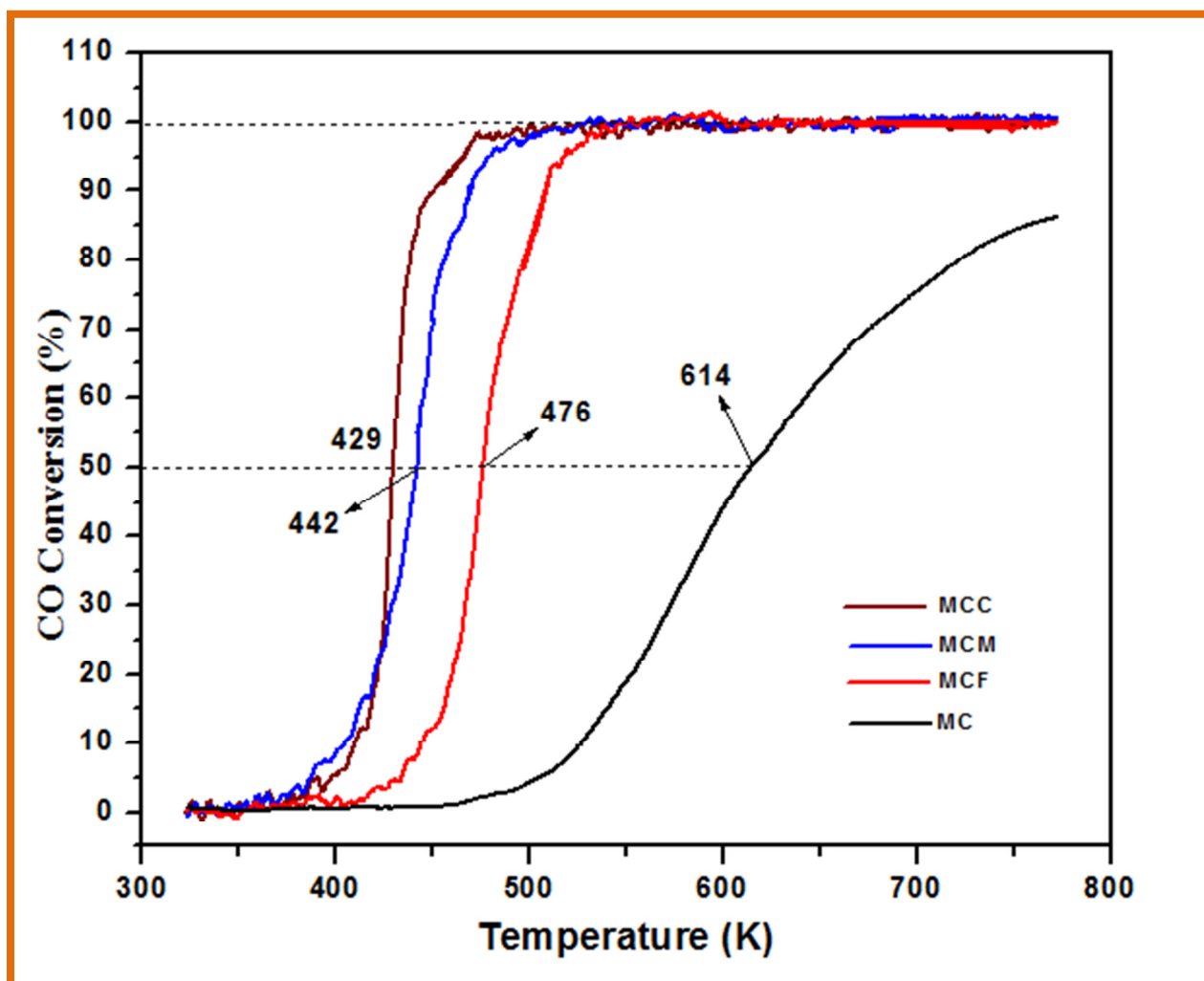
Figure 4.4:   Graph plotted between CO conversions against the reaction temperature of CeO₂ (MC), Ce–Mn (MCM), Ce–Fe (MCF), and Ce–Co (MCC) catalysts.

The doped ceria catalysts have shown better activity than pure ceria. The activity of MCM, MCF, and MCC catalysts were best compared with MC at light-off temperature i.e. temperature required for the 50% conversion (T 50) of carbon monoxide. Among the doped catalysts MCC have a T50 at 429 K whereas MCM and MCF has the T50 at 442 K and 476 K respectively. By observing these values it is concluded that MCC has best activity

compared to other counterpart catalysts. Besides this, all the doped catalysts have shown 100 % Carbon monoxide conversion. As well as the same trend as light–off temperature was reflected in the 100 % CO conversion also. Interestingly, the same is reflected in the oxygen storage capacity measurements. This shows that the CO oxidation involves both the surface, bulk reduction of the catalysts. Even the H_2TPR measurements support the activity trend. The better activity for the doped catalysts compared to bare ceria is due to the formation of solid solution between the dopants and ceria as confirmed from the XRD and Raman studies there by the creation of lattice defects, through which the diffusion of oxygen and storage of oxygen occurs.

There is some interesting literature available on the transition metal doped ceria catalysts. Reddy et. al [45, 53] studied the titled reaction over transition metal doped ceria, which were synthesized by the modified co-precipitation and hydrothermal synthesis with different morphologies. In co-precipitation method the best active catalysts was Mn doped ceria catalyst. On the other hand in hydrothermal synthesis Co doped ceria has shown better activity. In our present preparation method i.e MWCS Cobalt doped ceria shows better activity compared to other catalytic formulations. These cumulative observations lead us that the preparation method has a significant role in the physiochemical properties of ceria-based oxides. This might be due to the present preparation method employed is considerably very fast method which involves induction of combustion between the metal nitrates and fuel leading to the formation of solid solution.

4.4.   Conclusions

In summary, we have successfully adopted the MWCS method, for the synthesis of transition metal doped ceria and bare ceria in a single step by considering the advantages associated with it. The structural and physiochemical properties of the as-synthesized catalytic formulations were studied by XRD, Raman, BET surface area, and H_2-TPR. XRD and Raman studies confirm the formation of solid solution between ceria and the dopant metals. MCM, MCF, MCC have shown two fold increase in the surface area compared to bare ceria. The H_2 TPR measurements also confirm that the doped catalysts have reduced at

much low temperature especially the surface reduction which is key factor for the low temperature CO oxidation. The CO activity trend among the doped catalysts follows the order MCC>MCM>MCF>MC.

4.5.   References

[1]   Q. Fu, H. Saltsburg, M.F. Stephanopoulos, Science, 301 (2003) 935.

[2]   B.C.H. Steele, A. Heinzel, Nature, 414 (2001) 345.

[3]   M.F. Garcia, A.M. Arias, J.C. Hanson, J.A. Rodriguez, Chem. Rev. 104 (2004) 4063.

[4]   A. Trovarelli, in: Catalysis by Ceria and Related Materials, Catalytic Science Series, Hutchings, G. J. Ed., Imperial College Press, London, vol. 2, 2002.

[5]   A.M. Arias, A.B. Hungria, M.F. Garcia, J.C. Conesa, G. Munuera, J. Power Sources, 151 (2005) 32.

[6]   M. Machida, Y. Murata, K. Kishikawa, D. Zhang, K. Ikeue, Chem. Mater. 20 (2008) 4489.

[7]   B.M. Reddy, P. Bharali, P. Saikia, S.E. Park, M.W.E. van den Berg, M. Muhler, W. Grunert, J. Phys. Chem. C 112 (2008) 11729.

[8]   P. Venkataswamy, K.N. Rao, D. Jampaiah, B.M. Reddy, Appl. Catal. B: Environ. 162 (2015) 122.

[9]   D. Mukherjee, B. Govinda Rao, B.M. Reddy Appl. Catal. B: Environ. 197 (2016) 105.

[10]   G. Dutta, U.V. Waghmare, T. Baidya, M.S. Hegde, K.R. Priolkar, P.R. Sarode, Chem. Mater. 18 (2006) 3249.

[11]   K. Mudiyanselage,   H.Y. Kim, S.D. Senanayake, A.E. Baber, P. Liub, D. Stacchiola, Phys. Chem. Chem. Phys. 15 (2013) 15856.

[12]   N.V. Skorodumova, S.I. Simak, B.I. Lundqvist, I.A. Abrikosov, B. Johansson, Phys. Rev. Lett. 89 (2002) 166601-1.

[13]   G. Balducci, M.S. Islam, J. Kaspar, P. Fornasiero, M. Grazian, Chem. Mater. 12 (2000) 677.

[14]   B.M. Reddy, G. Thrimurthulu, L. Katta, J. Phys. Chem. C 113 (2009) 15882.

[15]   S. Collins, G. Finos, R. Alcantara, E. del Rio, S. Bernal, A. Bonivardi, Appl. Catal. A: Gen. 388 (2010) 202.

[16]   S.-L. Zhong, L.-F. Zhang, L. Wang, W.-X. Huang, C.-M. Fan, A.-W. Xu, J. Phys. Chem. C, 116 (2012) 13127.

[17]   X. Yao, C. Tang, Z. Ji, Y. Dai, Y. Cao, F. Gao, L. Dong, Y. Chen, Catal. Sci. Technol. 3 (2013) 688.

[18]   T. Masui, Y. Peng, K.I. Machida, G.Y. Adachi, Chem. Mater. 10 (1998) 4005.

[19]   H. Li, L. Zhang, H. Dai, H. He, Inorg. Chem. 48 (2009) 4421.

[20]   R. Wang, P.A. Crozier, R. Sharma, J.B. Adams, J. Phys. Chem. B 110 (2006) 18278.

[21]   X. Wang, J.C. Hanson, G. Liu, J.A. Rodriguez, J. Chem. Phys. 121 (2004) 5434.

[22]   K.J.D. Vries, G.Y. Meng, Mater. Res. Bull. 33 (1998) 357.

[23]   A.M. Arias, A.B. Hungria, M.F. Garcia, A.I. Juez, J.C. Conesa, G.C. Mather, G. Munuera, J. Power Sources, 151 (2005) 43.

[24]   J. Chen, S. Patil, S. Seal, J.F. McGinnis, Nat. Nanotech. 1 (2006) 142.

[25]   S. Patil, S. Reshetnikov, M.K. Haldar, S. Seal, S. Mallik, J. Phys. Chem. C 111 (2007) 8437.

[26]   J. Kaspar, P. Fornasiero, M. Graziani, Catal. Today, 50 (1999) 285.

[27]   P. Fornasiero, R.D. Monte, G.R. Rao, J. Kaspar, S. Meriani, A. Trovarelli, M. Graziani, J. Catal. 151 (1995) 168.

[28]   M. Ozawa, K. Matuda, S. Suzuki, J. Alloys Comp. 56 (2000) 303.

[29]   M. Boaro, A. Trovarelli, J.H. Hwang, T.O. Mason, Solid State Ionics, 147 (2002) 85.

[30]   J.A. Rodriguez, J.C. Hanson, J.Y. Kim, G. Liu, A.I. Juez, M.F. Garcia, J. Phys. Chem. B 107 (2003) 3535.

[31]   M. Luo, J. Chen, L. Chen, J. Lu, Z. Feng, Z. Li, Chem. Mater. 13 (2001) 197.

[32]   M. Alifanti, B. Baps, N. Blangenois, J. Naud, P. Grange, B. Delmon, Chem. Mater. 15 (2003) 395.

[33]   W. Shan, W. Shen, C. Li, Chem. Mater. 15 (2003) 4761.

[34]   M.M. Natile, A. Glisenti, Chem. Mater. 17 (2005) 3403.

[35]   B. Govinda Rao, D. Jampaiah, P. Venkataswamy, B.M. Reddy, Chemistry Select 1 (2016) 6681.

[36]   J. Zhang, J. Guo, W. Liu, S. Wang, A. Xie, X. Liu, J. Wang, Y. Yang European J. Inorg. Chem. 6 (2015) 969.

[37]   G. Thrimurthulu, K.N. Rao, D. Devaiah, B.M. Reddy, Res. Chem. Intermed. 38 (2012) 1847.

[38]   S. Royer, D. Duprez, Checatchem. 3 (2011) 24.

[39]   W.H. Weber, K.C. Hass, J.R. McBride, Phys. Rev. B 48 (1993) 178.

[40]   J-Y. Luo M. Meng, Y-Q. Zha, L-H. Guo, J. Phys. Chem. C 112 (2008) 8694

[41]   L. Kongzhai, W. Hua, W. Yonggang, L.J. Mingchun, Rare Earths, 26 (2008) 245.

[42]   G. Zhou, P.R. Shah, R.J. Gorte, Catal. Lett. 120 (2008)191.

[43]   G. Neri, A. Pistone, C. Milone, S. Galvagno, Appl. Catal. B: Environ. 38 (2002) 321.

[44]   D.W. Wheeler, I. Khan, Vib. Spectrosc. 70 (2014) 200.

[45]   D. Jampaiah, P. Venkataswamy, V. Elizabeth Coyle, B.M. Reddy, S.K. Bhargava, RSC Adv. 6 (2016) 80541.

[46]   D. Jampaiah, K.M. Tur, S.J. Ippolito, Y.M. Sabri, J. Tardio, S.K. Bhargava, B.M. Reddy, RSC Adv. 3 (2013) 12963.

[47]   J.E. Fallah, S. Boujana, H. Dexpert, A. Kiennemann, J. Majerus, O. Touret, F. Villain, F.L. Normand, J. Phys. Chem. 98 (1994) 5522.

[48]   S. Bernal, J.J. Calvino, G.A. Cifredo, J.M. Rodriguez-Izquierdo, J. Phys. Chem. 99 (1995) 11794.

[49]   E. Aneggi, M. Boaro, C. de Leitenburg, G. Dolcetti, A. Trovarelli, J. Alloys Compd. 408–412 (2006) 1096.

[50]   A. Jha, D.W. Jeong, Y.L. Lee, I.W. Nah, H.S. Roh, RSC sAdv. 5 (2015) 10302.

[51]   X. Tang, Y. Li, X. Huang, Y. Xu, H. Zhu, J. Wang, W. Shen, Appl. Catal. B: Environ. 62 (2006) 265.

[52]   D. Qiao, G. Lu, X. Liu, Y. Guo, Y. Wang and Y. Guo, J. Mater. Sci. 46 (2011) 3500.

[53]   P.V. Swamy, D Jampaiah, C.U. Aniz, B.M. Reddy, J. Chem. Sci. 127 (2015) 1347.

CHAPTER 5

STUDIES ON CeO$_2$ AND CeO$_2$-Sm$_2$O$_3$ FOR CO OXIDATION – INFLUENCE OF BALL MILL METHOD

5.1   Introduction

Cerium dioxide (CeO$_2$) has wide applications in the field of catalysis, even though its innovative properties are lost at higher temperatures for a long run in catalytic reactions due to rapid sintering. However, nanocrystallite ceria exhibits better catalytic activity and sinterability in comparison with coarse bulk material [1]. Nanocrystallite ceria has gained special interest of scientific research due to its peculiar physical and chemical properties with potential applications in present day situations.

Ceria exhibits high mechanical hardness, thermal stability, temperature coupled to redox activity, surface to volume ratio [2]. It exhibits unique UV absorptivity, optical characteristics [3, 4]. Pure ceria is a white crystalline solid, exhibits cubic fluorite structure. Nanocrystallite ceria is being a research interest because of its high chemical activity and surface area. Existed applications of ceria includes: as a promoter and support for three–way exhaust catalyst [5] and in fuel cells and gas sensors as oxygen ion conductor [6, 7].

From the reported work it is clear that ceria has been continuously used in material science research for developing scalable methods to synthesize nanocrystallite structures with different sizes, morphologies to study various applications involved with CeO$_2$ and doped-CeO$_2$ mixed oxides. Most of the chemical methods involved with synthesis of ceria aim to provide spherical particles with a high surface area, either weakly agglomerated or non-agglomerated. However, individual chemical methods produce solid solutions with different morphologies, defect densities resulting in different rates of catalytic activity.

To synthesize nanocrystallite ceria, numerous chemical methods are already reported in literature, very few of them includes: sol-gel techniques [8,9], microwave-assisted combustion synthesis [10], precipitation [11, 12, 13], micro emulsion [14], etc. Doping ceria with other metals, it's easy to modify the structure of ceria crystal leading to

changes in physiochemical properties. Among those different dopants reported, Sm^{3+} is one of the best dopant reported because of relatively close ionic radius with Ce^{4+}. Formation of solid solution is very important with a special emphasis for CO oxidation as there is involvement of surface and bulk oxygen in the catalytic reaction. Ceria-samarium based oxides are found to exhibit great properties towards low temperature solid oxide fuel cells. Yet these mixed oxides have to be explored in the CO oxidation reaction. As ceria and doped ceria are reported with wide range of applications, there is a huge demand for synthesizing in different sizes and morphologies.

In this chapter, we analyze CeO_2 and CeO_2-Sm_2O_3 samples obtained from MWCS and compared the results with those obtained after processing through ball mill method. To increase the CO oxidation activity, ball mill method was employed to CeO_2 and CeO_2-Sm_2O_3.

5.2   Experimental Procedure

The investigated CeO_2, CeO_2−Sm_2O_3 (8:2 based on oxide ratio) were prepared by MWCS and followed by Ball Mill Method. Complete preparation details are described under experimental section of chapter 2. The as-synthesized catalysts without any calcination are taken for analysis, for handiness named the prepared catalysts as MC for CeO_2, MCS for CeO_2−Sm_2O_3, MCB for ball milled CeO_2, and MCSB for ball milled-(CeO_2−Sm_2O_3).

5.3   Results and Discussions

XRD was employed on as-synthesized catalysts at room temperature in order to analyze crystalline phases and structural parameters (crystallite size, lattice parameter). XRD patterns obtained for MC, MCS, MCB, MCSB are shown in Figure 5.1. On detailed analysis of XRD patterns obtained for MC, MCS, MCB, MCSB had shown the resemblance with standard cubic fluorite phase of ceria, which are indexed as (111), (200),

(220), (311), (222), (400), and (420) [15, 16]. There are no patterns corresponding to oxides of samarium (MCS and MCSB).

Besides this, peak positions are slightly shifted to left side in all XRD patterns of samarium doped ceria [MCS, MCSB] compared to pure ceria [MC, MCB]. These shifts are observed because of variations in ionic radius of Sm^{+3} on comparison with Ce^{+4}.

All the above inferences confirm the formation of solid solution between samarium and ceria. Apart from this there is clear visualized crystallite peaks appeared for all the catalytic formulations which indicates that there is no requirement of further calcination unlike the other methods as enough crystallization was achieved. Required temperature for the crystallization of present catalysts is obtained from the flame generated during the synthesis for a short duration of time. This confirms the stoichiometry ratio between the metal nitrates and fuel is appropriate. In this MWCS the crystallization growth is very fast compared to other synthetic methods such as co-precipitation method, sol-gel method and hydrothermal method etc. For this reason all the catalysts obtained from MWCS have distinctive morphologies and properties. All the broadened diffraction patterns appeared for all the catalysts were due to the nano crystalline nature of sample.

There is an increase in extent of broadening when dopant samarium was introduced into the host lattice of ceria when compared to that of pure ceria. The peaks were further broadened for MCB, MCSB samples compared to MC, MCS samples respectively; this might be due to the ball milling procedure carried out on MWCS samples for 2 hrs.

The average crystallite size was calculated by considering one of most intense peak corresponding to (111) plane from the XRD patterns i.e. at around $2\theta = 28^0$ by applying the Debye–Scherer equation. The obtained average crystallite size was shown in the table 5.1. In case of pure ceria, crystallite size ranges from 8.9 to 32.5 nm [17] and the obtained is 14 nm for pure ceria. It is clearly evident that the samarium doped catalyst has a low crystallite size compared pure ceria. There is further reduction in average crystallite size when both the samples i.e. MC, MCS are ball milled. However, the ball milled ceria (MCB) has

bigger crystallite size when compared to the MCS. This gave the conclusion that the samarium doped ceria catalysts forms a solid solution which gives greater stability to the fluorite structure. The same peak i.e. (111) was used for calculation of lattice parameter which was also given in table 5.1. There is a slight increase in the values of lattice parameter for MCS, MCSB samples compared to MC, MCB. These shifts are observed because of variations in ionic radius of Sm^{+3} on comparison with Ce^{+4}.
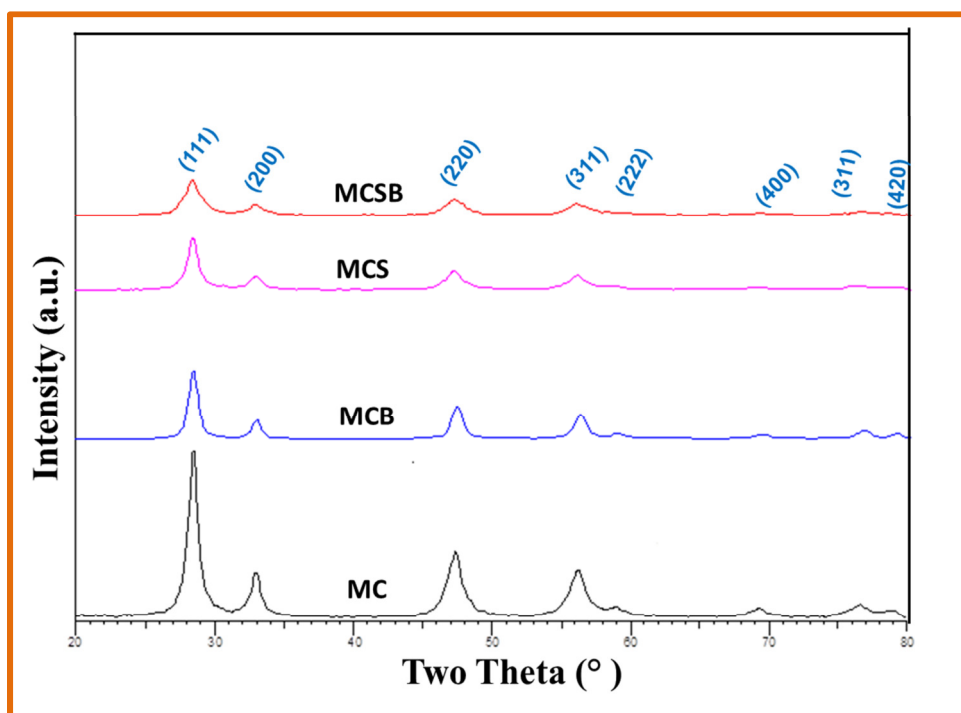

Figure 5.1: **Powder XRD patterns of CeO$_2$ (MC), CeO$_2$–Sm$_2$O$_3$ (MCS), and ball mill- CeO$_2$ (MCB), ball mill-CeO$_2$–Sm$_2$O$_3$ (MCSB) catalysts.**

Table 5.1 BET surface area, average crystallite size, lattice parameter, and oxygen storage capacity (OSC) values of Ceria and CeO$_2$–Sm$_2$O$_3$ solid solution.

Catalyst	Surface area (m^2/g)	Average Crystallite size (nm)	Lattice parameter (Å)	OSC μ mol of O$_2$/g ceria
MC	35	14	5.405	46
MCB	49	9	5.417	82
MCS	52	11	5.432	186
MCSB	70	7	5.441	234

The Raman spectroscopy was frequently employed to characterize the fluorite structure based oxides such as ceria and its mixed oxides. Generally the + 3 cations were introduced into the ceria lattice; it is expected to create oxygen vacancy in order to maintain electrical neutrality/electrostatic balance. The Raman spectrum is very sensitive to these kinds of vacancies. Hence, Raman spectroscopy was employed on the present catalysts and the obtained spectrum was shown in the Figure 5.2.

In the spectra, there is a strong intense peak for the catalytic formulations visualized at ~460 cm^{-1} equivalent to the symmetrical stretching of oxygen atoms around Ce atom (O-Ce-O) in a vibration unit with 8-fold coordination of ceria lattice which is generally denoted as Raman active F_{2g} band [18].
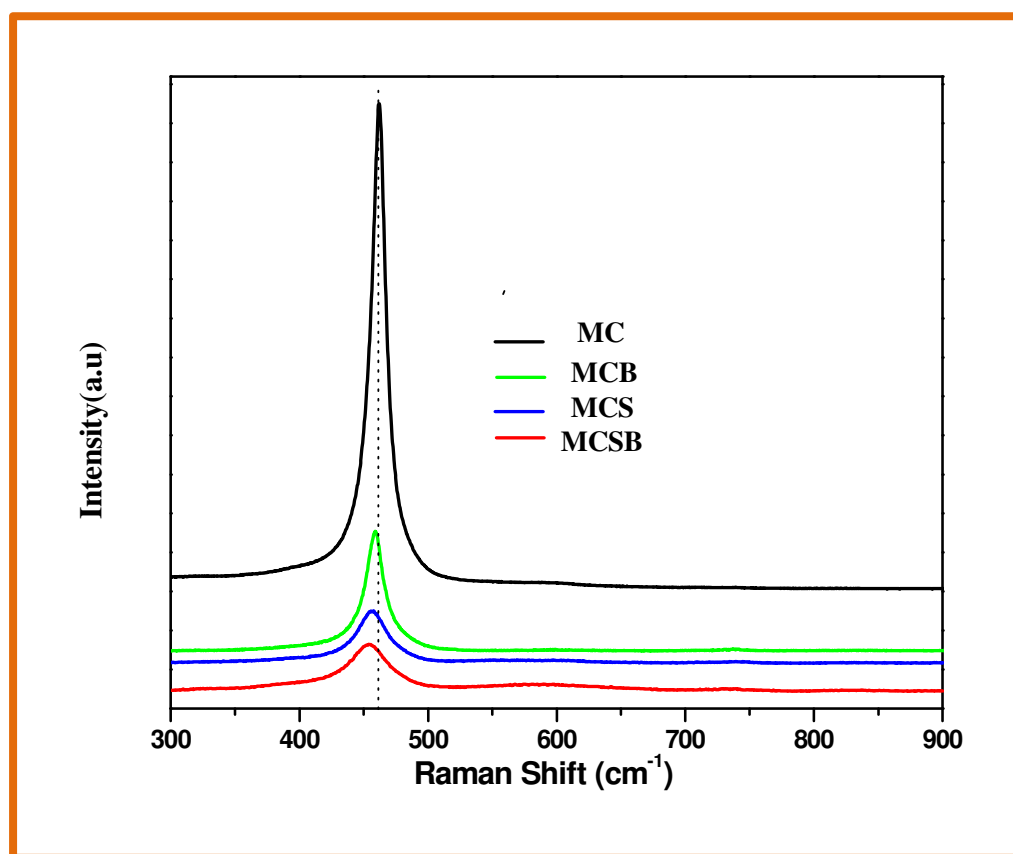

Figure 5.2: **Vis-Raman spectra ofCeO$_2$ (MC), CeO$_2$–Sm$_2$O$_3$ (MCS), and ball mill-CeO$_2$ (MCB), ball mill-CeO$_2$–Sm$_2$O$_3$ (MCSB) catalysts.**

In addition to this there is a small hump centered at 600 cm^{-1} for MC, MCB. On the other hand for MCS and MCSB catalysts a slit appears on the small hump, which are broad and continuously spread from 520 - 630 cm^{-1}. The slit in hump peak at 550 cm^{-1} for MCS and MCSB samples is due to the oxygen vacancy created for neutralizing the electronic charge between Ce^{+4} and Sm^{+3} and the peak at 600 cm^{-1} corresponds to the intrinsic oxygen vacancies. Further, upon comparing the intensity of peaks i.e. at 520-630 cm^{-1} there is an exponential increase in peak intensity of the samarium doped catalyst when compared with the pure CeO_2.

Besides this, it is evident the most intense peak at 460 cm^{-1} has been much broadened for all the catalysts. This indicated the nano crystalline nature of all oxides. Close examination of the Raman spectra reveals that assimilation of Sm^{3+} into the crystal lattice of CeO_2 significantly enhanced the number of defects or oxygen vacancies generated. The intensity of peak was decreased when the host lattice of ceria is doped with Samarium. Further increase in peak broadening was observed for MCB, MCSB. This indicates that doping, ball milling have shown strong influence on the Raman signals, which was evident from defect peak position as well as the main intense peak.

As the catalyst was ball milled there is a decrease in average crystallite size which impacted on the Raman signal. The decrease in crystallite size is also evident from XRD study. This indicated that the Raman peaks were also sensitive towards crystallite size. The same trend was observed for MCS, MCSB. It is also visualized that there is no peaks corresponding to samarium oxides or its daughter oxides in the Raman spectrum, which gives the conclusion that the unique formation of solid solution between Ce^{3+} and Sm^{3+} as evident in X-ray diffraction pattern. From the above illustrations it is evident that, significant role is being played by ball milling procedure on MWCS catalysts [MC, MCS].

UV-Vis DRS is one of the cheaper and easiest techniques to study the properties of metal oxides such as coordination environment and chemical valence of the metals on the surface. The present synthesized catalysts were examined in the wave length range of 200-800 nm. As cerium dioxide is strong UV-blocking agent, it absorbs the UV-light in

between the 250 to 400 nm. The recorded spectrum of all the synthesized catalysts is shown in the Figure 5.3.

All the peaks appear below to 400 nm indicates the charge-transfer transitions between Ce 4f levels and O 2p levels in MC, MCS, MCB, MCSB [18]. It shows that the ceria and ceria based materials are strong UV light absorbers.
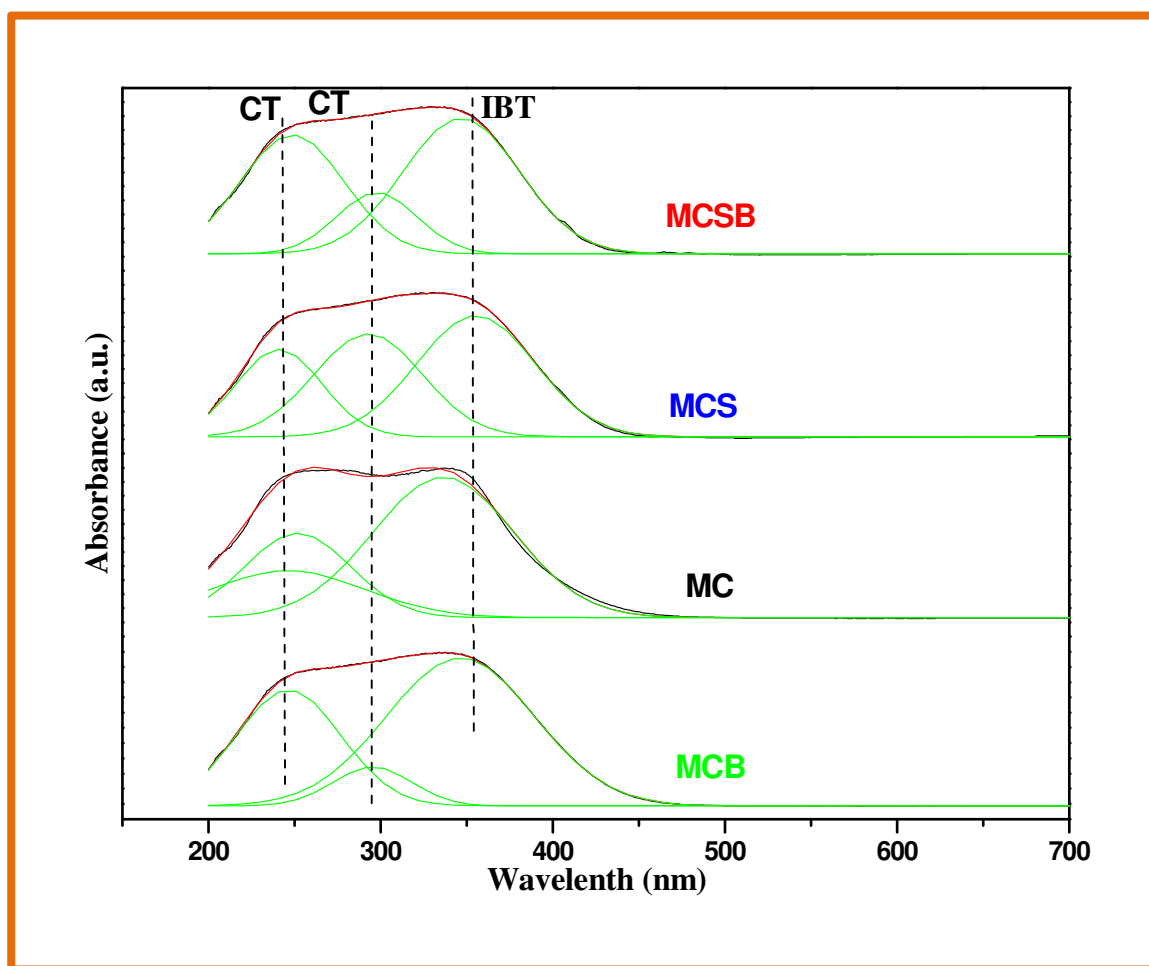

Figure 5.3: **UV-Vis DR spectra ofCeO$_2$ (MC), CeO$_2$–Sm$_2$O$_3$ (MCS), and ball mill-CeO$_2$ (MCB), ball mill-CeO$_2$–Sm$_2$O$_3$ (MCSB) catalysts.**

Apart from the absorption of light in the UV range no other information is extracted from the plot, hence we deconvoluted the peaks into three and those peaks are spotlighted at 255 nm, 282 and 300 nm. First two bands are metal to ligand charge transfer bands

corresponding to O^{2-} to Ce^{3+} and O^{2-} to Ce^{4+} and the later represents the inter band transitions [19]. The band at 255 nm gives information about the oxygen vacancies, as the peak relates to charge transfer of oxide ion to the Ce^{3+}. More intense peaks at 255 nm are observed for MCS, MCSB compared to MC, MCB are relating to the formation of ceria and the dopant.

Generally, metal oxides have the property of reducibility because of their variable oxidation states. Among the metal oxides CeO_2 belongs to the rare earth oxide with the property to reduce from Ce^{+4} to Ce^{+3} under reducing moiety and oxidize from Ce^{+3} to Ce^{+4} under oxygen rich environment.

Carbon monoxide oxidation reaction is also strongly influenced by the reducibility of the catalytic materials. Hence, the temperature programmed reduction studies by passing hydrogen gas over the ceria-based oxides have attracted much attention. Investigating reducible ability of ceria-based materials is an important topic to be concentrated for studying CO oxidation activity, and H_2-TPR is the best technique to be performed to examine reducible nature of ceria and ceria- based oxides [20]. Variation in the subsequent reduction temperatures is resulted from difference in energies of migrated oxygen [21]. The reduction profiles of all the catalytic materials against temperature from room temperature to 1000 K are shown in the Figure 5.4.

Ceria and ceria-based metal oxides exhibit two stage reductions: surface reduction (occurs at lower temperature), bulk reduction (occurs at higher temperature). In general for pure ceria, surface reduction occurs at 790 K, bulk reduction occurs at 1000 K due to capping of oxygen on surface phase and lattice oxygen in bulk phase respectively [22].

The present catalytic formulations also showed the same reduction patterns. The existence of two different types of oxygen species is also conveyed by the XPS study which will be discussed in later sections of this chapter. Although all the catalysts have same type of reduction patterns, there is dissimilarity in the temperature at which their respective reduction takes place and also the intensity of the peaks appeared.
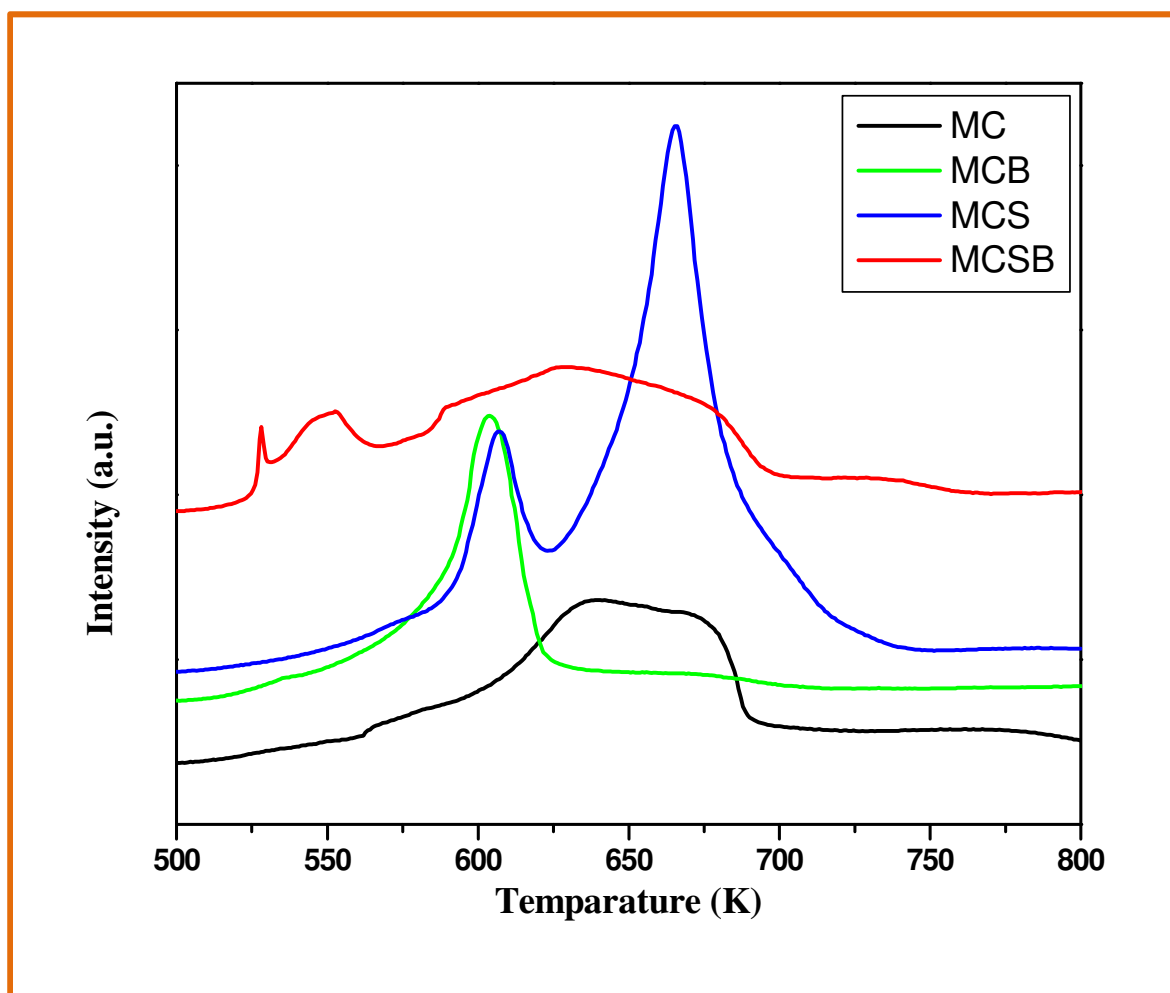
Figure 5.4: **H$_2$ TPR Studies of [CeO$_2$, (MC)], [CeO$_2$–Sm$_2$O$_3$ (MCS)], and [ball mill CeO$_2$ (MCB)], [(ball mill-CeO$_2$–Sm$_2$O$_3$) (MCSB)] catalysts.**

Pure ceria (MC) has shown a surface reduction at 653 K and the bulk reduction take place (with lesser intensity) at 773 K. Ball milling procedure had shown huge impact on surface reduction profiles of MCB sample. The surface reduction peak of MCB appeared at 605 K (lower temperature to MC), which is owing to increased surface area and decreased crystallite size. However, the ball milling method has no influence on the intensity of bulk reduction peaks for MCB sample which are same as MC catalyst.

On other hand, MCS and MCSB catalysts also showed surface and bulk reductions. Interestingly, for these catalysts there is large improvement in the bulk

reduction profiles occurred at 665 K and 635 K respectively. As the bulk reduction peak is visualized with huge intensity. These results from the smaller crystallite size and bigger surface area compared to the pure ceria catalysts (MC, MCB). H_2-TPR profile of MCS occurs at lower temperature compared to MC. This is probably from weakened Ce-O bond caused by doped Sm^{3+}. This relates to the induced structural modifications of host lattice (ceria) where, fewer Ce^{4+} ions are substituted by Sm^{3+}. Low reduction temperature of MCS sample might be due to the stronger interactions between Sm_2O_3 and CeO_2 ($Sm^{3+} \leftrightarrow Ce^{4+}$, $Sm^{3+} \leftrightarrow$ Oxygen $\leftrightarrow Ce^{4+}$). However, increased concentration of surface defects promote the H_2-adsorption over surface followed by dissociation of H_2, thereby resulting in improved consumption of H_2 [23]. Upon doping there is formation of oxygen vacancies which leads to easy liability of bulk oxygen by facilitating diffusion of oxygen to the surface of the catalyst. The formation of more oxygen vacancies over the surface is supported from the data of Laser Raman, XPS, and UV-Vis DRS studies.

However, the catalyst MCSB has shown three types of reduction peaks in contrast to others catalysts. The extra peak originated in MCSB is a result of sub surface reduction taking place which results from the drastic increase of surface area as well as decreased crystallite size of catalyst compared to their counterpart. The existence of three peaks was also pointed out in the literature for the samarium doped catalyst [24]. In addition to above bulk reduction peaks of MCSB appeared at much lower temperatures when compared to MC, MCB, and MCS. On the whole, compiling the reduction capability in terms of surface and bulk, the trend is as follows: MCSB>MCS>MCB>MC, this is because of implementation of ball milling procedure on catalytic samples prepared from MWCS.

XPS is the most efficient surface technique that can be applied over the catalytic materials to study the individual surface constituents and their oxidations states. We recorded XPS for all the catalysts, shown in the figures 5.5, 5.6, and 5.7 corresponding to Ce 3d core level spectra, O 1s spectra, and Sm 3d spectra respectively.
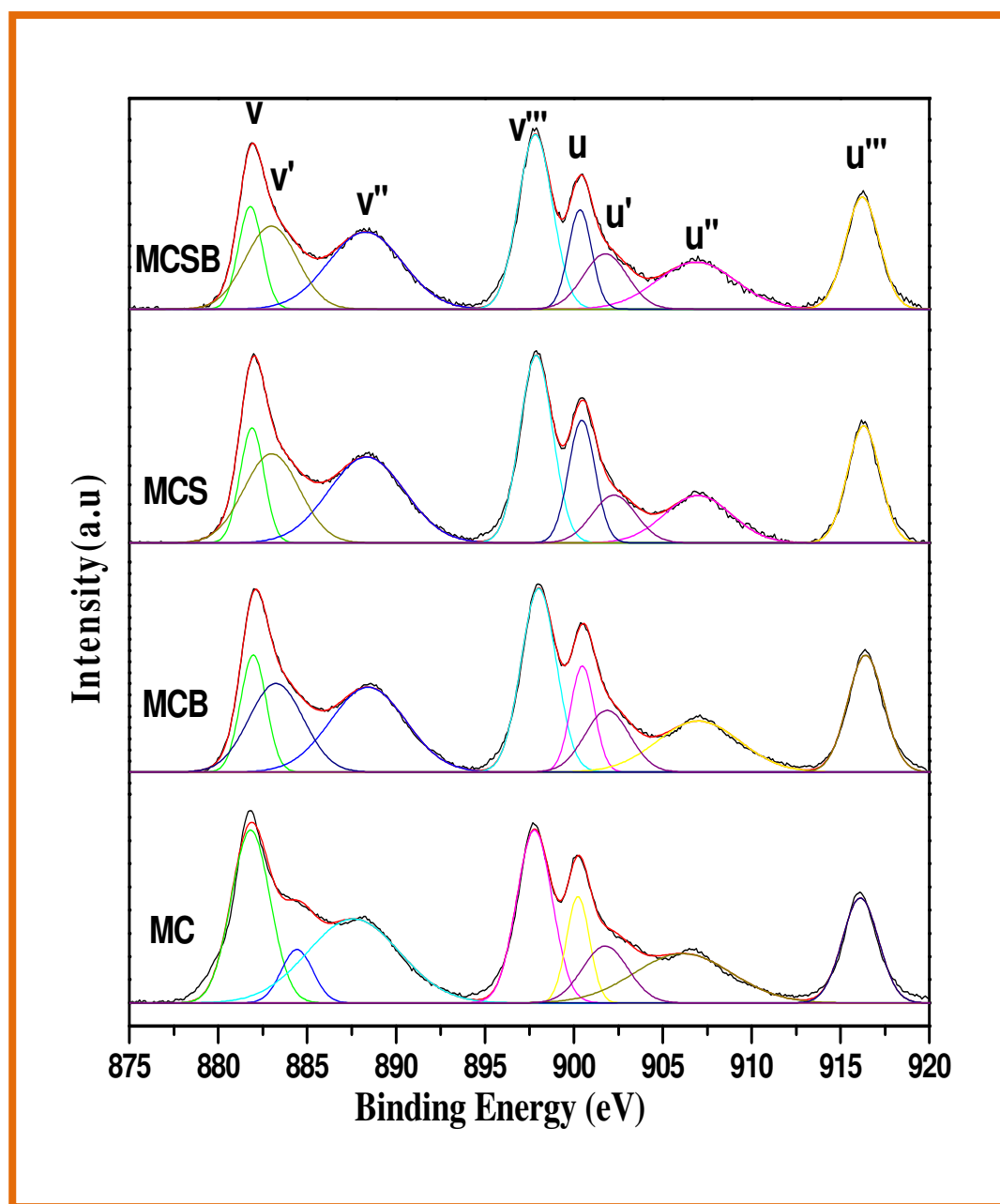
Figure 5.5:   **Ce 3d core level XPS profiles of CeO$_2$ (MC), CeO$_2$-Sm$_2$O$_3$ (MCS), ball mill-CeO$_2$ (MCB), ball mill-CeO$_2$-Sm$_2$O$_3$ (MSCB) catalysts**

From the Figure 5.5, the Ce 3d core level spectra is consisting two sets of peaks labeled as 'u' and 'v' featured as 3d$_{3/2}$ spin state, 3d$_{5/2}$ spin state, respectively [25, 26]. The peaks obtained within 880 and 897 eV related to Ce 3d$_{5/2}$ state where as peaks obtained

within 900 - 915 eV relate to Ce $3d_{3/2}$ state. From the figure 5.5 the spin-orbit states produced from photoemission of Ce 3d core level lead to 8 peaks [27]. According to the notation used in literature, the peaks 'u' and 'v' are assigned as main signals of Ce 3d and others are satellite. u′, v′ peaks correspond to Ce^{3+} ion and others correspond to Ce^{4+} ion.

Two peaks v′ and u′ appeared around 883 and 902 eV supports the Ce^{3+} ion presence, resulting from $3d^{10}4f^1$ configuration and remaining six peaks corresponds to Ce^{4+} ion due to $3d^{10}4f^0$ electronic configuration state [28]. Oxygen vacancies which are present in Ce-Sm samples support the above. From the above information Ce in 4+ and 3+ oxidation states coexist over the surface of samples comparatively high in Sm doped-Ceria. The intensity of v′ peak is increased for MCS, MCB, and MCBS when compared with MC.

The semi quantitative analysis of Ce^{3+} can be calculated by using the integrated peak areas(A) corresponding to their valence peaks by using the formula $[Ce^{3+}]/[Ce^{3+} + Ce^{4+}] = (A_{u'}+A_{v'})/ (A_u + A_{u''} + A_{u'''} + A_v + A_{v''}+A_{v'''})$ [29]. The percentage of Ce^{3+} present in all investigated catalysts is as follows MCSB (30%) > MCS (27%) > MCB (22%) >MC (18%).

Hence, from the above order, it is predicted that the same is observed for oxygen vacancy defect sites. The formation of defect peaks is also outlined from Laser Raman as well as UV-vis DRS. These defect sites also enhance reducible capacity of catalysts and OSC. MCB, MCSB has shown higher percentage of Ce^{3+} ions compared to MC, MCS respectively.

Figure 5.6 demonstrates the O 1s XPS of MC, MCS, MCB, and MCSB. Mainly two peaks are noticed from spectra with binding energies 529 eV and 532 eV corresponding to the lattice oxygen and surface oxygen respectively. The peak position was shifted towards higher binding energy side for MCS, MCB, MCSB compared to pure ceria (MC).
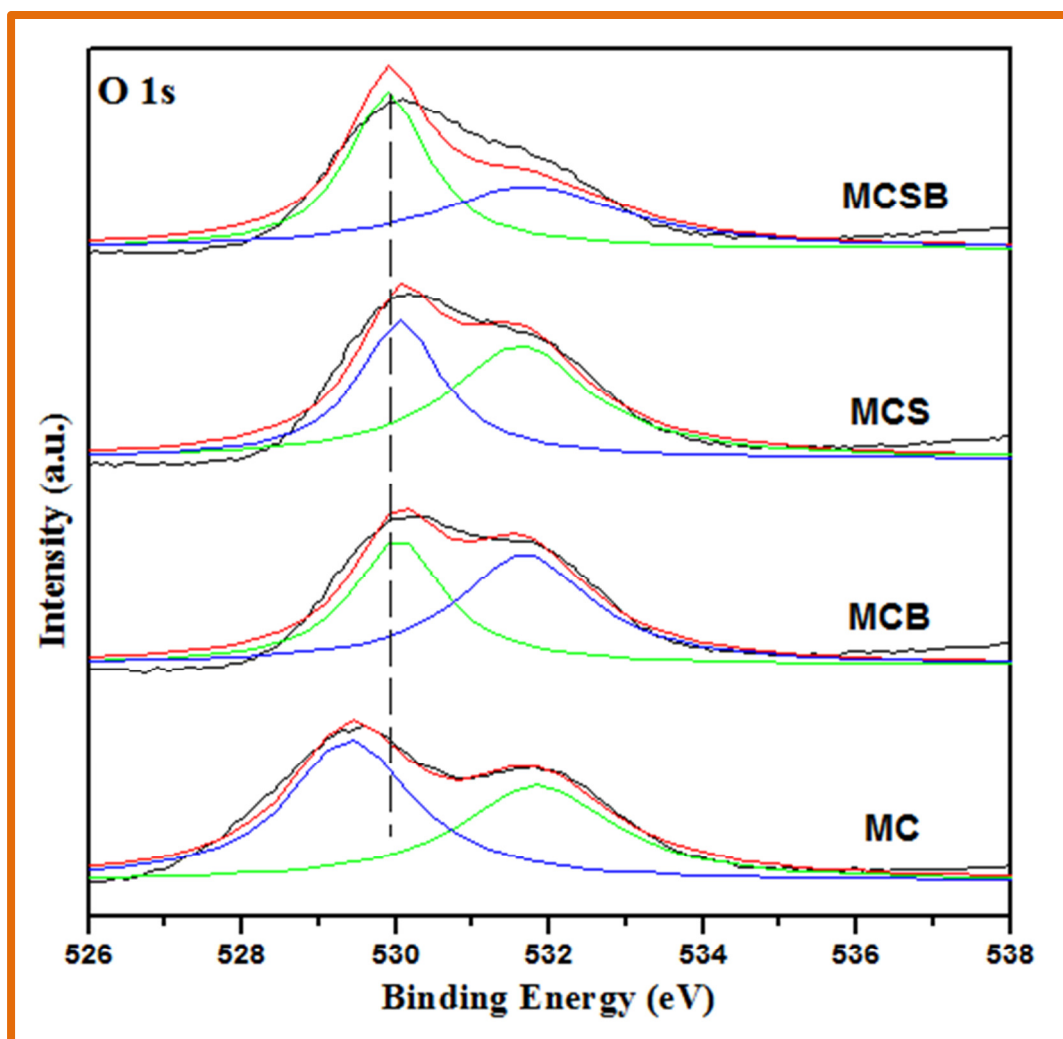
Figure 5.6:   O 1s XPS profiles ofCeO$_2$ (MC), CeO$_2$–Sm$_2$O$_3$ (MCS), and ball mill-CeO$_2$ (MCB), ball mill-CeO$_2$–Sm$_2$O$_3$ (MCSB) catalysts.

This indicates ball milling and Sm^{3+} dopant have shown significance effect on chemical nature of sample surfaces. Figure 5.7 demonstrates the Sm 3d core level spectra for MCS and MCSB catalysts. Major band observed for Samarium are at high binding energy side i.e. at 1084 eV and 1111 eV corresponds to 3d$_{5/2}$ and3d$_{3/2}$ spin-orbit states, indicates the ionization of Sm^{3+} [30, 31]. From the above it is evident that samarium exists on surface of MCS and MCSB in 3+ oxidation state.
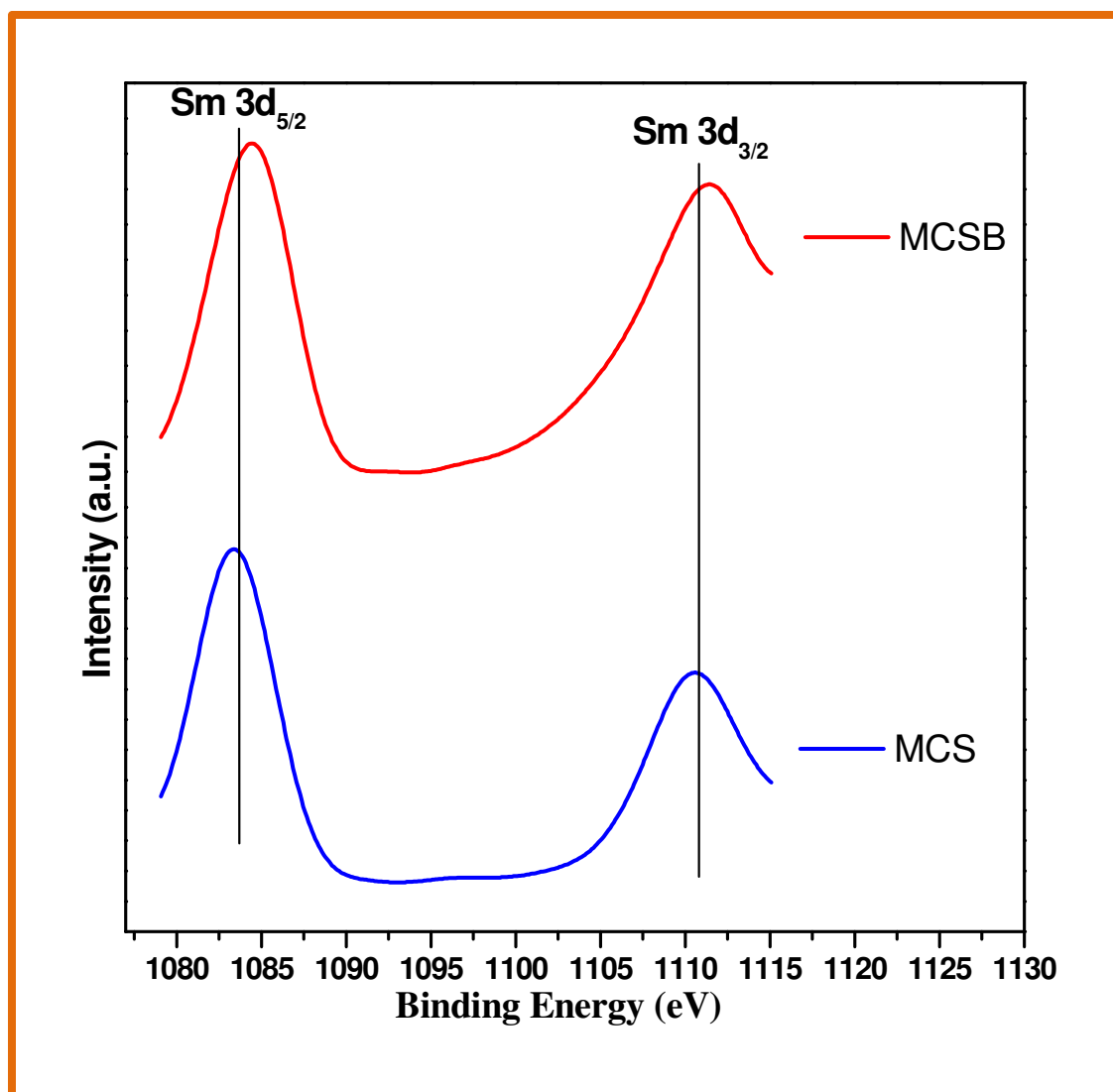
Figure 5.7: **Sm 3d XPS profiles of CeO$_2$–Sm$_2$O$_3$ (MCS) and ball mill-CeO$_2$–Sm$_2$O$_3$ (MCSB) catalysts.**

The specific surface area measurements, are carried on all the catalytic formulations and obtained valued are shown in the table 5.1.

The specific surface values of all the catalyst were improved compared to pure ceria synthesized by MWCS. Effect of preparation method has a significant role on the surface area values. Surface area of the MC catalyst is 35, whereas MCB surface area was increased dramatically i.e. almost two times. On the other hand surface area of MCS was 52 and MCSB was 70. This indicates ball milling procedure was effective on the doped

catalysts compared to the pure ceria catalysts. Furthermore the obtained surface area values correlate with XRD studies (Average crystallite size measured).

The oxygen storage capacity is one of the key factors for ceria and its mixed oxides as it indicates the redox couple involved between Ce^{4+} and Ce^{3+}. Hence, we measured OSC of all the catalytic materials in the temperature range of 373 K to 1073 K. In general, OSC migration of both surface and lattice oxygen will contribute to the total OSC measured. The obtained values indicate that MCS, MCSB have higher OSC values compared to the MC, MCB are given in the table 5.1. On comparison with pure CeO_2, the CeO_2-Sm_2O_3 mixed oxides showed higher OSC properties. From the above table it is also clear, that higher OSC values are observed for catalytic formulations after ball milling procedure. Since the defects generated while incorporating Sm^{3+} lead to easy creation of labile O_2 vacancy defects, those facilitated relatively high labile bulk lattice O_2 resulting in enhanced OSC values. This increase in OSC of the sample is accountable for improved redox activity thus increasing the number of "active oxygen" required for oxidation [32]. The observed OSC of MCS sample was found to be approximately 5 times greater than MC, and MCSB sample was found to be approximately times greater than MCB. This remarkable increase is mainly due to increase in oxygen vacancies, BET surface area and distortions of O^{2-} sub lattice. There is an increase in specific surface area, on doping Sm^{3+} into lattice of ceria. On doping Sm^{3+} into host lattice, smaller is the crystallite size. These resulted in increase of mobility of lattice oxygen which enhanced the OSC values of MCS sample compared to MC, MCSB sample compared to MCB.

CO oxidation activity of MC, MCS, MCB, MCSB is carried out from room temperature to 850 K under ambient conditions, is shown in the figure 5.8. It is noticed that the CO oxidation has improved linearly with increase in temperature. Most accepted mechanism involved with CO oxidation, is the Mars-van Krevelen-type [33], which was confirmed through isotopic studies by Liu et al. [34] that explains, $Ce^{4+} \leftrightarrow Ce^{3+}$ redox conversion results in surface defects and the restoration is successful with feed gas, used during oxidation of CO. Oxygen vacancies present in mixed oxides of ceria act as energetic centers for oxidation of CO [35].
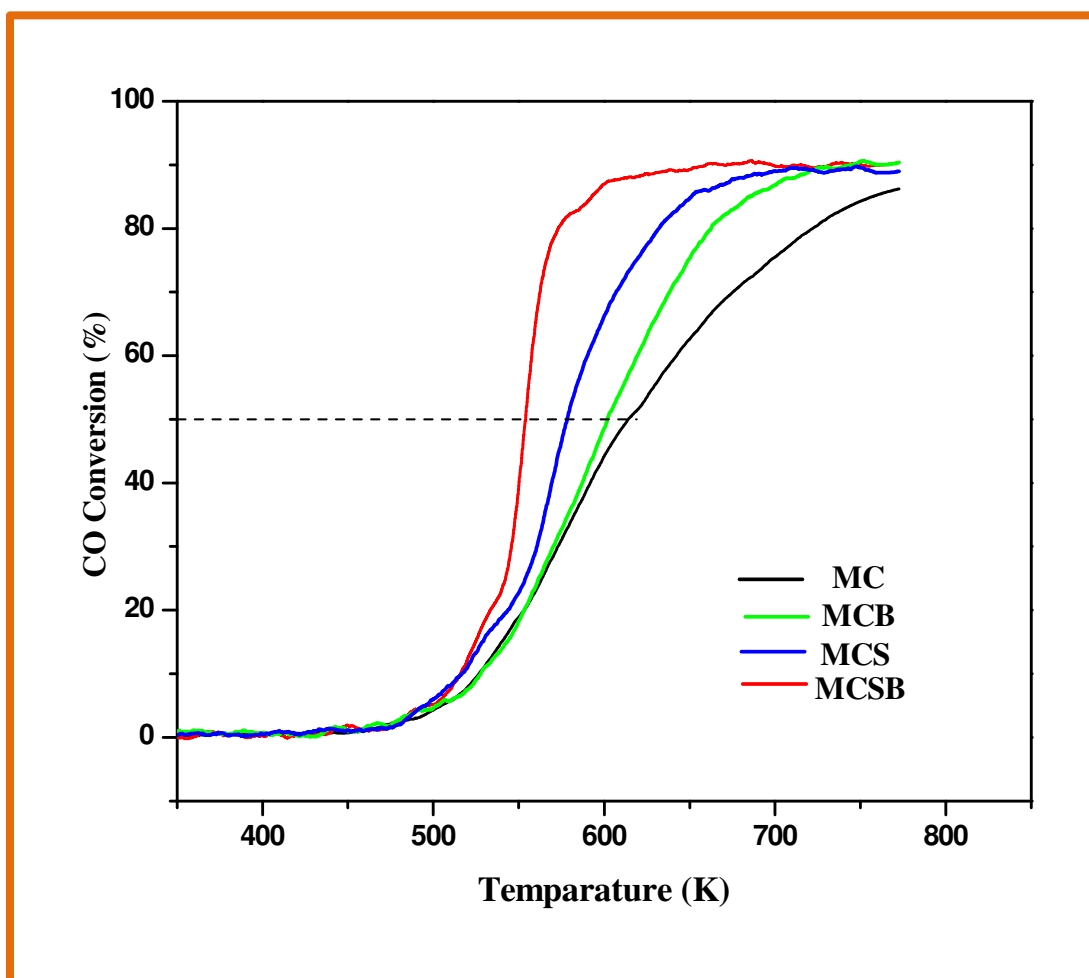
Figure 5.8:   **Graph plotted against CO conversion Vs Temperature of CeO$_2$ (MC), CeO$_2$–Sm$_2$O$_3$ (MCS), and ball mill-CeO$_2$ (MCB), ball mill-CeO$_2$–Sm$_2$O$_3$ (MCSB) catalysts.**

Among the studied catalysts, MCSB sample reflected in highest % of CO conversion and a lesser T50 compared to other catalytic formulations. The increased catalytic performance of MCSB sample might be due to the strong synergistic interactions between Sm$_2$O$_3$ and CeO$_2$ (Sm^{3+} ↔ Ce^{4+}, Sm^{3+}↔ Oxygen ↔Ce^{4+}), which also resulted in higher BET surface area, higher OSC, smaller crystallite size, enhanced surface reducibility. Even from Raman spectra it is revealed that incorporating Sm^{3+} into the lattice of ceria significantly enhanced the number of surface defects generated. Vacancies

generated play an important in catalytic performance of CeO_2 towards CO oxidation activity.

Catalytic performance of ceria and ceria based mixed oxides is explained by unique oxygen storage capacity of ceria and it is suggested as a suitable storage ingredient in formulations of TWC [36]. Noticed, that CO oxidation started at 465 K. To understand better, we included light-off temperature (T50) of ceria as reference, shown in table 5.1, at which 50% of CO conversion was achieved. Approximately a difference of 35 K is observed at T50 between MC and MCS, 12 K is observed at T50 between MC and MCB, 24 K is observed at T50 between MCS and MCSB. The activity trend among the catalysts is as follows MCSB>MCS>MCB>MC**.** From the observations it is revealed that doping of samarium as well as ball mill procedure has significantly enhanced the physiochemical properties of ceria towards CO oxidation. Further the CO oxidation order of samples is in direct correlation with the observations made from OSC values, average crystallite size, BET surface area values and TPR values.

5.4 Conclusions:

In summary, we have successfully prepared solid solution of samarium doped ceria ($Ce_{0.8}Sm_{0.2}O_2$) and bare ceria (CeO_2) by microwave induced combustion synthesis. In order to exploit the significance of this method we have adopted the Ball Mill method in conjunction with above method on the same catalysts. The physio-chemical properties of the MC, MCS, MCB, and MCSB were characterized and analyzed by following techniques: BET surface area, XRD, RS, TPR, UV-Vis DRS, XPS methods. The XRD and Laser Raman studies together confirm the solid solution formed between the guest ion i.e. samarium and host lattice ceria. After doping there is a substantial decrease in the average crystallite size and even further decrease in crystallite size values for the ball mill samples compared to their counter parts. Further, the Raman and XPS and UV-Vis studies also confirmed that there is an existence of oxygen vacancies in all the catalysts. The OSC values and H_2-TPR confirms that catalytic formulations showed an enhanced reducibility of the catalysts also. Samarium doped ceria catalysts obtained by both methods showed

enhanced reducibility compared to bare ceria. XPS line profiles and the subsequent BE's supported the presence of Ce^{3+} and Ce^{4+} ions. The CO oxidation activity was conceded over all prepared samples and the activity trend among the composition is as follows MCSB>MCS>MCB>MC. The activity studies were in excellent correlation with the various physiochemical properties of the catalytic formulation studied such as XRD, Raman, XPS, UV-Vis, and OSC. In short it is noticed that the implementation of Ball mill method on integration with microwave-assisted combustion synthesis, there is a significant improvement in physiochemical properties catalysts, there by the CO oxidation activity.

5.5   References

[1]   P. Fornasiero, R. Dimonte, G.R. Rao, J. Kaspan, S.Meriani, A. Trovarelli, M.Grazizni, J. Catal. 151 (1995) 168.

[2]   A. Trovarelli, C. Leitenburg, M. Boaro, G. Dolcetti, Catal. Today, 50 (1999) 353.

[3]   S. Tsunekawa, T. Fukuda, A. Kasuya, J. Appl. Phys. 87 (2000) 1318.

[4]   J. Spanier, R. Robinson, F. Zhang, S. Chan, I. Herman, Phys. Rev. B 64 (2001) 245407-1.

[5]   E. Bekyarova, P. Fornasiero, J. Kaspar, M. Graziani, Catal. Today, 45 (1998) 179.

[6]   H. Yahiro, Y. Baba, K.Eguchi, H. Arai, J. Electrochem. Soc. 135 (1988) 2077.

[7]   N.Izu, W. Shin, N. Murayama, S. Kanaki, Sensor. Actuat. B- Chem. 87 (2002) 95.

[8]   X. Chu, W. I. Chung, L. D. Schmidt, J. Am. Ceram. Soc. 76 (1993) 2115.

[9]   A.Makishima, H.Kubo, K.Wada, Y. Kitami, T.Shimohira, J. Am. Ceram.Soc. 69 (1986) C-127.

[10]   T. Masui, K. Fujiwara, K. I. Machida, G. Y. Adachi, Chem. Mater. 9 (1997) 2197.

[11]   W.P.Hsu, L. Ronnquist, E. Matijevic, Langmuir, 4 (1988) 31.

[12]   B. Djuricic, S. Pickering, J. Eur. Ceram.Soc. 19 (1999) 1925.

[13]   X. D. Zhou, W. Huebner, H. U. Anderson, Appl. Phys Lett. 80 (2002) 814.

[14]   O.H. Laguna, M.A. Centeno, M. Boutonnet, J.A. Odriozola, Appl. Catal. B: Environ. 106 (2011) 621.

[15]   M. J. Godinho, R.F. Gonçalves, L.P. Santos, J.A. Varela, E. Longo, E.R. Leite, Mat. Lett. 61 (2007) 1904.

[16]   G.R. Rao, H.R.Sahu, J. Chem. Sci. 113(2001) 651.

[17]   B.M. Reddy, G. Thrimurthulu, L. Katta, Catal. Lett. 141 (2011) 572.

[18]   P. Sudarsanam, B. Mallesham, P.S. Reddy, D. Gromann, W. Grunert, B.M. Reddy, Appl. Catal. B: Environ. 144 (2014) 900.

[19]   B.M. Reddy, L. Katta, G. Thrimurthulu, Chem. Mater. 22 (2009) 467.

[20]   F. Huang,Y. Zheng, Z. Li, Y. Xiao, Y. Zheng, G. Cai, K. Wei, Chem. Commun. 47 (2011) 5247.

[21]   D. Devaiah, D. Jampaiah, P. Saikia, B.M. Reddy, J. Ind. Eng. Chem. 20 (2014) 444.

[22]   I. Atribak, N. Guillen-Hurtado, A. Bueno-Lopez, A. Garcia-Garcia, Appl. Surf. Sci. 256, (2010) 7706.

[23]   N. Acerbi, S. Golunski, S.C. Tsang, H. Daly, C. Hardacre, R. Smith, P. Collier, J. Phys. Chem. C 116 (2012) 13569.

[24]   M. Wlodzimierz, A. Malgorzata, A. Malecka, P. K. Leszek, Appl. Catal. A: Gen. 368 (2009) 71.

[25]   D.R. Mullins, S.H. Overbury, D.R. Huntley, Surf. Sci. 409 (1997) 307.

[26]   A. Pfau, K.D. Schierbaum, Surf. Sci. 321 (1994) 71.

[27]   A. Bensalem, J.C. Muller, F. Bozon-Verduraz, J. Chem. Soc. Faraday Trans. 88 (1992) 153.

[28]   L. Katta, B.M. Reddy, M. Muhler, W. Grunert, Catal. Sci. Technol. 2 (2012) 745.

[29]   N. Sutradhar, A. Sinhamahapatra, S. Pahari, U. Jayachandra, Balasubramanian subramaniam, H.C. Bajaj, A.B. Panda. J. Phys. Chem. C 115 (2011) 7628.

[30]   M. Guo, J. Lu, Y. Wu, Y. Wang, M. Luo, Langmuir, 27 (2011) 3872.

[31]   Ch. Suzuki, J. Kawai, M. Takahashi, A.M. Vlaicu, H. Adachi, T. Muyokama, Chem. Phys. 253 (2000) 27.

[32]   D.M. Kempaiah, S. Yin, T. Sato, Cryst. Eng. Commun. 13 (2011) 741.

[33]   X. Li, S. Wei, Z. Zhang, Y. Zhang, Z. Wang, Q. Su, X. Gao, Catal. Today, 175 (2011) 112.

[34]   N. Guillen-Hurtado, A. Garcia-Garcia, A. Bueno-Lopez, J. Catal. 299 (2013) 181.

[35]   M. Fernandez-Garcia, A. Martinez-Arias, A. Iglesias-Juez, C. Belver, A.B. Hungria, J. C. Conesa, J. Soria, J. Catal. 194 (2000) 385.

[36]   C. Gao, Y.Y.J. Lin, Y. Li, D.G. Evans, D.Q. Li, Ind. Eng. Chem. Res. 48 (2009) 6544.

Publications:

[1]   **Lankela H. Reddy**, Gunugunuri K. Reddy, D. Devaiah, Benjaram M. Reddy

A rapid microwave-assisted solution combustion synthesis of CuO promoted CeO_2–MxOy (M = Zr, La, Pr and Sm) catalysts for CO oxidation.

Applied Catalysis A: General, 445– 446 (2012) 297– 305.

[2]   **Lankela H. Reddy**, Gunugunuri K. Reddy, Boningari Thirupathi, Benjaram M. Reddy

A facile microwave-assisted solution combustion synthesis of highly stable magnesium oxide for multicomponent Mannich reaction.

Current Catalysis, 1 (2012) 164-170.

[3]   D. Devaiah, **Lankela H. Reddy**, K Kuntaiah, Benjaram M. Reddy

Design of novel ceria-based nano-oxides for CO oxidation reaction and other catalytic applications.

Indian Journal of Chemistry, 51A (2012) 186-195.

[4]   Benjaram M. Reddy, Gunugunuri K. Reddy, **Lankela H. Reddy**, Ibram Ganesh

Synthesis of nanosized Ceria-Zirconia solid Solutions by a rapid microwave-assisted combustion method.

The Open Physical Chemistry Journal, 3 (2009) 24-29.

Articles in Periodicals:

[1]   **Lankela H. Reddy**, Benjaram M. Reddy

Increasing applications of microwave-assisted synthesis in chemical industry

Chemical Industry Digest, November (2010) 60-69.

Book Chapters

[1]   **Lankela H. Reddy**, D Devaiah, Benjaram M. Reddy

Microwave Assisted Synthesis: A Versatile Tool for Process Intensification: In **Industrial Catalysis and Separations: Innovations for Process Intensification (Eds., K V Raghavan and B M Reddy), AAP/CRC Press, NJ, USA, Chapter 10, 2014, pp. 375 – 405.**

<u>Symposia/ Conference/Workshops:</u>

[1] **Lankela H. Reddy**, D. Devaiah, D. Jampaiah, P. Venkata Swamy, Benjaram M. Reddy

Influence of foreign cations (Zr^{4+}, La^{3+}, Pr^{3+}, and Sm^{3+}) on CuO–CeO_2: Microwave induced solution combustion synthesis, characterization, and CO oxidation activity **(Poster Presentation).**

21st National symposium on catalysis: Catalysis for sustainable development, CSIR–IICT, February 11–13, 2013, Hyderabad, India.

[2] **Lankela H. Reddy,** G. K. Reddy, D. Das, K. Kuntaiah, Benjaram M. Reddy

Synthesis and characterization of nanosized ceria-based solid solutions by microwave-induced combustion synthesis **(Poster Presentation).**

20th National symposium on catalysis: Catalysis for energy conversion and conservation of environment, **IIT Madras, India,** December, 2010.

[3] P. VenkataSwamy, P. Sudarsanam, **Lankela H. Reddy**, B. Mallesham, Benjaram M. Reddy.

Design of novel nanosized noble–metal free copper–ceria catalysts for diesel soot oxidation **(Poster Presentation).**

5th International conference on nanoscience and technology, ARCI, Hyderabad, India, January 20-23, 2012.

[4] **Workshop** on chromatography equipment's on 2nd - 3rd November, 2010.
Central Facilities for Research and Development (CFRD), **Osmania University, Hyderabad,** India.

Abstract of Published Paper:

A rapid microwave-assisted solution combustion synthesis of CuO promoted CeO$_2$–M$_x$O$_y$ (M = Zr, La, Pr and Sm) catalysts for CO oxidation

Lankela H. Reddy, Gunugunuri K. Reddy, Damma Devaiah, Benjaram M. Reddy*

Inorganic and Physical Chemistry Division, Indian Institute of Chemical Technology, Uppal Road, Hyderabad 500607, India

ARTICLE INFO

ABSTRACT

A series of copper oxide promoted CeO$_2$–M$_x$O$_y$ (M$_x$O$_y$ = ZrO$_2$, La$_2$O$_3$, Pr$_2$O$_3$ and Sm$_2$O$_3$) mixed oxides were synthesized by microwave-assisted solution combustion method using urea as the fuel and the respective metal nitrates as the precursors. The physico-chemical properties of the synthesized materials were analysed by BET surface area, X-ray diffraction (XRD), Raman spectroscopy, temperature programmed reduction/oxidation (TPR/TPO), X-ray photoelectron spectroscopy (XPS) and oxygen storage capacity (OSC) methods. XRD measurements confirmed the formation of solid solutions between ceria and the doped metal oxides in the presence of copper promoter. Raman measurements suggested defective structure of the mixed oxide solid solutions resulting in the formation of oxygen vacancies. The TPR/TPO studies revealed that the reduction behaviour of ceria depends on the type of metal dopant. XPS studies confirmed the presence of cerium in both Ce^{3+} and Ce^{4+} oxidation states in all mixed oxides. All the doped mixed oxides exhibited better CO oxidation activity compared to the undoped copper–ceria catalysts. Among various samples, ZrO$_2$ doped copper–ceria showed a high activity ($T_{1/2} \sim 378$ K) followed by samarium, praseodymium and lanthanum oxide doped samples, respectively. Significance of the combustion synthesis method has been addressed that include simplicity, flexibility and the control of different favourable factors.

MICROWAVE - ASSISTED SOLUTION CONBUSTION SYNTHESIS AND CHARACTERIZATION OF CERIA - BASED OXIDES FOR CO OXIDATION

Catalysis and Separations, 2014.
Publication

4   Benjaram M. Reddy. "Nanosized CeO2–SiO2, CeO2–TiO2, and CeO2–ZrO2 Mixed Oxides: Influence of Supporting Oxide on Thermal Stability and Oxygen Storage Properties of Ceria", Catalysis Surveys from Asia, 09/2005
Publication

<%1

5   Submitted to Pondicherry University
Student Paper

<%1

6   eprints.csirexplorations.com
Internet Source

<%1

7   Reddy, Benjaram M., Gode Thrimurthulu, Lakshmi Katta, Yusuke Yamada, and Sang-Eon Park. "Structural Characteristics and Catalytic Activity of Nanocrystalline Ceria−Praseodymia Solid Solutions", The Journal of Physical Chemistry C, 2009.
Publication

<%1

8   Reddy, Benjaram, M., Lakshmi Katta, and Gode Thrimurthulu. "Novel Nanocrystalline $Ce_{1-x}La_xO_{2-\delta}$ (x = 0.2) Solid Solutions: Structural Characteristics and Catalytic Performance", Chemistry of Materials, 2010.
Publication

<%1

9   Venkataswamy, Perala, Komateedi N. Rao,

<%1

Deshetti Jampaiah, and Benjaram M. Reddy. "Nanostructured manganese doped ceria solid solutions for CO oxidation at lower temperatures", Applied Catalysis B Environmental, 2015.
Publication

10 amsdottorato.unibo.it
    Internet Source   <%1

11 Submitted to RMIT University
    Student Paper   <%1

12 Submitted to Higher Education Commission Pakistan
    Student Paper   <%1

13 Submitted to Jawaharlal Nehru Technological University
    Student Paper   <%1

14 El Fray, M., D. Strzalkowska, C. Mandoli, F. Pagliari, P. Di Nardo, and E. Traversa. "Influence of ceria nanoparticles on chemical structure and properties of segmented polyesters", Materials Science and Engineering C, 2015.
    Publication   <%1

15 Pal, Nabanita, Eun-Bum Cho, Dukjoon Kim, and Mietek Jaroniec. "Mn-Doped Ordered Mesoporous Ceria–Silica Composites and Their Catalytic Properties toward Biofuel Production",   <%1

The Journal of Physical Chemistry C, 2014.
Publication

16 Vinodkumar, T., D. Naga Durgasri, Benjaram M. Reddy, and Ivo Alxneit. "Synthesis and Structural Characterization of Eu2O3 Doped CeO2: Influence of Oxygen Defects on CO Oxidation", Catalysis Letters, 2014.
Publication

<%1

17 Rao, K.N.. "Supported copperceria catalysts for low temperature CO oxidation", Catalysis Communications, 20100511
Publication

<%1

18 www.microscopy.cz
Internet Source

<%1

19 Gunugunuri K. Reddy. "A Rapid Microwave-Induced Solution Combustion Synthesis of Ceria-Based Mixed Oxides for Catalytic Applications", Catalysis Surveys from Asia, 12/04/2009
Publication

<%1

20 Reddy, Gunugunuri K., P. Boolchand, and Panagiotis G. Smirniotis. "Unexpected Behavior of Copper in Modified Ferrites during High Temperature WGS Reaction—Aspects of Fe^{3+} $\leftrightarrow Fe^{2+}$ Redox Chemistry from Mössbauer and XPS Studies", The Journal of Physical Chemistry C, 2012.

<%1

Publication

21 addi.ehu.es
    Internet Source   <%1

22 Jampaiah, Deshetti, Katie M. Tur, Samuel J.   <%1
    Ippolito, Ylias M. Sabri, James Tardio, Suresh
    K. Bhargava, and Benjaram M. Reddy.
    "Structural characterization and catalytic
    evaluation of transition and rare earth metal
    doped ceria-based solid solutions for elemental
    mercury oxidation", RSC Advances, 2013.
    Publication

23 Ozawa, M.. "Microstructure and oxygen release   <%1
    properties of catalytic alumina-supported
    CeO"2-ZrO"2 powders", Journal of Alloys and
    Compounds, 20000524
    Publication

24 www.ias.ac.in   <%1
    Internet Source

25 Benjaram M. Reddy. "Single step synthesis of   <%1
    nanosized CeO2–M x O y mixed oxides (M x O
    y = SiO2, TiO2, ZrO2, and Al2O3) by
    microwave induced solution combustion
    synthesis: characterization and CO oxidation",
    Journal of Materials Science, 06/2009
    Publication

26 www.benthamscience.com   <%1
    Internet Source

27 Katta, Lakshmi, Gode Thrimurthulu, Benjaram M. Reddy, Martin Muhler, and Wolfgang Grünert. "Structural characteristics and catalytic performance of alumina-supported nanosized ceria–lanthana solid solutions", Catalysis Science & Technology, 2011.
Publication

<%1

28 VENKATASWAMY, P, D JAMPAIAH, C U ANIZ, and BENJARAM M REDDY. "Investigation of physicochemical properties and catalytic activity of nanostructured Ce0.7M0.3O2−δ (M = Mn, Fe, Co) solid solutions for CO oxidation", Journal of Chemical Sciences, 2015.
Publication

<%1

29 J. Requies. "Biobutanol Dehydrogenation to Butyraldehyde over Cu, Ru and Ru–Cu Supported Catalysts. Noble Metal Addition and Different Support Effects", Catalysis Letters, 11/05/2011
Publication

<%1

30 Zhang, Xueying, Jingjing Wei, Hongxiao Yang, Xiufang Liu, Wei Liu, Cong Zhang, and Yanzhao Yang. "One-Pot Synthesis of Mn-Doped CeO 2 Nanospheres for CO Oxidation", European Journal of Inorganic Chemistry, 2013.
Publication

<%1

31 Jaimy, Kanakkanmavudi B., V. P. Safeena, Swapankumar Ghosh, Neha Y. Hebalkar, and K. G. K. Warrier. "Photocatalytic activity enhancement in doped titanium dioxide by crystal defects", Dalton Transactions, 2012.
Publication   <%1

32 M. R. Mohammadizadeh. "Pr at Gd or Ba site in GdBa_{2}Cu_{3}O_{7}:   Appearance of superconductivity", Physical Review B, 09/2003
Publication   <%1

33 Lei Li. "Water–Gas Shift Reaction over CuO/CeO2 Catalysts: Effect of the Thermal Stability and Oxygen Vacancies of CeO2 Supports Previously Prepared by Different Methods", Catalysis Letters, 03/04/2009
Publication   <%1

34 Handbook of Materials Modeling, 2005.
Publication   <%1

35 Benjaram M. Reddy. "Catalytic Efficiency of Ceria–Zirconia and Ceria–Hafnia Nanocomposite Oxides for Soot Oxidation", Catalysis Letters, 07/2008
Publication   <%1

36 Phung, Quoc Tri Maes, Norbert Jacques, D. "Effect of limestone fillers on microstructure and permeability due to carbonation of cement pastes u", Construction and Building Materials,   <%1

May 1 2015 Issue
Publication

37 She, Y.. "Rare earth oxide modified CuO/CeO"2 catalysts for the water-gas shift reaction", International Journal of Hydrogen Energy, 200911
Publication

<%1

38 Katta, Lakshmi, T. Vinod Kumar, D. Naga Durgasri, and Benjaram M. Reddy. "Nanosized Ce1âˆ'xLaxO2âˆ'Î´/Al2O3 solid solutions for CO oxidation: Combined study of structural characteristics and catalytic evaluation", Catalysis Today, 2012.
Publication

<%1

39 eprints-phd.biblio.unitn.it
Internet Source

<%1

40 Submitted to University of KwaZulu-Natal
Student Paper

<%1

41 www.researchgate.net
Internet Source

<%1

42 Vincenzo Esposito. "Design of Electroceramics for Solid Oxides Fuel Cell Applications: Playing with Ceria", Journal of the American Ceramic Society, 4/2008
Publication

<%1

43 mdpi.com

Internet Source

<%1

44 Papista, E., E. Pachatouridou, M. A. Goula, G. E. Marnellos, E. Iliopoulou, M. Konsolakis, and I. V. Yentekakis. "Effect of Alkali Promoters (K) on Nitrous Oxide Abatement Over Ir/Al2O3 Catalysts", Topics in Catalysis, 2016.
Publication

<%1

45 Hu Yucai. "Hydrothermal Synthesis of Nano Ce-Zr-Y Oxide Solid Solution for Automotive Three-Way Catalyst", Journal of the American Ceramic Society, 6/12/2006
Publication

<%1

46 www.jbclinpharm.com
Internet Source

<%1

47 Ashok, J.. "Catalytic decomposition of CH"4 over Ni-Al"2O"3-SiO"2 catalysts: Influence of pretreatment conditions for the production of H"2", Journal of Natural Gas Chemistry, 200806
Publication

<%1

48 Ashok, J.. "CO"X-free H"2 production via catalytic decomposition of CH"4 over Ni supported on zeolite catalysts", Journal of Power Sources, 20070210
Publication

<%1

49 jocpr.com
Internet Source
<%1

50 Reddy, Benjaram M., Pankaj Bharali, Pranjal Saikia, Sang-Eon Park, Maurits W. E. van den Berg, Martin Muhler, and Wolfgang Grünert. "Structural Characterization and Catalytic Activity of Nanosized CexM1-xO2 (M = Zr and Hf) Mixed Oxides", The Journal of Physical Chemistry C, 2008.
Publication
<%1

51 Sedmak, G.. "Kinetics of selective CO oxidation in excess of H"2 over the nanostructured Cu"0"."1Ce"0"."9O"2"-"y catalyst", Journal of Catalysis, 20030125
Publication
<%1

52 digbib.ubka.uni-karlsruhe.de
Internet Source
<%1

53 Submitted to University of Glasgow
Student Paper
<%1

54 D. A. Andersson. "Modeling of CeO_{2} , Ce_{2}O_{3} , and CeO_{2−x} in the LDA+U formalism", Physical Review B, 01/2007
Publication
<%1

55 Jha, Ajay, Dae-Woon Jeong, Yeol-Lim Lee, Won-Jun Jang, Jae-Oh Shim, Kyung-Won Jeon, Chandrashekhar V. Rode, and Hyun-
<%1

Seog Roh. "Chromium free high temperature water–gas shift catalyst for the production of hydrogen from waste derived synthesis gas", Applied Catalysis A General, 2016.
Publication

56 Bueno-Lopez, A.. "On the mechanism of model diesel soot-O"2 reaction catalysed by Pt-containing La^3^+-doped CeO"2", Catalysis Today, 20070330
Publication   <%1

57 www.jnanochem.com
Internet Source   <%1

58 Reddy, Benjaram M., Pranjal Saikia, Pankaj Bharali, Sang-Eon Park, Martin Muhler, and Wolfgang Grünert. "Physicochemical Characteristics and Catalytic Activity of Alumina-Supported Nanosized Ceria−Terbia Solid Solutions", The Journal of Physical Chemistry C, 2009.
Publication   <%1

59 www.getskinned.org
Internet Source   <%1

60 Venkataswamy, Perala, Deshetti Jampaiah, Deboshree Mukherjee, C. U. Aniz, and Benjaram M. Reddy. "Mn-doped Ceria Solid Solutions for CO Oxidation at Lower Temperatures", Catalysis Letters, 2016.   <%1

Publication

| 61 | www.scribd.com
Internet Source | <%1 |

| 62 | Katta, Lakshmi, Putla Sudarsanam, Baithy Mallesham, and Benjaram M. Reddy. "Preparation of silica supported ceriaâ€"lanthana solid solutions useful for synthesis of 4-methylpent-1-ene and dehydroacetic acid", Catalysis Science & Technology, 2012.
Publication | <%1 |

| 63 | ethesis.nitrkl.ac.in
Internet Source | <%1 |

| 64 | Krishna, K.. "Potential rare earth modified CeO"2 catalysts for soot oxidation", Applied Catalysis B, Environmental, 20070926
Publication | <%1 |

| 65 | eprints.bham.ac.uk
Internet Source | <%1 |

| 66 | dro.deakin.edu.au
Internet Source | <%1 |

| 67 | Carabineiro, S.A.C.. "Effect of chloride on the sinterization of Au/CeO"2 catalysts", Catalysis Today, 20100915
Publication | <%1 |

Ayastuy, J.L.. "CuO/CeO"2 washcoated ceramic

68 monoliths for CO-PROX reaction", Chemical Engineering Journal, 20110615
Publication

<%1

69 Hocevar, S.. "Wet Oxidation of Phenol on Ce"1"-"xCu"xO"2"-"@dCatalyst", Journal of Catalysis, 19990515
Publication

<%1

70 file.scirp.org
Internet Source

<%1

71 Tang, C.W.. "Influence of pretreatment conditions on low-temperature carbon monoxide oxidation over CeO"2/Co"3O"4 catalysts", Applied Catalysis A, General, 20060717
Publication

<%1

72 Huizhi Bao. "Structure-activity Relation of Fe2O3–CeO2 Composite Catalysts in CO Oxidation", Catalysis Letters, 09/2008
Publication

<%1

73 Song, Daheoi, and Miewon Jung. "Ni-coated La2 Ce2 O7 /SiC Membrane via DC Magnetron Sputtering : Ni-coated La2 Ce2 O7 /SiC Membrane via DC Magnetron Sputtering", Bulletin of the Korean Chemical Society, 2016.
Publication

<%1

74 F. M. Aquino. "Thermal decomposition kinetics of PrMO3 (M = Ni or Co) ceramic materials via

<%1

thermogravimetry", Journal of Thermal Analysis and Calorimetry, 12/08/2010
Publication

75   dyuthi.cusat.ac.in
Internet Source   <%1

76   Mohebbi, H.. "Synthesis of nano-crystalline (Ni/NiO)-YSZ by microwave-assisted combustion synthesis method: The influence of pH of precursor solution", Journal of Power Sources, 20080315
Publication   <%1

77   www.unesco-ihe.org
Internet Source   <%1

78   Iafisco, Michele <1980>(Roveri, Norberto). "Interaction between biomimetic inorganic materials and biomolecules: towards nanotechnological applications ", Alma Mater Studiorum - Università di Bologna, 2011.
Publication   <%1

79   Feng, R.m.. "Hydrothermal synthesis of stable mesoporous $ZrO_2-Y_2O_3$ and $CeO_2-ZrO_2-Y_2O_3$ from simple inorganic salts and CTAB template in aqueous medium", Materials Chemistry & Physics, 20080115
Publication   <%1

80   Benjaram M. Reddy. "Characterization and   <%1

photocatalytic activity of TiO2–M x O y (M x O y = SiO2, AI2O3, and ZrO2) mixed oxides synthesized by microwave-induced solution combustion technique", Journal of Materials Science, 07/29/2009

Publication

81 Ramana, Singuru, Bolla Govinda Rao, Perala Venkataswamy, Agolu Rangaswamy, and Benjaram M. Reddy. "Nanostructured Mn-doped ceria solid solutions for efficient oxidation of vanillyl alcohol", Journal of Molecular Catalysis A Chemical, 2016.

Publication

<%1